Technical Report No. 3

08160-3-T

HOLOGRAM INTERFEROMETRY

August 1968 to August 1969

ORL Subcontract R66-2476

Under Contract NOw-65-0123-d

Prepared by

Lyman W. Orr
Norman E. Barnett

Cooley Electronics Laboratory
Department of Electrical Engineering
The University of Michigan
Ann Arbor, Michigan

for

Ordnance Research Laboratory
The Pennsylvania State University
State College, Pennsylvania

August 1969

ABSTRACT

The development of interferometry with special application to the analysis of surface vibrations has been continued. A complete analysis is given of the contrast of real-time fringes for the extreme cases of non-depolarizing and completely depolarizing objects, and several methods are shown for advantageously manipulating fringe contrast in practical laboratory work. Techniques are analysed for vibrational sensitivity enhancement, for stroboscopic interferometry, and for phase modulation of the holographic reference beam. The latter technique may be applied both to the sensing of vibrational phase and to the detecting of small vibrational amplitudes. Effects relating to underwater interferometry are discussed and the acoustic pressure modulation of the index of refraction of water is found to create a fundamental difficulty.

A digest is presented of the useful application of holographic interferometry to the study of large vibrating objects under the constraint of the limited axial coherence length associated with most CW gas laser systems. Photographic results on a full-sized section of torpedo shell demonstrate this application.

Two sonar transducers (2 by 2 arrays with rubber faces operating in the 19 to 30 kHz frequency range) were examined interferometrically in air and in water. These studies were directed at

discovering the problems of applying hologram interferometry techniques underwater. For such transducer experiments, an anechoic water tank is needed but pressure modulation of the index of refraction of the water may still introduce interpretational complexity. The well-known acoustical effects caused by air bubbles were observed during hologram interferometry in water. Many of the transducer results also are displayed by means of photographic reconstructions from the corresponding holograms.

TABLE OF CONTENTS

TABLE OF CONTENTS (Cont.)

LIST OF FIGURES

LIST OF FIGURES (Cont.)

LIST OF FIGURES (Cont.)

1. INTRODUCTION

The activities of the Cooley Electronics Laboratory for the period August 1968 to August 1969 on ORL subcontract R66-2476 are reported. This research is a continuation of the development of hologram interferometry with special application to the analysis of surface vibrations. The previous work has been reported[1] in Technical Report No. 1. For convenient reference, the table of contents from Technical Report No. 1 has been included in this report as an appendix. Section 3 of this report contains a digest of material which was recently reported[2] as Technical Report No. 2 and given small circulation.

In this report, we first discuss further developments in the techniques of hologram interferometry and then present the results of interferometric studies on a full-sized section of torpedo shell in air and also two four-element sonar transducers both in air and in water.

---

[1] Technical Report No. 1, "Hologram Interferometry in Cylindrical Shell-Vibration Analysis" by L. W. Orr and N. E. Barnett, Cooley Electronics Laboratory, The University of Michigan, December 1968.

[2] Technical Report No. 2, "Holographic Interferometry of Large Cylinders" by L. W. Orr, Cooley Electronics Laboratory, The University of Michigan, July 1969.

2. TECHNIQUES FOR HOLOGRAM INTERFEROMETRY

2.1 Real-Time Fringe Contrast Enhancement

For dynamic studies of vibrating objects it is clearly advantageous to obtain real-time fringes of good contrast. A typical arrangement for real-time fringe interferometry is shown in Fig. 1. Here the reference beam acts as a playback beam to reconstruct the virtual image. With proper placement of the hologram, this image is in almost exact register with the object. As viewed from behind the hologram, the light forming the image is coherent with that reflected from the object, giving rise to a regular pattern of bright and dark fringes.

The contrast ratio R_c of the fringe pattern is defined as

$$R_c = I_{max}/I_{min} \tag{1}$$

that is, the ratio of intensities of an adjacent pair of bright (I_{max}) and dark (I_{min}) fringes. This ratio depends only on the intensity I_i of the reconstructed virtual image, the intensity I_o of the corresponding object as viewed through the hologram, and the degree of coherence between them.

We shall now examine two cases (a) for non-depolarizing objects and (b) for totally depolarizing objects. In each case the maximum value and variation of the fringe contrast ratio will be found. Theoretically, R_c has a maximum value of infinity in case (a); however, it is found in practice that values of R_c in excess of 30 are satisfactory for nearly all real-time interferometry.

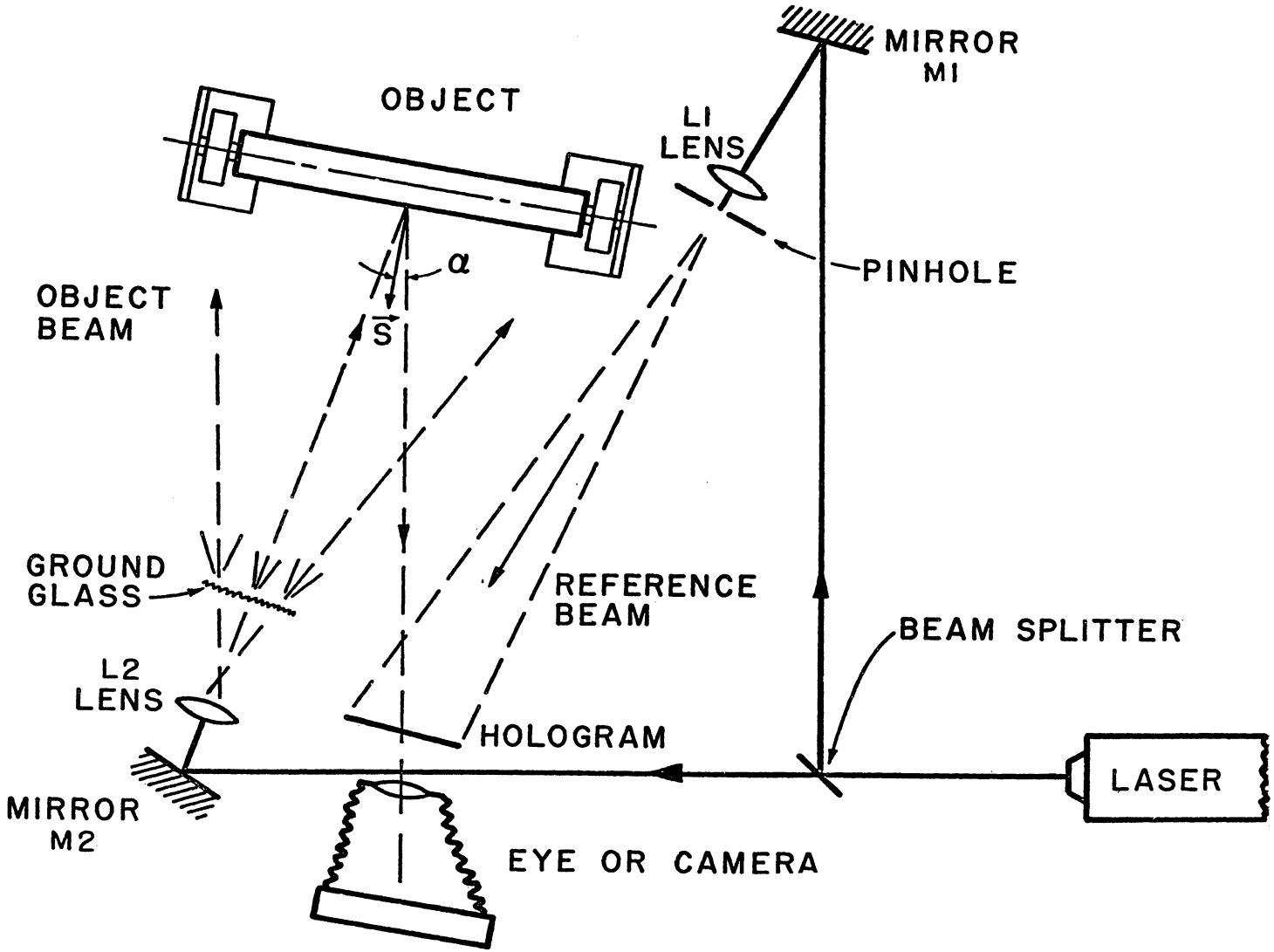

Fig. 1. Plan view of holographic setup

2.1.1 Non-Depolarizing Objects. For lasers equipped with Brewster windows, the output beam is plane polarized. In the arrangement depicted in Fig. 1, we therefore will have, for a non-depolarizing object, two polarized beams (from object and virtual image) which have the same plane of polarization. Since these two beams are completely coherent, we must use vector addition of the amplitude vectors of the two beams. Thus the combined amplitude may range from a maximum of $A_i + A_o$ to a minimum of $A_i - A_o$. Since the intensity is the square of the amplitude, we may write

$$I_{max} = (A_i + A_o)^2 = \left[(I_i)^{\frac{1}{2}} + (I_o)^{\frac{1}{2}}\right]^2 \tag{2}$$

$$I_{min} = (A_i - A_o)^2 = \left[(I_i)^{\frac{1}{2}} - (I_o)^{\frac{1}{2}}\right]^2 \tag{3}$$

Substitution in Eq. 1 thus gives the desired expression for the fringe contrast ratio in this case.

$$R_c = \left[\frac{(I_i)^{\frac{1}{2}} + (I_o)^{\frac{1}{2}}}{(I_i)^{\frac{1}{2}} - (I_o)^{\frac{1}{2}}}\right]^2 \tag{4}$$

In the above expressions, A_i and I_i represent the amplitude and intensity of some specified unit area of the virtual image as reconstructed by the playback beam, while A_o and I_o are the corresponding quantities

for that portion of the reflected object light which is transmitted through the hologram to the viewer. The ratio of intensities I_i/I_o of these exit beams is termed the exit beam ratio, and the variation of R_c vs I_i/I_o for this case is shown by curve A of Fig. 2.

If our criterion is that $R_c > 30$, it is clear from this figure that the exit beam ratio may vary from 0.5 to 2.0 and still satisfy our requirements for satisfactory interferometry. The practical limit on R_c determined by plate noise is on the order of 100 depending on the emulsion characteristics.

2.1.2 Totally Depolarizing Objects. In this case the plane polarized light from the laser forms a virtual image which is also plane polarized. However the object exit beam is completely depolarized, so that only a portion of it will interfere with the virtual image. With no loss in generality, the depolarized beam may be considered as composed of two plane polarized component waves with their planes at right angles. We chose the two components I_{o1} parallel and I_{o2} normal to the plane of polarization of the virtual image. In computing the maximum and minimum amplitudes, the parallel vector components may be added numerically as before, but the normal component must be added vectorially.

The maximum and minimum intensities in the fringe pattern now become,

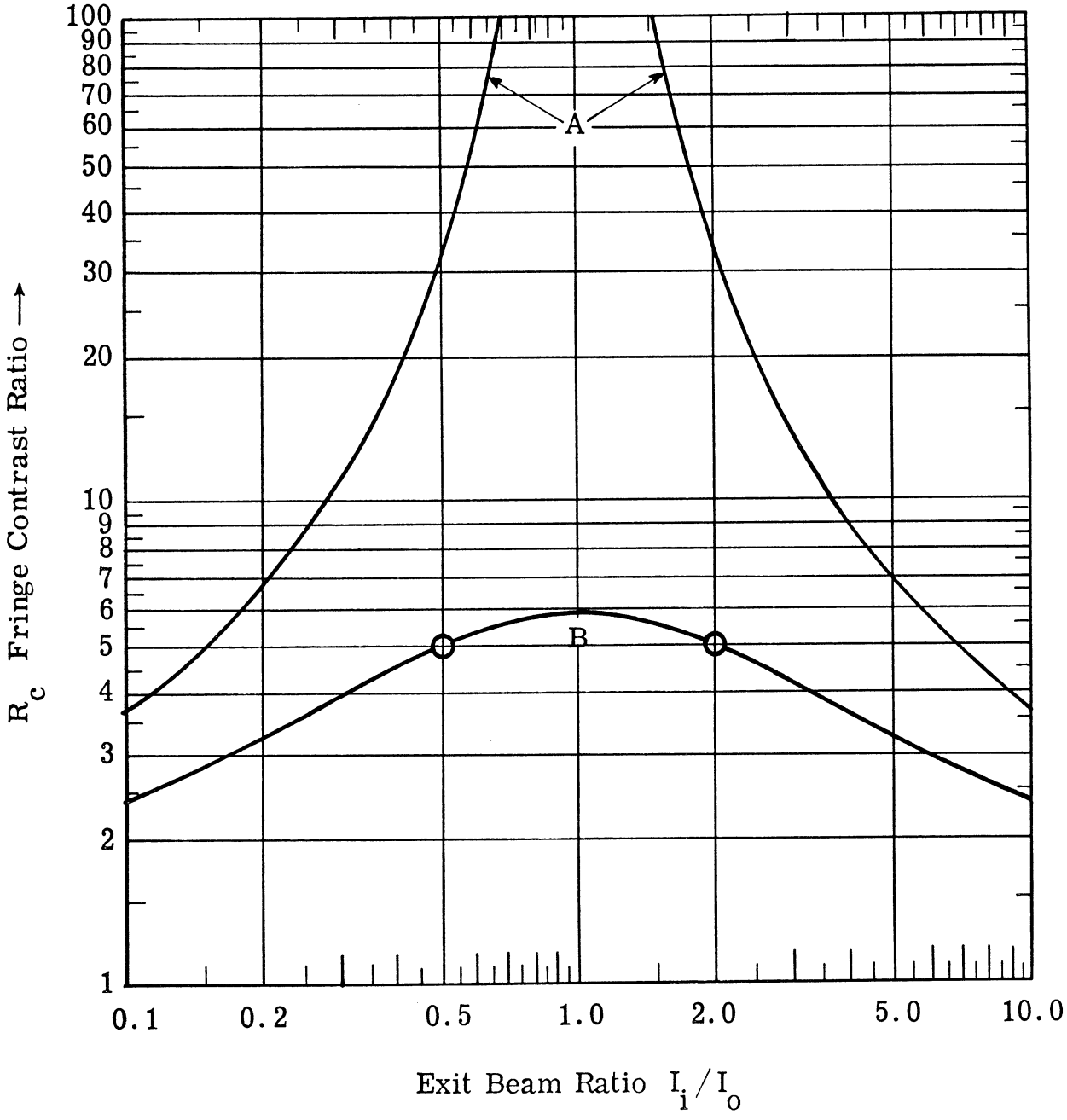

Fig. 2. Fringe contrast ratio vs exit beam ratio
A - Non-depolarizing objects
B - Totally depolarizing objects

$$I_{max} = \left[(I_i)^{\frac{1}{2}} + (I_{o1})^{\frac{1}{2}}\right]^2 + I_{o2} \tag{5}$$

$$I_{min} = \left[(I_i)^{\frac{1}{2}} - (I_{o1})^{\frac{1}{2}}\right]^2 + I_{o2} \tag{6}$$

Substituting in Eq. 1 now gives the following:

$$R_c = \frac{\left[(I_i)^{\frac{1}{2}} + (I_{o1})^{\frac{1}{2}}\right]^2 + I_{o2}}{\left[(I_i)^{\frac{1}{2}} - (I_{o1})^{\frac{1}{2}}\right]^2 + I_{o2}} \tag{7}$$

For a completely depolarized object exit beam, one has

$$I_{o1} = I_{o2} = \frac{1}{2} I_o \tag{8}$$

Substitution in Eq. 7 now gives the desired equation for the fringe contrast ratio for totally depolarizing objects:

$$R_c = \frac{\left[(I_i)^{\frac{1}{2}} + \left(\frac{1}{2} I_o\right)^{\frac{1}{2}}\right]^2 + \frac{1}{2} I_o}{\left[(I_i)^{\frac{1}{2}} - \left(\frac{1}{2} I_o\right)^{\frac{1}{2}}\right]^2 + \frac{1}{2} I_o} \tag{9}$$

Curve B in Fig. 2 shows this relationship. R_c reaches a maximum of only 5.828, but the actual value of exit beam ratio is not at all critical. I_i / I_o may range all the way from 0.5 to 2.0 while R_c remains in excess of 5.0 over this range. In some instances $R_c \cong 5$ may be adequate for

visual observation or recording. In others, a much greater contrast is required, for example, where subtle fringe washouts are being observed in a frequency survey.

We now show a method for making a dramatic improvement in R_c from totally depolarizing objects, in fact, R_c may be made almost arbitrarily large, as in case (a). This method involves the use of a Polaroid filter between the hologram plate and the eye (or camera). When this filter is properly aligned, the I_i and I_{o1} components are transmitted while the I_{o2} component is stopped. The result of $I_{o2} = 0$ in Eq. 7 is to reduce it to Eq. 4, so that curve A in Fig. 2 may be used again. We need only note here that now the exit beam ratio is measured after transmission through the Polaroid filter. The practical limit on R_c is determined only by plate noise and filter characteristics.

The loss of combined image-object brightness, which always results with this method, is normally of little consequence. The dramatic fringe contrast enhancement is always beneficial for photographic recording, and usually quite helpful in visual observation. However situations have arisen where the image brightness is so low that observers may prefer the greater visibility associated with the brighter but less contrasting fringe pattern.

2.1.3 Exit Beam Ratio Control. Several methods of control over the exit beam ratio (I_i/I_o) are available to furnish the desired fringe contrast in real-time interferometry. It will be sufficient here to discuss

two of these methods which use (a) control of the plate density alone, and (b) control of both plate density and playback factor, k .

Method (a) uses the conventional real-time interferometer arrangement, as in Fig. 1, without any added optical components. Curve I_i in Fig. 3a shows the relative intensity of the reconstructed virtual image as a function of semidiffuse density, D , of a hologram made on an Agfa 10E70 plate. Maximum playback efficiency is seen to occur at $D = 0.6$.

The corresponding curve of object intensity, I_o , which is the specular component of the transmitted object beam, also varies with density, and is shown plotted on the same scale. The match point P , where $I_i = I_o$, usually occurs at $D \approx 1.2$. However we have learned that some flexibility is allowed, and the exposure is usually made with a target point such as Q giving $D \approx 1.0$. This does not produce an exact match, but still produces good fringe contrast, and with a brighter image than one obtains at point P .

We have used this method[1] for several years. Its chief advantage is its simplicity, requiring no additional optical parts. However, the combined image brightness in a number of situations may still be so dim as to fatigue the viewer, and an alternative method of R_c control with a greater image brightness is obviously desirable.

---

[1] See, for instance, Appendix A, Technical Report No. 1, December 1968, ORL Subcontract R66-2476.

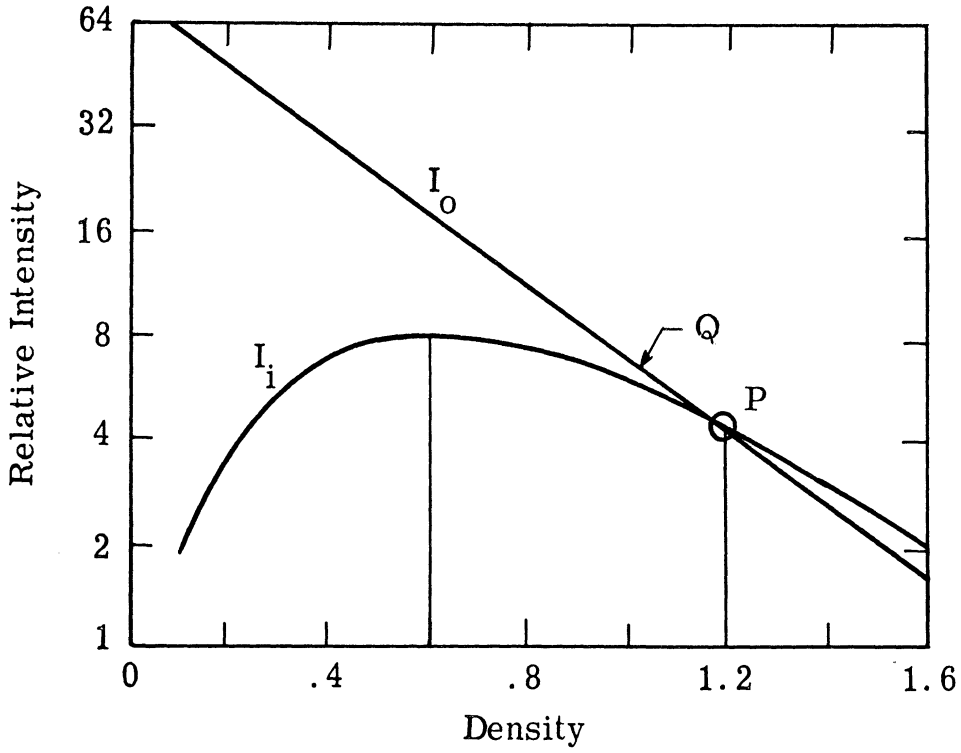

(a) Density Control Alone

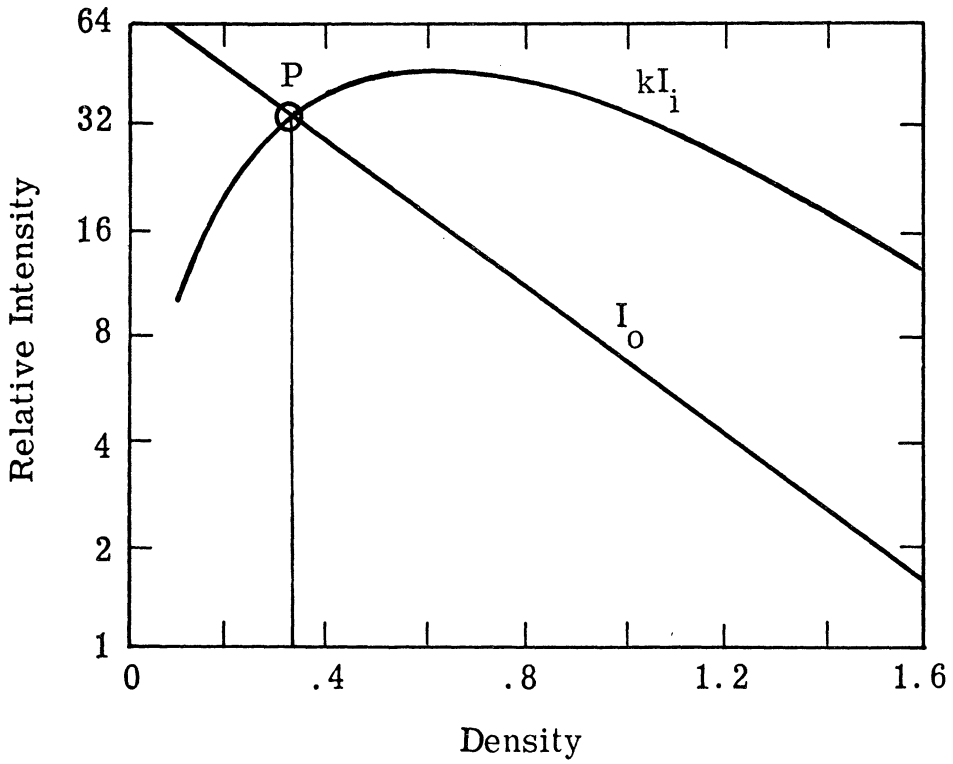

(b) Density and Playback Factor Control

Fig. 3. Control methods of exit beam ratio

Method (b) offers a great improvement in image brightness with no sacrifice in fringe contrast. This method uses the same optical arrangement as in Fig. 1, with the addition of an optical attenuator placed between the beam splitter and mirror M_1. Lens L_1 may require a change in focal length, and perhaps also in distance from the hologram, in order to maintain the usual reference-to-object beam ratio of about 4, in exposing the hologram.

On playback, the attenuator is either reduced or removed altogether, giving a playback ratio of $k > 1.0$ where $k = I_{pb}/I_{ref}$, the intensity ratio of the beam in the playback and reference situations. The resulting proportional increase in intensity of the reconstructed image is indicated by curve kI_i in Fig. 3b. This is the same curve as in Fig. 3a, but displaced upward by the factor k. The match point, P, where this curve crosses the I_o line shows greatly improved intensity and at a much lower plate density than before.

This curve was drawn for $k = 6.3$ (obtained with a neutral density filter $D_f = 0.8$ as the attenuator, which was removed entirely on playback). It illustrates an intensity improvement factor of about 6 over method (a). In making the hologram exposure, P is used as the target density (approximately 0.3) since for useful values of k, there is no advantage in departing from point P.

This example is typical of our experimental procedure in which Wratten No. 96 gelatin neutral density filters (Eastman Kodak Co.) were

used successfully. They can be inserted or removed from the reference beam without spoiling the alignment of the interferometer. They have been quite satisfactory provided they remain clean and reasonably flat. (During one period of very hot, humid weather the gelatin neutral density filters could not be used successfully for reasons not fully understood. Otherwise, they have been very effective, convenient and economical.)

Neutral density filters of the evaporated metal film variety mounted in glass have not been used as successfully. The greater optical thickness of the glass tends to misalign the interferometer, and internal reflections may introduce interference fringes, which are hard to remove with the pinhole spatial filter, into the reference beam.

Some advantage is gained by the use of stepped or continuously variable attenuators since closer control may be enjoyed after the hologram is exposed. In this case also, the optical quality of the attenuator must be such as to avoid adverse diffraction or beam displacing effects that can seriously degenerate the quality of the hologram. Some variable attenuators specifically designed for interferometry are starting to appear on the market.

Two Polaroid filters can function as a variable attenuator in the reference beam. The first Polaroid is rotatable and varies the intensity of the polarized reference beam transmitted to the second Polaroid. The latter is required to restore the plane of polarization of the output beam to its original orientation. This restoration is essential for good

interferometry of both depolarizing and non-depolarizing objects. Correct orientation of the second filter is done simply by maximizing the transmitted light with the first Polaroid filter temporarily removed.

This method of variable attenuation is attractive, but we have experienced uneven and sometimes unsatisfactory hologram quality when two glass-mounted filters of photographic grade were employed.

These several methods for adjusting the exit beam ratio provide the holographer with flexible and positive control, improving the overall quality and usefulness of real-time hologram nterferometry.

2.2 Vibrational Sensitivity Enhancement

Time-average hologram interferometry (TAHI) is used widely for mapping vibration-amplitude contours on objects in controlled sinusoidal vibration.[1] The contour indicated by the first dark fringe represents a projected[2] single-peak amplitude of $0.191\,\lambda$. (This is 4.768 microinches for $\lambda = 632.8$ nm.) In cases where the projected vibration is considerably smaller than this, the conventional methods of TAHI are inadequate. This section discusses a method of enhancing the sensitivity of the technique to smaller vibrations by almost an order of magnitude.

---

[1] A full discussion of the theory of TAHI is found in Technical Report No. 1.

[2] This is the projection of the vibration vector on the sensitivity vector.

The electric field vector E_p for a point P on the reconstructed image of a time-average interferogram is given by

$$E_p = E_o J_o(\phi) \tag{10}$$

where E_o is the magnitude of the electric field vector for no vibration, J_o is the zero order Bessel function of the first kind, and ϕ is the optical phase excursion (referred to the fixed phase of the reference beam) of the reflected light from P due to the vibration. Figure 4 is a plot of Eq. 10. This shows that the light vector falls to zero at certain values of the vibration amplitude. The first zero is at point A, and it follows that the corresponding dark fringe represents a vibration amplitude of d_1.

Suppose that the entire hologram could be biased by the amount E_2, so that the first zero would occur at point B. In this case the first dark fringe would represent a vibration amplitude of d_2. This would depict, in the reconstructed image, a contour representing a considerably smaller vibration amplitude than with normal time-average interferometry. Furthermore, a set of such holograms could be made with different bias levels each one giving a new contour with a different value of d_2.

Such a biased hologram may be made as follows. Two exposures are made. The first is an exposure of t_1 seconds with the object vibrating. Before making the second exposure, the phase of the reference beam is shifted by π radians. During the second exposure of t_2 seconds,

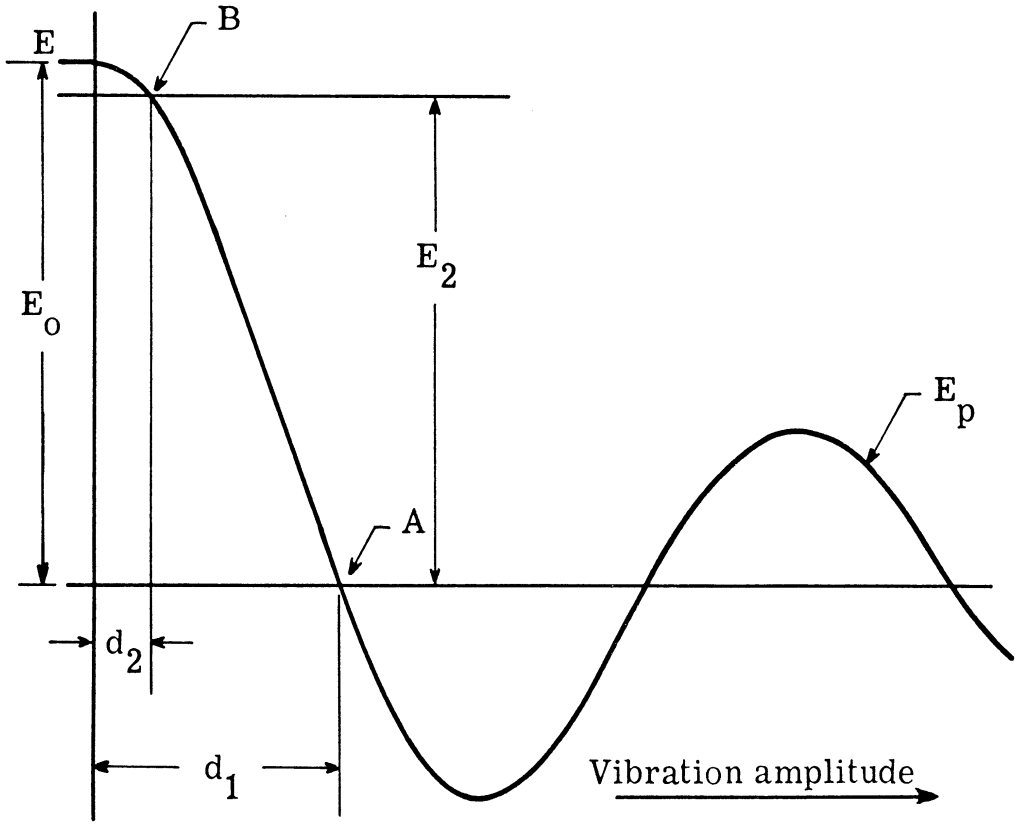

Fig. 4. Variation of time-average electric field vector for a point P with vibration amplitude

the object is not permitted to vibrate. Exposure times are suitably adjusted to give an acceptable density to the finished hologram.

By making a phase shift of π radians in the reference beam between exposures, the stored amplitudes in the second hologram will all be rotated by π radians from those of the first. In the finished hologram they will therefore subtract.

If we make $t_2 = t_1$, then the bias level due to the second exposure would amount to just E_o, and a "zero" difference hologram[1] would result. However if t_2 is made less than t_1 by the proper amount, then the desired bias E_2 (less than E_o) will result.

The reason this method can function is due first to the capability of storing a number of holograms on one plate, and second, to the fact that the phase and amplitude of the light vectors are preserved so that they may interact together in playback. The actual intensity variation of the resulting image will, as always, be the square of the resultant amplitude. In this case it will be the square of the difference between the horizontal line at level E_2 due to the second exposure, and the curve E_p due to the first.

A number of ways are available for performing the required reference beam phase shift of π radians between exposures. Collins[2] has

---

[1] See, for instance, L. F. Collins, "Difference Holography," Applied Optics, 7, 203, January 1968.

[2] Op. cit.

used a gas cell within which a controlled step change in pressure gave the required phase shift. It should be noted that the phase shift should be made as accurately as possible, as errors in this adjustment become serious with large sensitivity enhancements.

It is believed that an enhancement factor approaching an order of magnitude may be realized in practice. A second method of vibrational sensitivity enhancement involving phase modulation of the reference beam in a singly exposed interferogram is discussed in Section 2.4.

2.3 Stroboscopic Hologram Interferometry (SHI)

Stroboscopic Hologram Interferometry (SHI) is becoming increasingly important in the analysis of surface vibrations. The interference fringe patterns are somewhat easier to read and will accommodate much larger vibration amplitudes without loss in fringe brightness than in Powell and Stetson time-average interferograms. However, the great significance of SHI is in its application to non-sinusoidal periodic vibrations.

The concept of SHI was developed some time ago at the Cooley Electronics Laboratory and has been discussed with ORL personnel at various times over the past two years. Unfortunately, due to financial limitations, this technique has not been supported by experimental work at our laboratory. However, we have followed with interest the developments at other laboratories, and these will be referred to below.

The basic optical arrangement in all cases is similar to Fig. 1 with the addition of a light chopper or pulse modulator placed in the laser beam between the laser and the beam splitter. Alternatively, a pulsed gas laser could be used to advantage. In either case, pulses of laser light are presented to the optical system with a phasing and repetition rate related to those of the vibrating object, and with a pulse duration which is short compared to the period of vibration.

Two types of SHI have evolved. In frozen fringe SHI, the interference pattern is permanently stored in the hologram. In real-time SHI, the dynamics of the vibration may be viewed by observing a changing interference fringe pattern in real time.

2.3.1 Frozen Fringe SHI. In frozen fringe stroboscopic hologram interferometry[1, 2] two separate exposures are made on the same hologram plate. During the first exposure the object is held motionless. The exposure is made with continuous laser light for one-half the normal exposure time. During the second exposure, the laser beam is chopped by a slotted rotating disk or by a pulse-modulated Pockels cell, and the object is permitted to vibrate at constant amplitude such that one of the

---

[1] B. M. Watrasiewicz and P. Spicer, "Vibrational Analysis by Stroboscopic Holography," Nature, 217, 1968, p. 1142.

[2] P. Shajenko and C. D. Johnson, "Stroboscopic Holographic Interferometry," Applied Physics Letters, 13, 1 July 1968, p. 44.

extremes of vibratory motion coincides with the light pulses. The second exposure is made long enough so that the accumulated light pulses give, as before, one-half the normal exposure.

In playback, the hologram reconstructs the two stored images of the object in its zero and extended positions. These two images interfere with each other, producing a fringe distribution pattern wherein the fringes are essentially contour lines representing equal increments of vibrational displacement. This fringe pattern is frozen in the hologram plate forming a permanent record. The fringes are regularly spaced at half-wave intervals of displacement in the sensitivity direction, and are of equal brightness as distinct from the successively decreasing brightness obtained in Bessel fringes in a Powell and Stetson (time-average) interferogram. This fact has the disadvantage that the vibratory nodes are not easily identified as in Bessel fringe patterns, but has the advantage that large amplitudes of vibration may be accommodated.

To increase the sensitivity, the first exposure may also be made stroboscopically with the pulses of light so phased as to coincide with the opposite extreme of vibratory motion. In this case the fringes depict the interference between the object in its two extremes of motion, and the fringe density is doubled. Moving in the other direction, the sensitivity may be decreased to an arbitrarily small value by suitable phase control of the light pulses in the second exposure.

This technique does not sense the phase of the vibrational anti-nodes, since in almost all frozen fringe interferograms, the sign ambiguity in vibration amplitude is not resolved.[1]

2.3.2 Real-Time SHI. Archbold and Ennos[2] first proposed the use of real-time stroboscopic hologram interferometry for the analysis of surface vibrations in 1968. They employed a small hole drilled in the shaft of a high-speed air turbine as the light chopper in a narrowly focussed helium-neon laser beam. A second optical path involving a rotating polarizer on the turbine shaft was used for phase control of the vibration drive.

In their technique, an ordinary hologram is made with unchopped laser light while the object is held fixed. The hologram is processed and then replaced in exact register in its holder to give the zero fringe condition,[3] the combined object and its virtual image being exactly superimposed, and thus appearing equally bright (or dark) over the entire surface.

---

[1] Vibrational phase sensing in a frozen fringe interferogram is discussed in Section 2.4.

[2] Edward Archbold and A. E. Ennos, "Observations of Surface Vibration Modes by Stroboscopic Hologram Interferometry," Nature, 217, March 9, 1968, p. 942. See also Ennos and Archbold, "Vibrating Surface Viewed in Real Time by Interference Holography," Laser Focus, 4, October 1968, p. 58.

[3] The zero fringe condition is quite difficult to achieve without a special holder suitably equipped with kinematic adjustments. As an alternative, the plate could be processed in situ giving the zero fringe condition automatically, but again requiring a special holder of a different variety.

The object is now permitted to vibrate, and the chopper is placed in operation. By a suitable phase adjustment, the light pulses are made to coincide with one of the vibrational extremes. Now the observer sees, in real time, interference fringes between the extended object and the reconstructed image of its zero position. By varying the amplitude or phase of the vibrational drive, the dynamic behavior of the object may be studied in real time and from a single hologram. Furthermore, by slowly scanning the frequency, the resonances and their distributions may be found.

The chief disadvantage of this method is the great loss of total light due to the chopper, which tends to cause fatigue in viewing the dim fringe patterns. Light conservation techniques, and the use of a more powerful laser, are helpful inthis regard. The most important advantage of the technique is its usefulness in making cleanly observable frequency surveys and dynamic observations of complex motions in real time, and from a single hologram.

In common with the frozen fringe method, these real-time SHI fringes are all spaced at half-wave displacement intervals and are of equal brightness. Also non-sinusoidal vibrations are clearly represented.

Since the fringes representing a positive displacement are identical in behavior and appearance to those representing a negative one, it appears unlikely that the sign ambiguity in vibration amplitude can be resolved with only the zero fringe setting. Archbold and Ennos claim that it can be done but do not elucidate.

2.3.3 Modified Real-Time SHI. The real-time SHI system conceived by us at the Cooley Electronics Laboratory differs from the one described above in two respects.

(a) The hologram is reinserted, after processing, in its original position and adjusted not for zero fringe, but for a regularly spaced parallel fringe pattern[1] under the condition of no vibration.

(b) The chopper is replaced by a pulse-modulated Pockels cell, electrically controlled from the driving oscillator through a continuously rotatable electronic phase shifter. This method extends the frequency range, and furnishes excellent stability and phase control.

Action of the system is similar to the previous one; however, the appearance and behavior of the fringes are different. Without vibration, the fringes remain straight and parallel. When vibration is induced in the object, and the Pockels modulator is operated at a certain phase, the fringes will appear bunched, curved and shifted. A lateral fringe shift occurs where the object is being extended in the direction of the sensitivity vector at the moment of strobing. Fringe curvature describes explicitly the distribution of extension since the fringe was originally straight. Also, a forward vibrational movement of the object shifts the fringes in one direction, while a backward movement shifts them in the other direction. By observing such shifts stroboscopically in real time,

---

[1] These conditions are identical with those conventionally used in real-time interferometry as described in Section 2.1.

while the vibration amplitude is caused to increase or decrease, the sign ambiguity of the vibration phase may be resolved.

Considerable benefit is obtained by making a motion picture of the fringe motions. This may be done one frame at a time, the strobe phase being advanced between frames until a full cycle has been recorded. By splicing copies of this full cycle together, a film of arbitrary length may be made. The dynamics of motion may now be studied at leisure without fatigue in essentially any desired time scale, and features about the vibration may be revealed, which are too dim to be observed in real time. Furthermore, quantitative data on the relative phasing of various vibrating regions, as well as their velocity and acceleration may be obtained.

Advantages of this method may be summarized as follows:

(a) Periodic vibration of any complexity may be studied in real time.

(b) The dynamics of motion may be observed directly.

(c) Any number of frequency or amplitude surveys may be made in real time using only a single hologram.

(d) The phase sense of various vibrating regions may be resolved by direct observation.

(e) A permanent film record may be made for future dynamic study, and without fatigue.

2.4 Phase Modulation of the Reference Beam (PMRB)

Different forms of beam modulation were examined for application in the analysis of surface vibrations, and two useful applications of phase modulation of the reference beam (PMRB) were found. These are in vibrational phase sensing and in vibrational sensitivity enhancement.

2.4.1 PMRB for Vibrational Phase Sensing. Phase modulation of the reference beam[1] (PMRB) has an attractive use in resolving the sign ambiguity of the vibration in a time-average interferogram, i.e., in vibrational phase sensing (VPS). Although this is also an important feature of the real-time stroboscopic interferometric system discussed in Section 2.3.3 the use of PMRB for VPS has the advantage of using the total available light from the continuous-wave laser, rather than the small fraction of this light, which remains after strobing.

It should be noted at the outset that this is a time-average method of interferometry with the fringes frozen in the hologram. As such, the interference pattern is viewable only after processing, and the method is applicable only to steady sinusoidal vibrations.

In this method, a singly exposed, time-average hologram is made of the vibrating object while the reference beam is phase modulated at the same frequency as the vibration. An optical arrangement similar to

---

[1] See, for instance, C. C. Aleksoff, "Time Average Holography Extended," Applied Phys Letters, 14, January 1, 1969, p. 23, or C. C. Aleksoff, "Modulated Reference Wave Holography," Paper WB21 Opt. Soc of of America Meeting, San Diego, California, March 1969.

Fig. 1 may be used with the addition of some means of modulating the phase of the reference beam. This may be accomplished by using a piezoelectric crystal modulator between the beam splitter and mirror M_1 in Fig. 1. The electro-optic properties of the crystal cause a change in refractive index in the direction of light transmission, which may be cycled electrically to produce the desired phase modulation. As an alternative, a vibrating mirror may be used.

When a hologram is made of a vibrating object with a phase-modulated reference beam, we now wish to find the relative amplitude of the light from some point P on the reconstructed image of the vibrating object. As before, the time averaging process stores only the carrier term of the phase-modulated light reflected from P into the hologram, but now, this phase modulation must be taken with reference to the varying phase of the reference beam.

Suppose reflected light reaches the hologram from a point P on the object, its vibration producing optical phase modulation of depth a, and phase angle α. Then the instantaneous phase of object light will be given by

$$\phi_p = a \cos(\omega t + \alpha) \tag{11}$$

where ω is the angular vibration frequency. If, in addition, the reference beam is also phase-modulated at frequency ω with depth b and phase angle β, then its instantaneous phase at the hologram will be given by

$$\phi_r = b \cos(\omega t + \beta) \tag{12}$$

Since these motions are sinusoidal, we may use the vector representation in Fig. 5. The magnitudes of the phase vectors are represented by a and b, while c is the vector difference between them. The magnitude of the vector c is the phase modulation depth of the light reflected from P, when referred to the time varying phase of the reference beam. Its value is readily found from the cosine law.

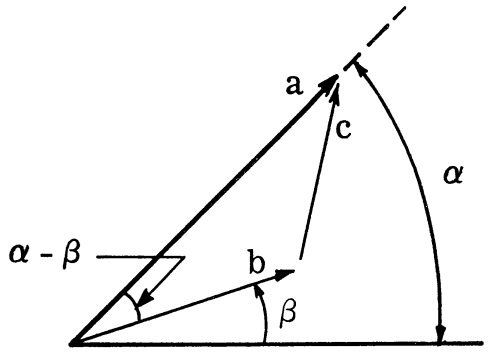

Fig. 5. Vector phase diagram

$$c^2 = a^2 + b^2 - 2ab \cos(\alpha - \beta) \tag{13}$$

In this case the vector b may be thought of as a phase bias applied to the recording characteristics of the hologram. The amplitude of the reconstructed image point P is given by replacing ϕ by c in Eq. 10

$$E_p = E_o J_o(c) \tag{14}$$

where c is given by Eq. 13.

For vibrational phase sensing (VPS) we consider the special case in which, by suitable phase adjustment of the reference beam modulator, we obtain

$$\alpha - \beta = 0 \tag{15}$$

Then the vibration of the object point P is in phase with the reference modulation, and Eq. 13 reduces to

$$c = a - b \tag{16}$$

A plot of Eq. 14 is shown in Fig. 6. Here we illustrate that with no phase bias, (b = 0), an object phase modulation of +a gives the light vector amplitude of E_1, while an object phase modulation of -a gives the equal valued E_2. Since these amplitudes are equal, there is nothing to distinguish them apart.

In the presence of a reference beam phase modulation of b radians, the corresponding relative phase modulations would be (-b + a) giving a vector amplitude E_4, and (-b - a) giving a vector amplitude E_5. The considerably smaller value of E_5 makes it easy to distinguish between these two situations and hence between two vibration regions of opposite phase. In this manner, phase ambiguity of the vibration may be resolved in a time-average interferogram.

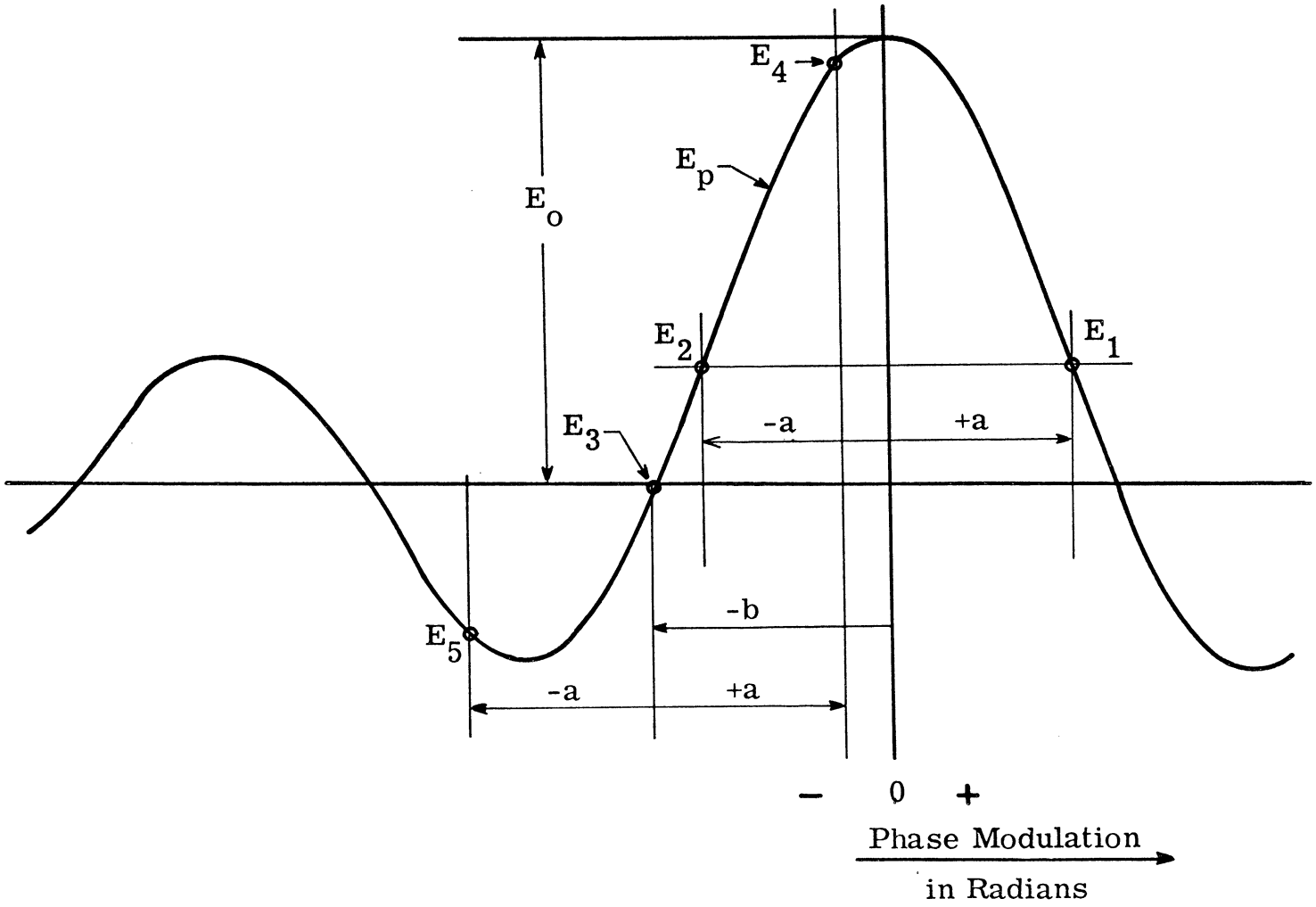

Fig. 6. Variation of time-average electric field vector with phase modulation

Note that in this example, relatively small values of phase modulation are used to simplify the explanation. In general, it may be necessary to make two or more time-average holograms, one being without bias, for positive identification.

2.4.2 PMRB for Vibrational Sensitivity Enhancement. In Fig. 6 the particular value of reference beam modulation shown is $b = 2.405$ radians. This is the value giving $E_3 = 0$ or zero light in unmodulated regions of the virtual image. In this case all vibrational nodes would record dark, and in fact, with no vibration of the object, the entire image would be dark, producing the so-called null hologram.

In this case we have a potential method of enhancing the vibrational sensitivity since very small object vibrations will produce departures from the point E_3, which can easily be detected. For maximum sensitivity enhancement, the beam modulation should be in phase with the vibration to be sensed, and the depth of modulation should be adjusted as close to 2.405 radians as possible.

This method of vibrational sensitivity enhancement, in a time-average interference hologram, is termed the phase bias method, as distinct from the amplitude bias method discussed in Section 2.2. It has the advantages that all critical adjustments may be made in advance, that only one exposure is required, and that the sensitivity enhancement is greater than in the amplitude bias method.

As a final observation, it is possible to achieve identical results both in vibrational phase sensing and in phase-bias-sensitivity enhancement by phase modulating the subject-illuminating beam instead of the reference beam.

2.5 Underwater Interferometry of Vibrating Objects

Underwater interferometry may be performed much the same as air interferometry. A convenient arrangement is shown in Fig. 7. Here the vibrating object is placed on a rigid mounting inside a water tank containing a window which permits entry and exit of the object beam. The chief difference in underwater interferometry is that a portion of the object beam optical path is in water with a refractive index ($n = 1.333$) which differs from air. The consequences of this fall into two categories, (a) static effects and (b) dynamic effects.

2.5.1 Static Effects. For satisfactory holography, the total path lengths of the reference beam and the object beam must not differ by more than the axial coherence length of the laser. This is approximately 20 cm for the Model 125 Spectra-Physics laser. When one of the paths is partly in water, its equivalent air path length must be computed. This is done by merely multiplying the water path section by n, the refractive index for water. The criterion is now applied to the equivalent air path of the object beam.

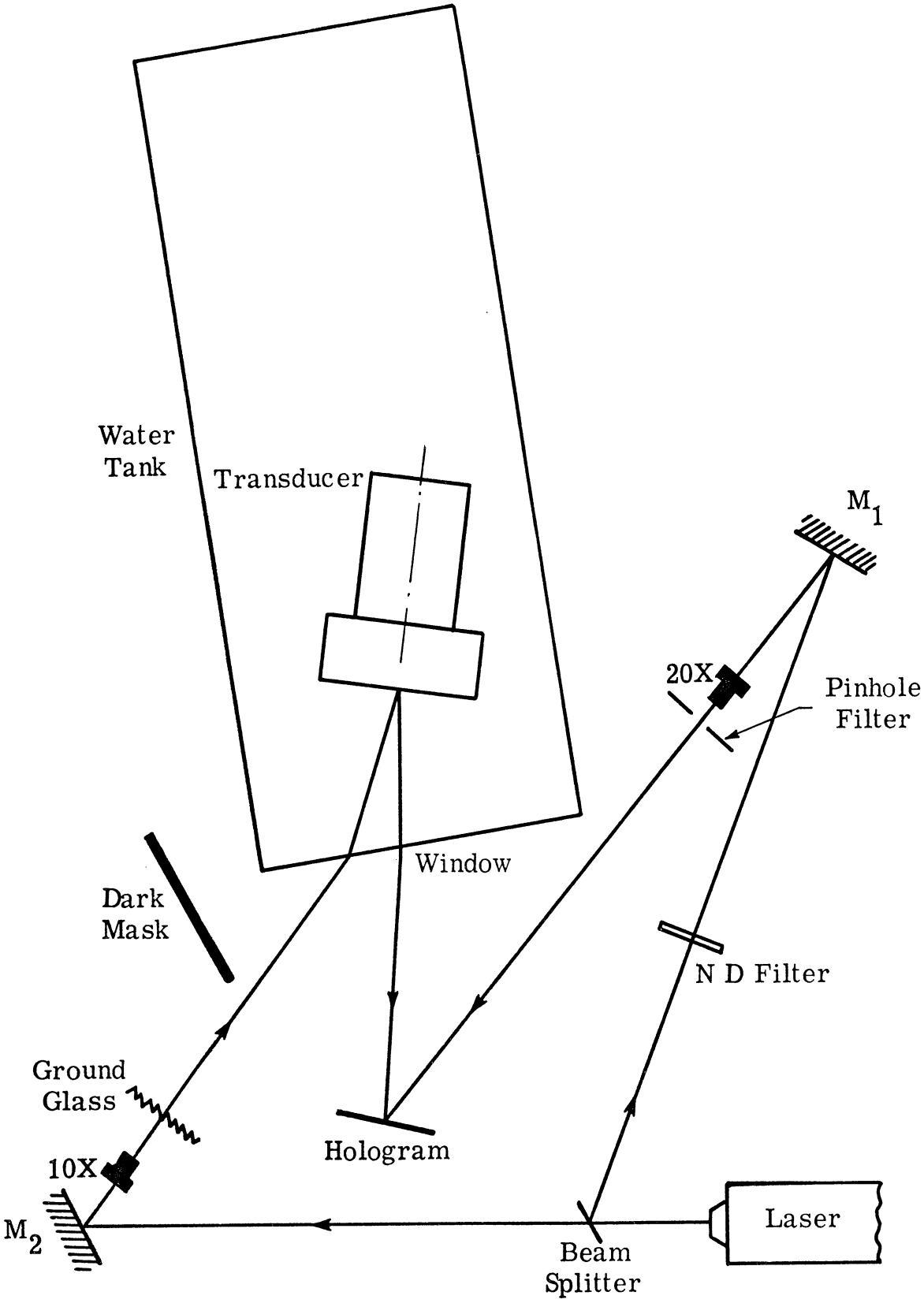

Fig. 7. Arrangement of apparatus for underwater interferometry

A second consequence of the water is the reduced coherence depth of a scene which may be registered in the hologram. If this depth is 20 cm in air, it is reduced in water by the factor $1/n$, i.e., to 15 cm.

As in air interferometry, stability of all optical components is required for satisfactory results. This requires attention in design and assembly to guarantee the ruggedness of the tank window and object mounting system. In addition, it requires freedom from variation of tank and water temperature during the exposure. After assembly, the tank and object must be allowed a suitable settling time of several hours or preferably a day prior to making holograms.

2.5.2 Dynamic Effects. The three important dynamic effects which are different in underwater interferometry, are the increase in vibration sensitivity and the undesired effects due to window vibration and due to acoustic modulation of the refractive index of the water.

The vibration sensitivity in underwater interferometry increases by a factor equal to the refractive index, n. It was seen in Section 2.2 that the first dark fringe in a time average interferogram represents a vibration amplitude of $\pm 0.191\lambda$. This is ± 4.768 microinches in air for $\lambda = 632.8$ nm. In water this is reduced to ± 3.576 microinches due to the reduced wavelength in the water medium.

Vibration of the glass window may cause problems in underwater interferometry, particularly in sonar transducer studies. This may be caused either by the object under study or by some outside influence.

A window vibration in which the front and back surface of the glass move together by an amount x toward the hologram will thus produce an increase of x in the water path (equivalent to nx in air) and at the same time reduce the air path by x. The combined effect is an increase in equivalent air path of $(n-1)x$. This change in equivalent air path produces a phase modulation of the object beam.

The phase modulation due to a window vibration of amplitude x is about one-fourth as great $[(n-1)/n]$ as that due to an object in water vibrating with amplitude x. This phase modulation will add vectorially to that of the vibrating object seen through the vibrating window, and the interferogram may be difficult to interpret unless window vibrations remain less than 2 or 3 microinches.

A satisfactory method of measuring the window vibrations is to temporarily apply a diffusing coat of dulling spray to the window. When this has dried, hologram interferometry of the diffusely reflecting window reveals any existing vibration distribution.

A vitally important feature of underwater interferometry is the modulation of the refractive index of the water due to pressure waves. In the region between the object and the window, water index variations can produce phase modulation of the object beam both on its path toward the object, and on its return path to the hologram.

An elementary example illustrates the magnitude of the effect. Consider the following problem: How many waves of laser light

(λ_{air} = 633 nm) are added per meter path length when the water pressure is raised one atmosphere?

The value of the pressure coefficient for the refractive index of water, dn/dP, is 14.8×10^{-6} per atmosphere (14.8×10^{-11} m^2/N), as given by Rosen,[1] for water at 25°C and λ_{air} = 579 nm. The number of waves per meter in water at one atmosphere is given by

$$N_1 = n/\lambda_{air} \tag{17}$$

At 2 atmospheres it is given by

$$N_2 = (n + dn/dP) / \lambda_{air} \tag{18}$$

And the difference is

$$N_2 - N_1 = \frac{dn}{dP} \cdot \frac{1}{\lambda_{air}} \tag{19}$$

$$= 14.8 \times 10^{-6} / .633 \times 10^{-6}$$

$$= 23.4 \text{ waves per meter (per atmosphere)} \tag{20a}$$

$$= 1 \text{ wave per } 4.28 \text{ cm} \tag{20b}$$

---

[1] Joseph S. Rosen, "The Refractive Index of Alcohol, Water and their Mixtures at High Pressures," J. Opt. Soc. Am., 37, November 1947, p. 932. (The variation in pressure coefficient between λ_{air} = 579 nm and λ_{air} = 633 nm is insignificant in this approximate calculation.)

This example illustrates the important point that a dynamic pressure change of one atmosphere averaged over a path length of only 4.28 cm can cause an optical phase modulation of 2π radians.

A practical example is the interferometric study of a sonar transducer at 20 kHz. Suppose that between the transducer and the window, there is a well-developed standing wave pattern. A laser beam traversing the length of this pattern in one direction would experience no phase modulation for an even number of standing waves because the alternating sign of successive pressure waves cancels the index modulation. For an odd number, the beam would be phase modulated. The modulation depth would depend on the length L and the mean acoustic pressure $\overline{P}$ of the uncancelled half-wave section.

The mean acoustic pressure $\overline{P}$ averaged over the distance L cannot exceed $\frac{2}{\pi} P_{max}$ for a sinusoidal distribution, thus, $\overline{P} \leq \frac{2}{\pi} P_{max}$. These considerations give an optical modulation depth of

$$\phi_{max} = 2\pi \frac{dn}{dP} \cdot \frac{1}{\lambda_{air}} \cdot L \cdot \overline{P} \quad \text{radians} \tag{21}$$

$$\leq 4 \frac{dn}{dP} \cdot \frac{1}{\lambda_{air}} \cdot L \cdot P_{max} \quad \text{radians} \tag{22}$$

where P_{max} is the peak pressure of the acoustic wave. Taking $c = 1500$ m/sec as the velocity of sound in water at 25°C, the acoustic half-wavelength at 20 kHz is $L = 3.75 \times 10^{-2}$ m and for $\lambda_{air} = 633$ nm, Eq. 22 becomes

$$\phi_{max} \leq 3.51\ P_{max} \quad \text{radians} \tag{23}$$

for P_{max} expressed in atmospheres. And in a worst case for light traversing the standing-wave region in both directions, which is the more common situation, we obtain double the phase modulation depth, i.e.,

$$\phi_{max} \leq 7.02\ P_{max} \quad \text{radians} \tag{24}$$

This situation can cause serious concern for even modest acoustic pressures. At an acoustic peak-pressure of 1/3 atmosphere, we can see from Eq. 24 that ϕ_{max} may approach the value 2.4 radians which will produce the first dark fringe in a time-average interferogram.

Concern for this pressure modulation phenomenon is not limited to acoustical standing-wave fields. It is equally applicable to interferometry through an uncancelled acoustic half-wave path in a traveling-wave field. Consider the acoustic relationship for plane waves[1]

$$P = A \cdot 2\pi f \rho_o c \tag{25}$$

where

P = peak acoustic pressure, N/m^2

A = peak displacement amplitude, m . (as for a transducer face)

---

[1]Kinsler and Frey, Fundamentals of Acoustics, 2nd. Ed., John Wiley and Sons, New York, 1962, Ch. 5, p. 121.

f = frequency, Hz

ρ_o = density of water (1×10^3 kg/m^3 at 25^o C)

c = velocity of sound in water (1.5×10^3 m/sec at 25^o C)

and for L = one-half wavelength of sound in water

$$L = c/2f \tag{26}$$

Substituting Eqs. 25 and 26 into Eq. 22 yields

$$\phi_{max} \leq \frac{4\pi}{\lambda_{air}} \cdot \frac{dn}{dP} \rho_o c^2 A \tag{27}$$

This expression represents the optical phase modulation due to pressure modulation with normal viewing of a transducer face-operating in the regime of unity radiation impedance. The optical phase modulation expected due to the displacement amplitude only of the transducer face in water is

$$\phi_{displacement} = \frac{4\pi n}{\lambda_{air}} \cdot A \tag{28}$$

Taking the ratio of Eq. 27 to Eq. 28, we obtain a modulation magnitude ratio R_{mod}

$$R_{mod} = \frac{\phi_{max(pressure\ modulation)}}{\phi_{(displacement\ modulation)}} \leq \frac{dn}{dP} \frac{\rho_o c^2}{n} \tag{29}$$

an expression which contains only parameters of the fluid medium.

Substituting numbers appropriate to water

$$R_{mod} \leq 0.25 \tag{30}$$

or if the optical path traverses the uncancelled pressure region twice

$$R_{mod} \leq 0.50 \tag{31}$$

Clearly, when examining transducer motion underwater, the pressure modulation can be of consequence. For free-field acoustic conditions, the two modulations will have a quadrature temporal relationship that must be taken into account for a more specific analysis.

The example above does not necessarily represent an extreme upper limit. In a standing-wave field, the peak pressure can be larger than for the plane-wave relationship which was assumed. Also, the optical paths may be at an angle to the acoustical wavefronts and thus traverse longer pressure-modulated paths than assumed in the calculations. Perhaps this pressure modulation phenomenon could be utilized to visualize the wave fields themselves by some rearrangement of the holographic apparatus.

These pressure modulation effects can produce serious ambiguities in the interpretation of sonar transducer interferograms. Several examples are shown and discussed in Section 4.3.

3. INTERFEROMETRIC STUDIES OF A LARGE TORPEDO SECTION

3.1 Introduction

The purpose of this development is to demonstrate the quality and spatial depth of interferograms made on a full-size torpedo section, 21 inches in diameter and 32 inches long, using a conventional laser. The limited axial coherence length of many CW gas lasers places a constraint on the depth of the scene which can be recorded in a reflection hologram. The Spectra-Physics Model 125 laser used in our experiments had an axial coherence length of approximately 20 cm.

The coherence requirements for making holograms are satisfied if the subject (or as much of it as possible) is placed within the coherence volume of the holographic arrangement. For subject illumination diverging from a source point A, the coherence volume is an ellipsoidal shell having a radial depth L, which approximates the coherence length. See Figure 8. The shell boundaries are two ellipsoids of revolution, E_1 and E_2, with common foci A and B. The point B represents the center of the hologram plate. The dotted circle represents the optimum position for the cylindrical torpedo section. Its radius, 10.5 inches, is greater than dimension L by approximately 2.5 inches, so that slightly less than half the cylinder can be recorded in the hologram.

At the time of this development it was realized that a number of techniques were available for extending the scene depth of a hologram.

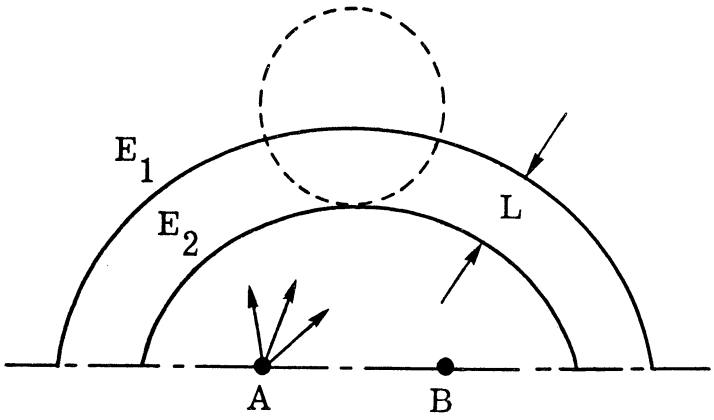

Fig. 8. The coherence volume

These techniques include (a) backlighting, (b) multiple subject-beam illumination, (c) warping the shape of the coherence volume by special optics, and (d) increasing the coherence length of the laser. Of these methods, (c) and (d) are particularly applicable to interferometry. However it was the purpose of these tests to demonstrate the quality and coverage of interferograms of large objects made without recourse to such techniques. And with due consideration of the noted limitations, a moderate degree of success may be claimed for our results.

3.2 Optical Arrangement

A plan view of the optical arrangement used for large-cylinder interferograms is shown in Fig. 9. The length of the subject beam from beam splitter to plate is 97.0 inches for the nearest point of the cylinder. This is 7.5 inches shorter than the corresponding reference beam path length of 104.5 inches. When this difference was increased to 8.0 inches,

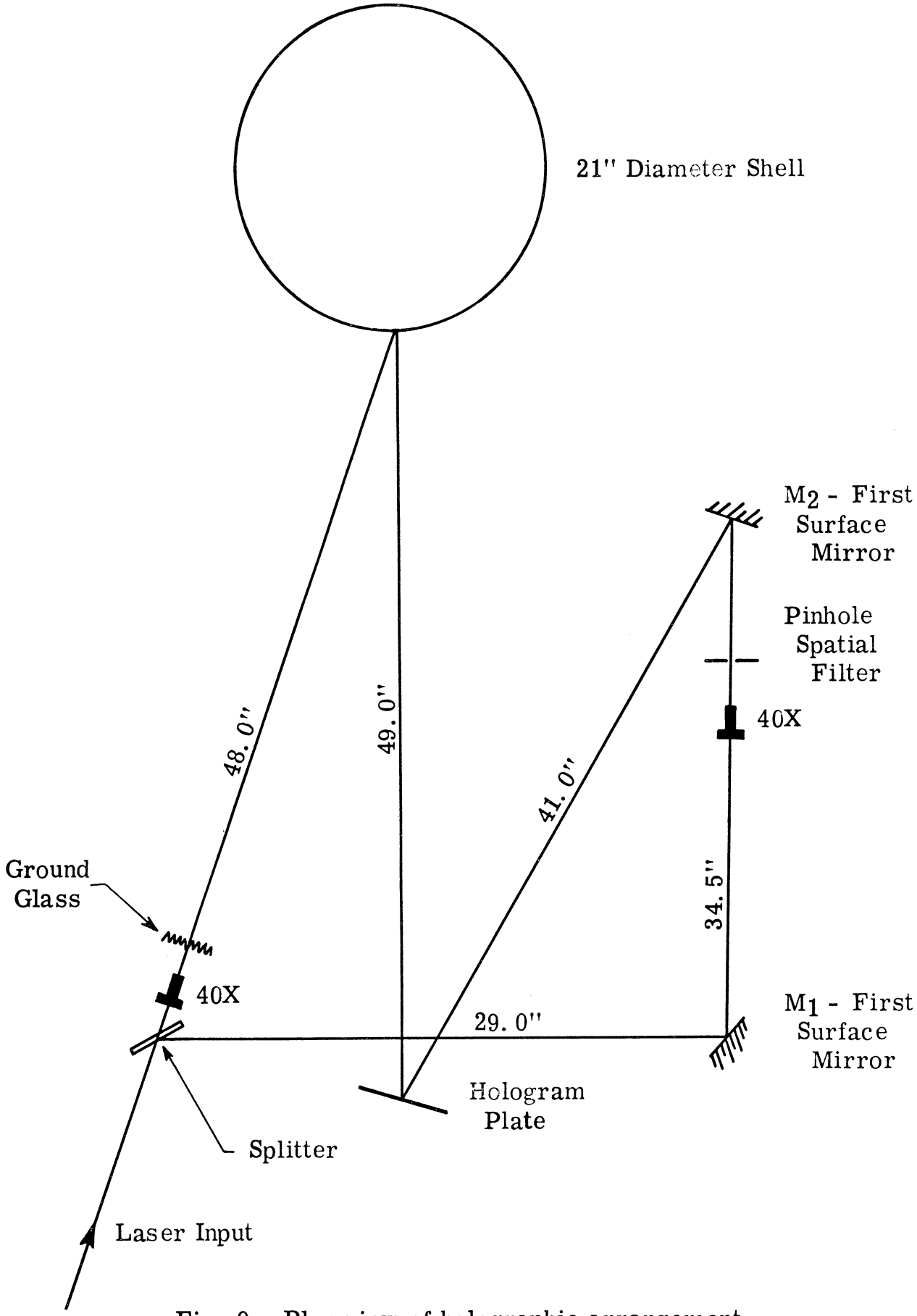

Fig. 9. Plan view of holographic arrangement

we judged that there was too great a loss in intensity in the reconstructed image for good interferometry. The farthest boundary of the coherence volume in this case is approximately 7.5 inches farther back than the nearest point on the cylinder.

Two views of the setup are shown in Figs. 10a and 10b. All components except the laser are supported on the large slab of granite. A magnetic driver was used for vibrating the large cylinder. It may be seen at the left side of the cylinder in Fig. 10a.

In Fig. 10b the hologram plate holder is seen in the center foreground supported by two granite parallel blocks. The cylinder is seen in the central background, while beam splitter, 40X expander and ground-glass screen are shown at the left.

3.3 Mechanical Stability

Providing sufficient mechanical stability for satisfactory interferograms of the large torpedo section was a difficult task. After several other mounting arrangements had failed, the cylinder section was finally supported by three half-rounds of brass. These made three radial line contacts with the lower edge of the cylinder on their rounded surfaces. The machined flat surfaces were turned down against the granite slab. The stability of the cylinder appeared sensitive to its position on the granite slab. Ultimately an optimum position was located, but even with the best arrangement, there were certain times when a slight disturbance

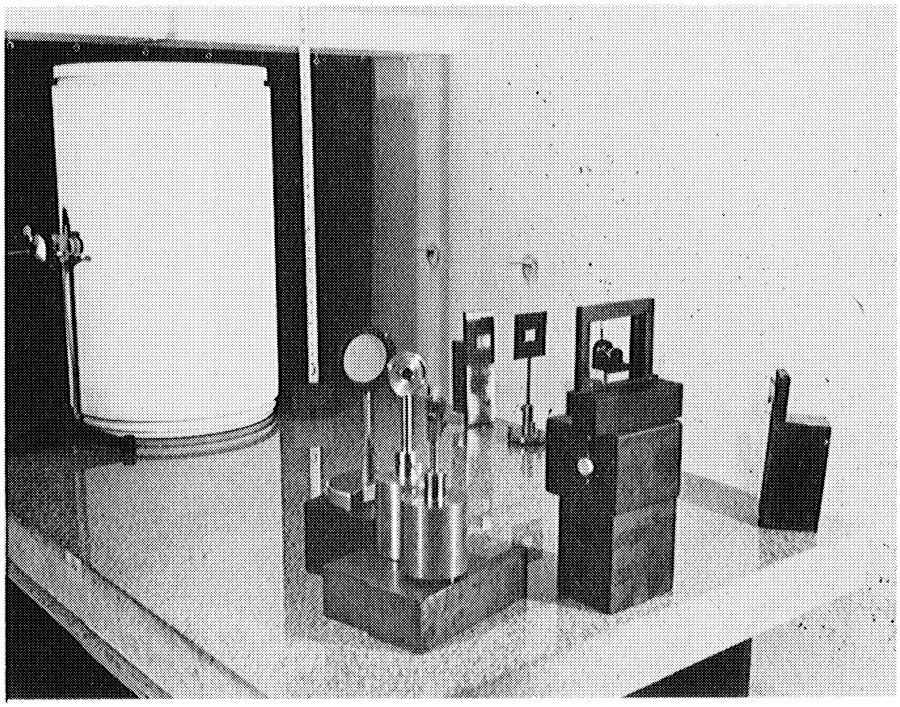

(a)

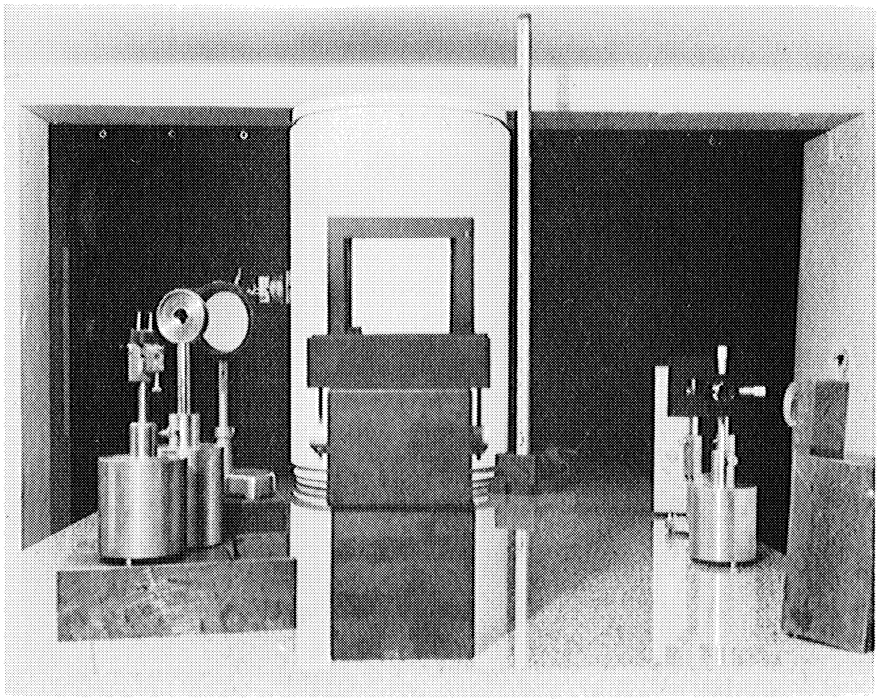

(b)

Fig. 10. Two views of the hologram setup

would spoil the hologram. The massiveness and large size of the torpedo section appeared to aggravate the problem.

This problem was somewhat relieved by making as short a hologram exposure as possible. By the use of the faster Agfa 10E70 emulsion, and by light conservation measures, the hologram exposure was cut down to 2.0 seconds, an unusually short exposure for such a large object.

3.4 Results

A hologram of the torpedo section was made without vibration, and its reconstructed image is shown in Fig. 11. The barrel-shaped appearance of the illuminated area was anticipated, and is a consequence of the outer boundary of the ellipsoidal coherence volume cutting off a portion of the cylinder which is slightly narrower at the top and bottom than in the middle. The slightly darkened central region in Fig. 11 is due to the nearest portion of the cylinder approaching the inner boundary of the coherence volume.

Time-average interferograms were made of the torpedo section when driven into resonance by the magnetic driver. In these interferograms the reader is reminded that dark fringes depict contours of constant projected[1] vibration amplitude. Typical results are shown for selected resonance conditions by the reconstructions in Figs. 12 through 18.

---

[1] Projected on the sensitivity vector.

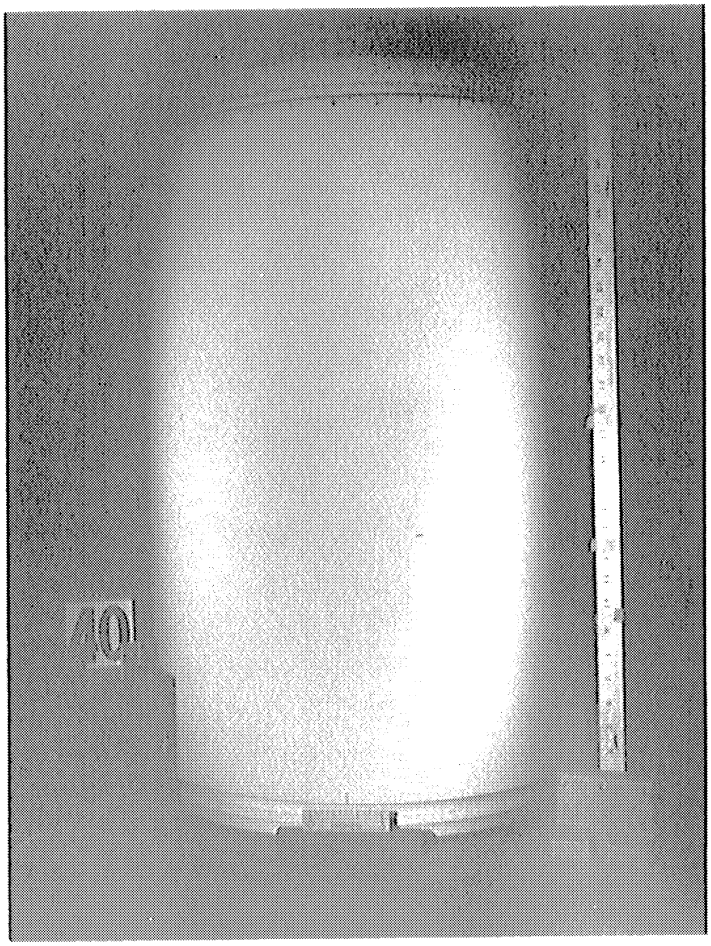

Fig. 11. Hologram reconstruction of torpedo section--no vibration

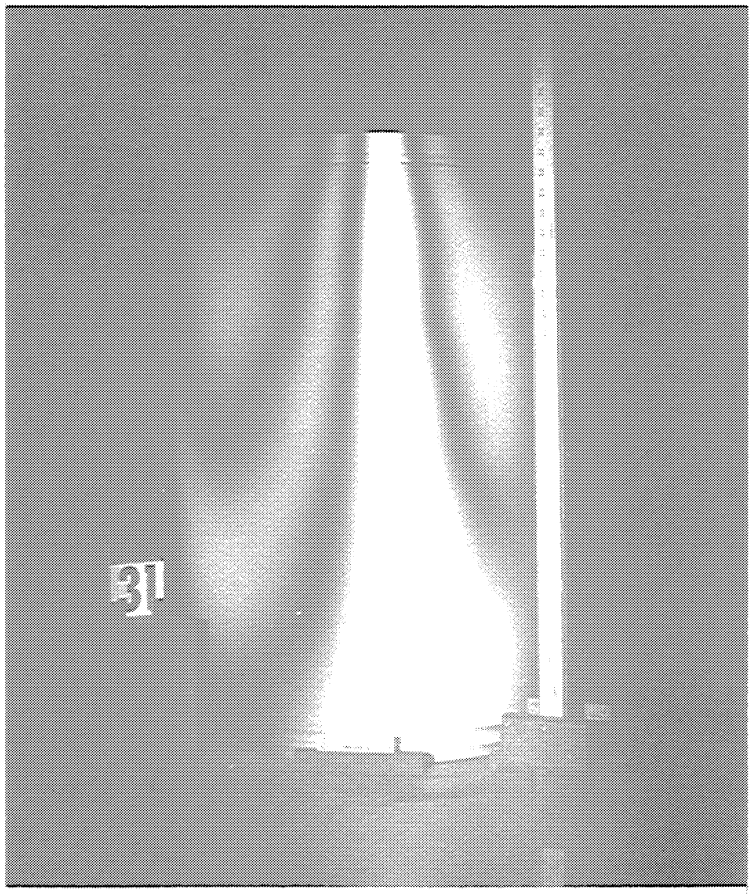

Fig. 12. Resonant response at f_r = 387.73 Hz

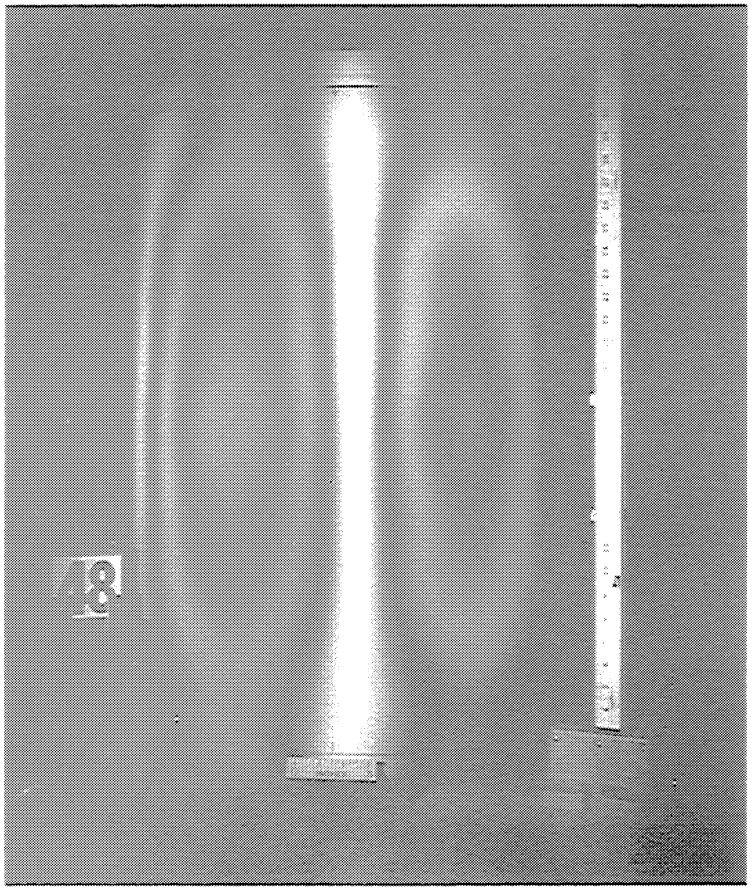

Fig. 13. Resonant response at f_r = 483.44 Hz

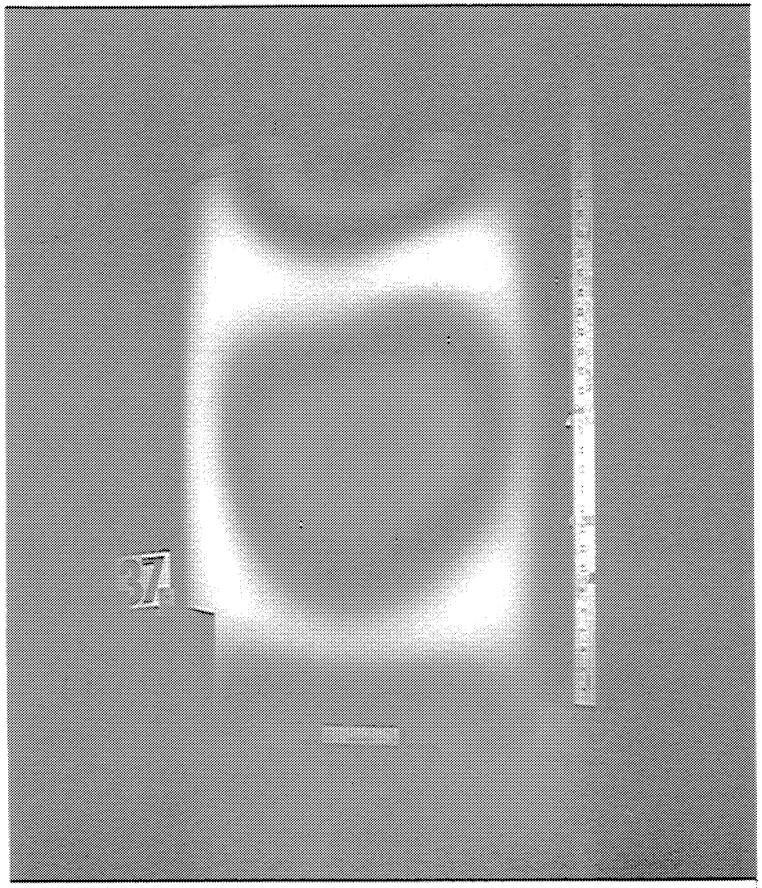

Fig. 14. Resonant response at f_r = 984.59 Hz

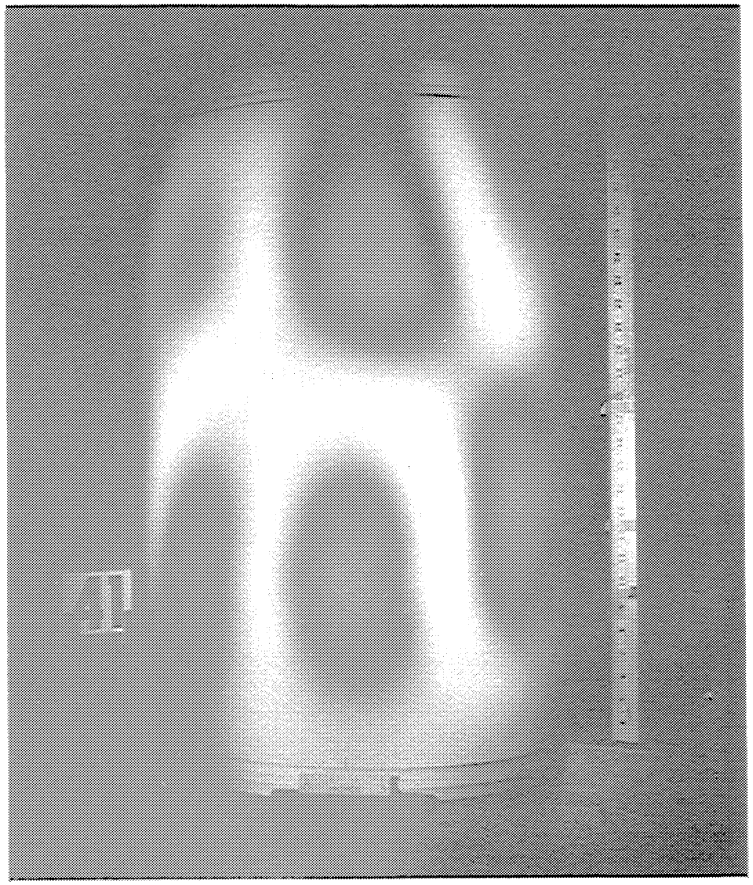

Fig. 15. Resonant response at f_r = 1099.7 Hz

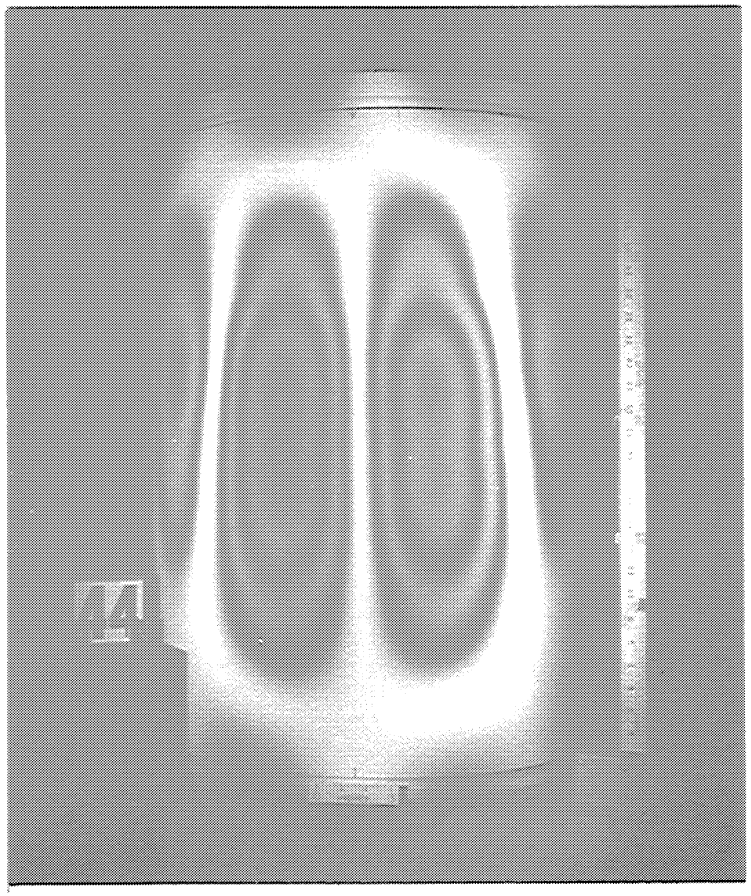

Fig. 16. Resonant response at f_r = 1263.4 Hz

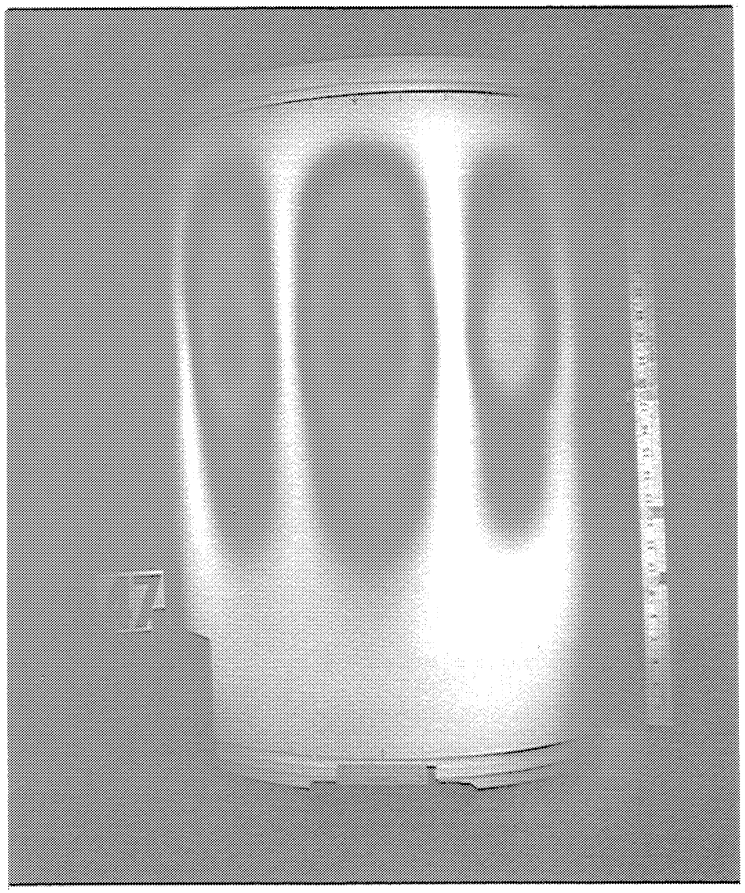

Fig. 17. Resonant response at f_r = 1317.3 Hz

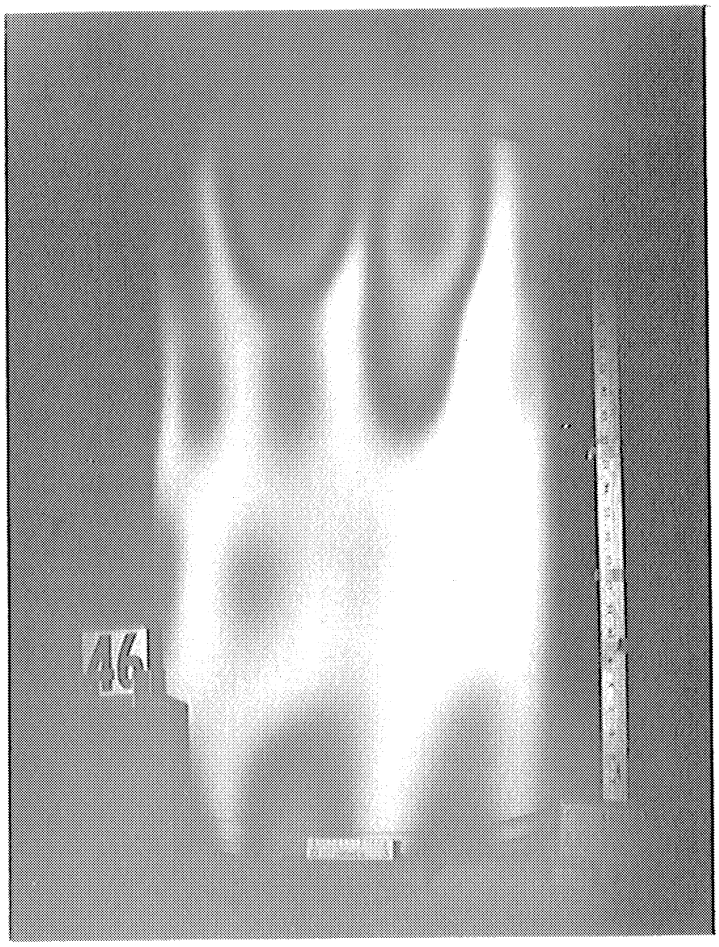

Fig. 18. Resonant response at $f_r = 1547.6$ Hz

These interferograms, arranged in order of increasing resonant response frequency, f_r, show a variety of vibration distributions.

Figure 12, for the lowest frequency resonance at $f_r = 387.7$ Hz shows a distribution pattern resembling an inverted bell type of response, with the vibration amplitude increasing toward the top. The slight irregularities in the otherwise uniform fringe just to the right of center are believed due to the ribbed structure on the interior of the torpedo section.

Figure 13, for $f_r = 483.4$ Hz, was the strongest resonance for this particular method of mounting and excitation. The driver voltage used here was only 37 percent of that used in Fig. 12, yet a well-developed pattern resulted. The pattern is almost exactly symmetric, with motion extending to both the cylinder ends. Here again there are suggestions of slight fringe irregularities indicative of the ribbed inner structure.

Figure 14 shows a resonant mode at $f_r = 984.6$ Hz having three well-developed antinodes arranged vertically. The heart-shaped central antinode is not as strongly developed as the one above it on the upper rim. This mode was difficult to excite. In making the hologram the drive voltage here was nine times as great as that in Fig. 13.

Figures 13, 14 and 18 show evidence of considerable motion at the bottom end of the cylinder. It is uncommon to find this distribution when the bottom end is used for support. Examples of irregular vibration distributions are shown in Figs. 15 and 18. These represent considerable

departures from any regular pattern. Such irregularities are fairly typical of complex structures at certain frequencies, and usually are revealed at the higher frequencies, where higher order resonances abound.

The more regular distributions shown in Figs. 16 and 17 illustrate that not all high frequency resonances are irregular. Although these two patterns have similarities, Fig. 17 is unique in that there is no evidence of any vibration at the free upper rim of the cylindrical shell.

In this investigation the primary purpose was to demonstrate the potential of a technique, rather than make a detailed analysis of the torpedo section. The reconstructed patterns do show considerable detail, although in some cases not to the extreme edges of the cylinder. We therefore conclude that much can be done with large-object interferometry even with lasers of limited axial coherence.

4. TRANSDUCER STUDIES

The goal of these studies was to observe interferometrically the distribution of displacement amplitudes over the face of a transducer operating in water. For this purpose, the transducer was immersed in a water-filled, glass-walled aquarium. Two transducers were studied. The first was a 2 by 2 array which operated in the vicinity of 30 kHz and, as furnished, was filled with air. This transducer subsequently became erratic and was returned to ORL. A second 2 by 2 array transducer was supplied to permit these studies to continue. The second unit was slightly larger than the first. Also, it was liquid-filled and operated in the vicinity of 20 kHz.

The first transducer was immersed in water after only a cursory test in air. Later, because of a suspected leak into its case and because of questions about interpretation of certain results in water, a more complete study was undertaken in air. The case was opened to gain access to the electrical connections to the individual elements of the array and various reconnections were utilized during the ensuing air studies. This transducer developed an erratic electrical behavior before further tests could be undertaken in water.

The second transducer was studied in air before it was immersed in water. This transducer was sealed so that all experiments, both in air and in water, had to be performed with all four elements excited according to permanent internal electrical connections.

The following subsections describe our observations in air and in water on both transducers. Chronological order has not been followed rigorously in these descriptions. Additional observations are related which, although peripheral to the mainstream of the transducer studies, have experimental significance.

4.1 First Transducer Operating in Air

The apparatus was arranged as shown previously in Fig. 7. Before filling the aquarium with water for the first time, some holograms were made to verify the mechanical stability of the setup and to determine an illumination suitable for rendering the flat-black rubber face of the transducer. Among these were three time-average interferograms taken in the vicinity of the transducer's resonance in air near 34 kHz at 40 Vac drive. These interferograms served their original purpose but they later assumed additional importance by providing a limited record of behavior in air before this transducer was immersed in water. The flat-black rubber faces of both transducers were found to be non-depolarizing both in air and in water.

The first transducer was studied in air after it had been removed from the water because of a suspected leak. The case was opened, the electrical leads to the individual elements were separated, and the accumulated moisture was dried by circulating air through the case. Then a related series of experiments were undertaken.

4.1.1 Behavior of Individual Elements. The first tests involved exciting each element independently. Figure 19 gives the details of the excitation and monitoring electronic instrumentation. A high-impedance ac voltmeter, connected in shunt across the element under investigation, showed a slight dip in reading near 34.6 kHz. In addition, the method of real-time fringes was used to identify the frequency setting which produced a maximum mechanical response for each element. The tuning was broad and a mean value of about 34.6 kHz was found. It was used for most of the subsequent experiments in air. The interferograms were obtained with a conventional arrangement of the holography apparatus like that shown in Fig. 1.

Figure 20 shows the time-average motional response produced by a 16 Vac sinusoidal driving signal. The inserted sketch gives the identification which we assigned to the individual elements. The sensitivity vector was positioned to be normal to the transducer's face. The vibratory displacement was assumed to be essentially normal to the rubber face. Definitive verification was not obtained but, on the other hand, none of the interferograms produced any hint of major displacements in other directions. Under the assumption, the fringes can be simply interpreted. They represent contours of equal amplitude of displacement where the first dark fringe corresponds to about 5×10^{-6} inch single peak displacement and each additional dark fringe represents an increment of about 6×10^{-6} inch.

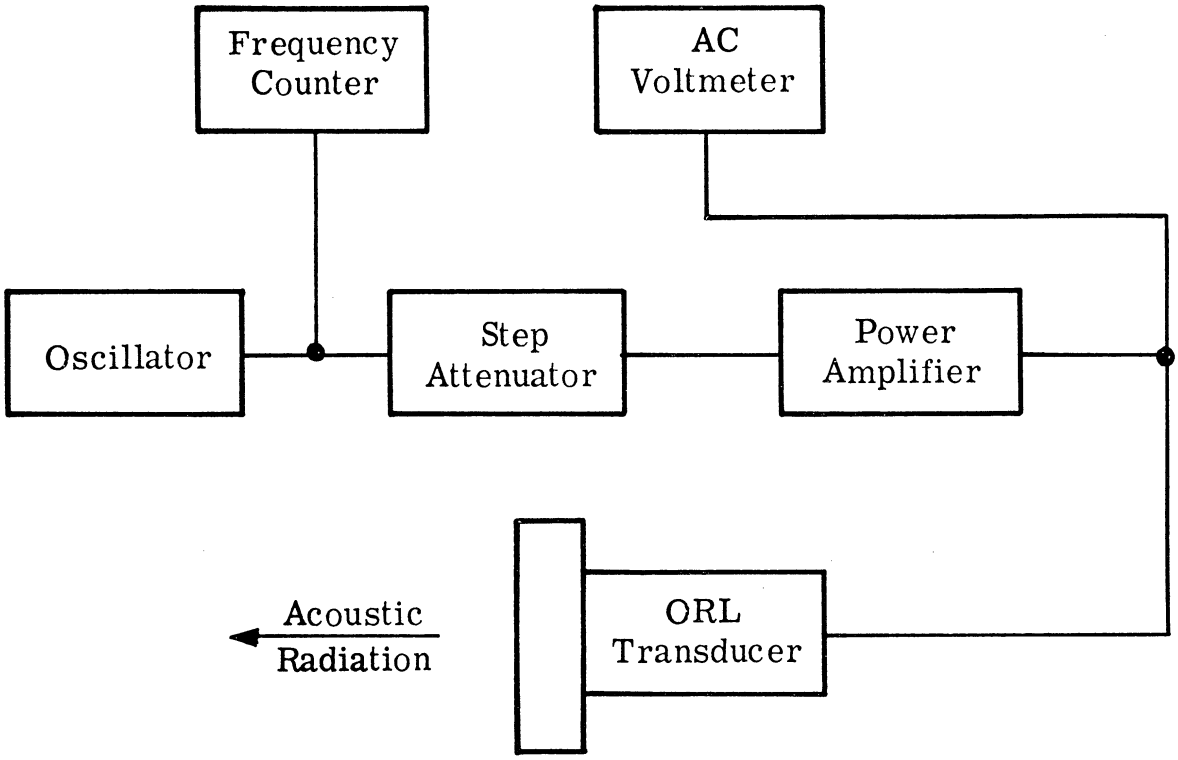

Frequency Counter: Hewlett Packard Model 5216A Electronic Counter

AC Voltmeter: Hewlett Packard Model 3400A RMS Voltmeter

Oscillator: Hewlett Packard Model 203A Variable Phase Function Generator (sinusoidal output was used)

Step Attenuator: Daven Type VT-790G Attenuation Network (110 dB by 1 dB steps)

Power Amplifier: McIntosh MC-225 Power Amplifier (used one side connected for single ended output at nominal 200 ohms output impedance)

Fig. 19. Diagram of excitation and monitoring system

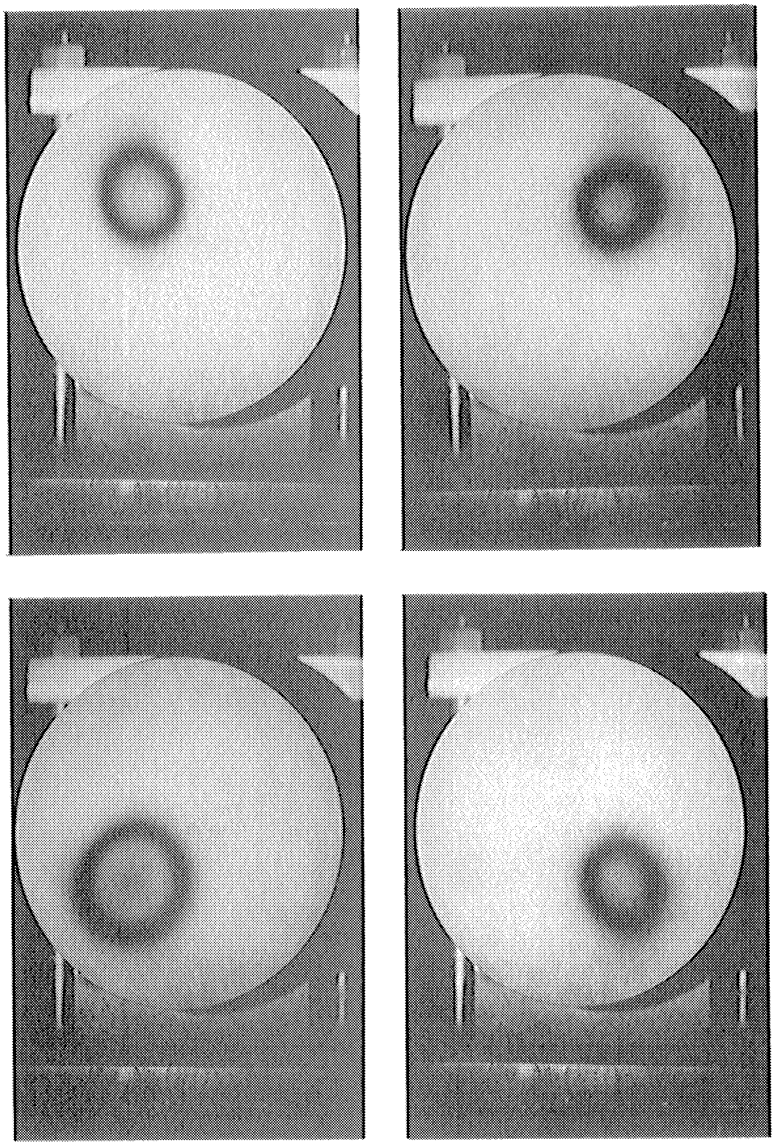

Element Identification

Fig. 20. Response uniformity of individual transducer elements operated in air at 34.600 kHz and 16.0 Vac

In Figure 20, we can see that elements A, C and D responded in almost identical fashion; i.e., their respective fringe patterns were nearly the same size and shape. The light gray centers of these patterns indicate motion corresponding approximately to the second maximum of the J_o^2 function representing a single-peak displacement of about 8×10^{-6} inch. This deduction has been further verified by the use of the time-average interferogram to form real-time fringes as described in Section 4.4.2. Clearly, element B produced a larger response; its pattern is larger and the center of the pattern has started to darken again implying a displacement amplitude approaching that for a second dark fringe or roughly 11×10^{-6} inch single-peak displacement. Thus, in this experiment, element B exhibited roughly 25 percent larger displacement amplitude than elements A, C and D. All of the fringe contours in Fig. 20 look slightly elliptical with the major axis of each pattern oriented in a radial direction.

During trials at tuning each element for maximum amplitude response, judged from the blurring of real-time fringes, it appeared that element C peaked closer to 34.2 kHz than 34.6 kHz and that element B peaked about 34.8 kHz. Elements A and D appeared to peak at 34.6 kHz. Figure 21 relates to a further investigation of the above observations. The interferograms demonstrate a remarkable lack of sensitivity to small changes in driving frequency. The pattern for element C is just detectably larger at 34.2 kHz than at 34.6 kHz while

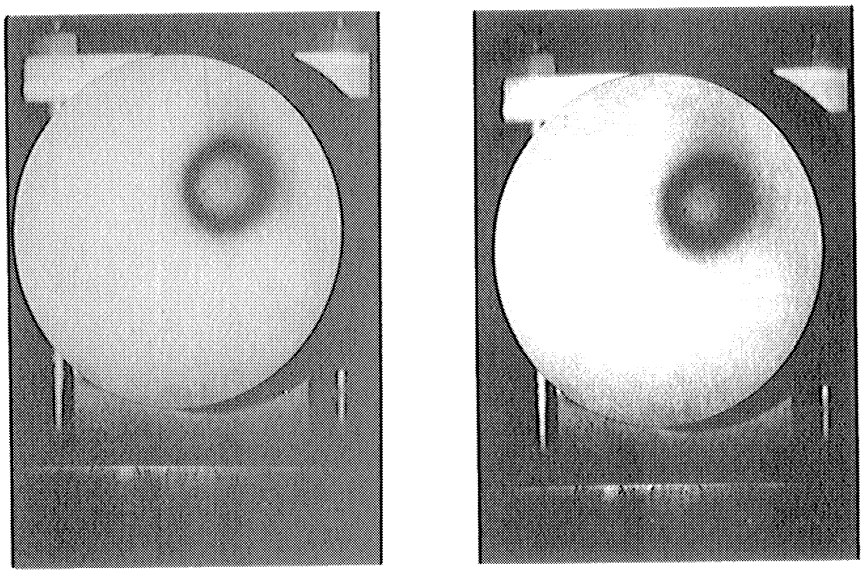

34.201 kHz 34.600 kHz

Element C operating in air at 16.0 Vac

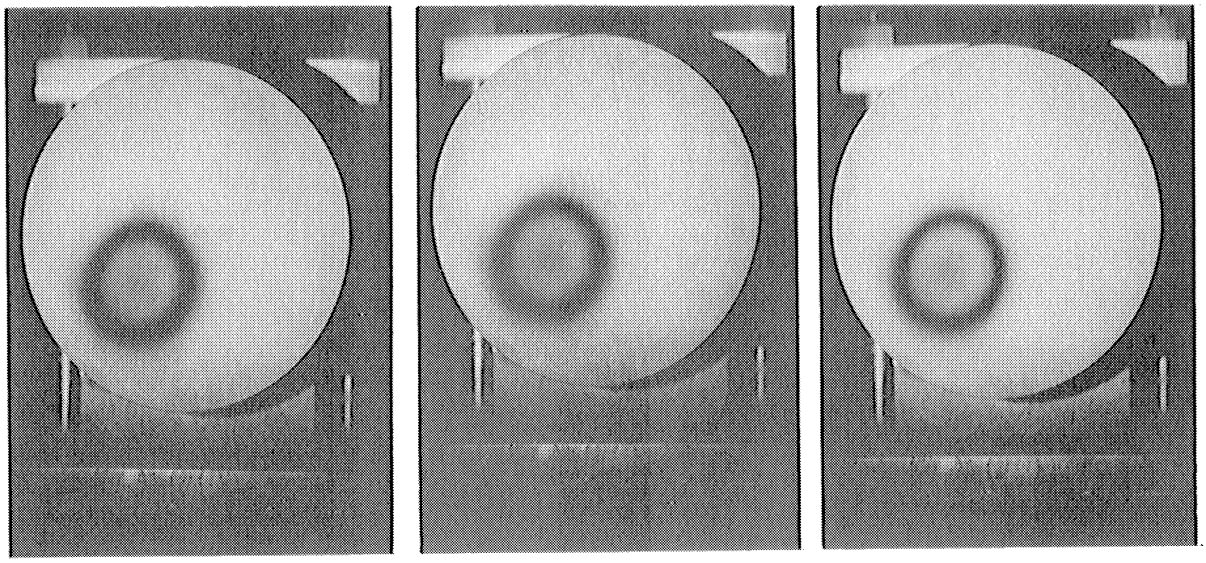

34.401 kHz 34.600 kHz 34.799 kHz

Element B operating in air at 16.0 Vac

Fig. 21. Sensitivity of response to small changes in frequency

element D responded with essentially equal amplitude across the range tested. We concluded that a single excitation frequency of 34.600 kHz would be satisfactory for experiments in air.

4.1.2 Behavior of Pairs of Elements. The next experiments involved exciting pairs of elements, both in phase and counter-phased. Figure 22 shows the results. Recall that ordinary time-average interferograms can not resolve ambiguities in temporal phase relationships of the mechanical displacements. However, the gross effects of in-phase and counter-phase electrical connection of pairs of elements are discernible by the form of the corresponding time-average patterns. The counter-phased condition reveals an enforced optical nodal line between the participating elements. We feel justified in the assumption that the particle displacement on the rubber surface was sufficiently rectilinear and normal so that the simplest interpretation suffices.

There are several features about Fig. 22 which are difficult to present because detailed comparisons among several interferograms are involved. The surface displacement of the rubber is suppressed by the counter-phase operation. The fringe patterns are displaced away from one another in the region between elements while the outer parts of the pattern correspond closely to contours for those same elements operated individually. The maximum displacements have remained essentially equal to the displacements obtained when the elements were operated individually for the case of diagonal pairs of elements.

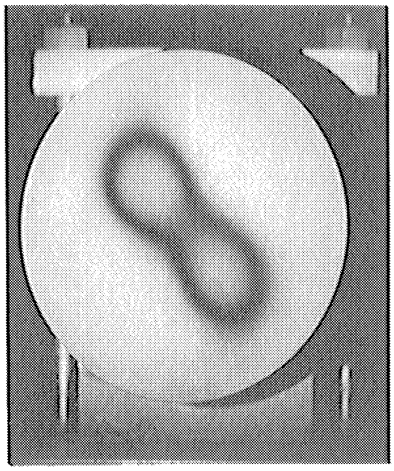

Elements A & D

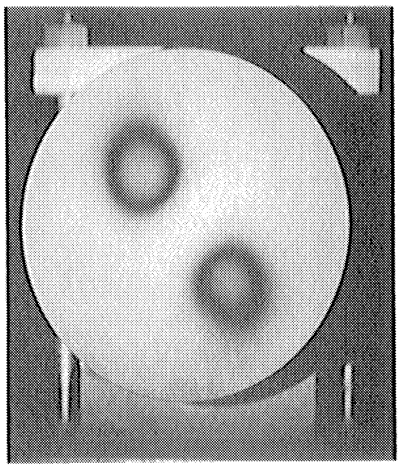

Elements A & D

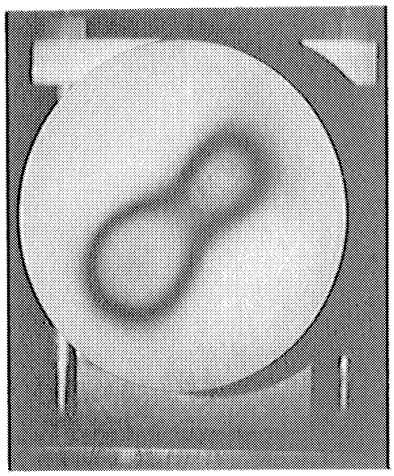

Elements B & C

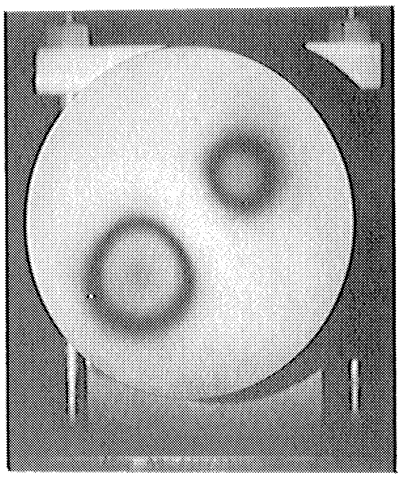

Elements B & C

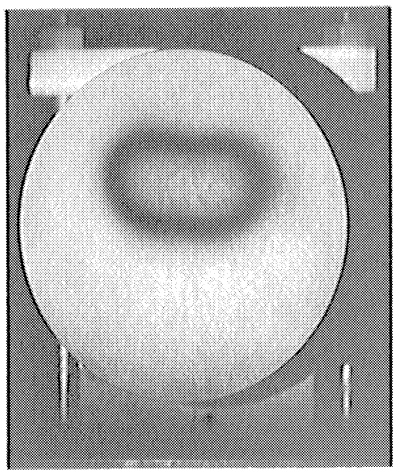

Elements C & D

In Phase

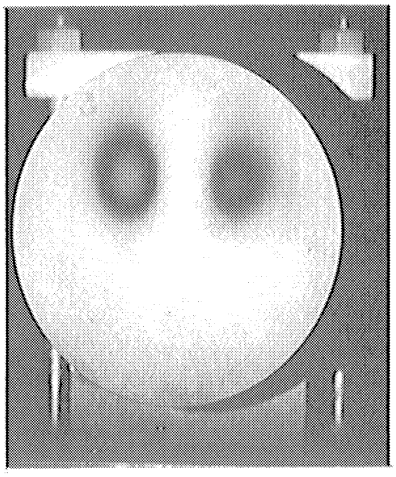

Elements C & D

Counter Phased

Fig. 22. Pairs of elements operated in air at 34.600 kHz and 16.0 Vac

Of course, the area partaking of this maximum displacement has been reduced because the fringe contours have been slightly altered as noted above.

The situation changes for adjacent pairs of elements, for example, elements C and D, operated counter-phased (Fig. 22). These elements are spaced so closely, compared to the thickness of the rubber layer, that a suppression of amplitude can be observed.

When pairs of elements are operated in phase, the peak amplitudes appear to be preserved equal to those for the individual elements. The patterns expand in area into the region between element pairs. Diagonal pairs of elements are separated far enough that a saddle-shaped pattern occurs between them. An elongated plateau of constant amplitude occurs between adjacent element pairs. It also appears that the lateral extent of the dark fringe is not quite as large as for the corresponding elements individually.

4.1.3 Behavior of All Four Elements. Figure 23 shows some results obtained by operating all four elements simultaneously. At an excitation of 16 Vac, operating the elements in-phase resulted in a squarish fringe pattern. The peak amplitude corresponds to that found for the individual elements A, C and D when excited by the same voltage signal. The amplitude over element B has been slightly suppressed compared to operating it individually. Nevertheless, element B makes its greater responsiveness felt by stretching the square contour slightly

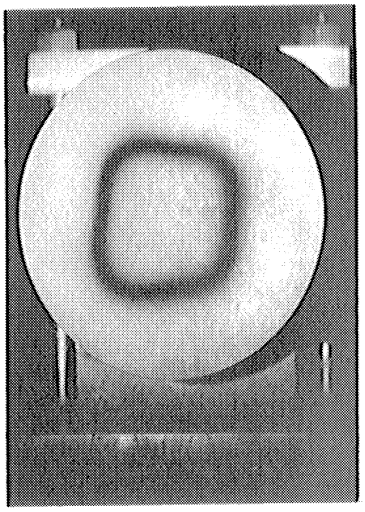

Elements A, B, C, & D excited in phase at 16.0 Vac

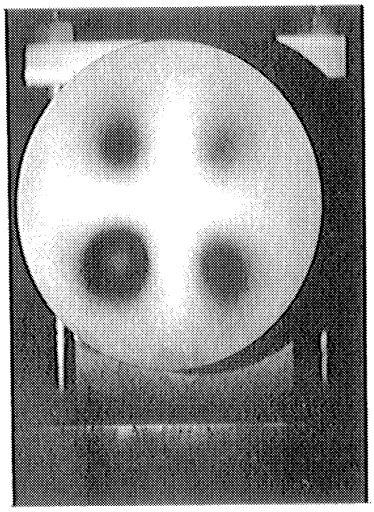

Elements B & C counter-phased with respect to A & D at 16.0 Vac

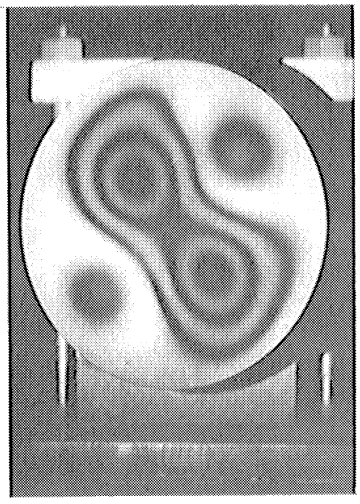

Elements A, B, C, & D excited in phase at 40.0 Vac

Fig. 23. Response of all four elements operating in air at 34.600 kHz

near its corner. Notice also that the dark fringe is more curved between A and C than on other sides; the reason is unknown at present.

Although the peak displacement amplitude remains the same as for the individual elements, the square pattern is smaller in area than a superposition of the four individual patterns from Fig. 20 would imply. The lateral dimensions are only about 80 percent as large as expected.

When diagonal pairs of elements were counter-phased, four separated spots appeared as might have been anticipated. Both the peak amplitudes and the active areas were significantly reduced compared to the responses of the individual elements. Element B still exhibited the largest pattern but the patterns for elements C and D were smaller than for element A, whereas, when operated individually, the patterns for elements A, C and D were essentially equal in size.

The third interferogram in Fig. 23 is especially interesting. All four elements were connected in phase but driven more forcefully with 40 Vac. The pattern of surface displacement has changed dramatically from the square pattern. Now, the major response is along the diagonal containing elements A and D. The peak displacements above these two elements correspond to the locations for the elements operated individually. The appearance of a third dark fringe is consistent for the magnitude of the driving signal assuming linearity of displacement amplitude with voltage. The two small spots of response along the other diagonal are roughly in the direction of elements B and C but are closer

to the edge of the transducer face. This can be seen by comparing Fig. 23 with Fig. 20. The phase relationships among various parts of this interferogram are unresolved. One might suspect the two small dots to be out of phase with the main figure-eight pattern but this is only conjecture.

4.1.4 Behavior as a Function of Voltage. The two distinctly different and unexpected patterns of response shown in Fig. 23 led to a study of transducer response as a function of applied voltage. The results are shown in Fig. 24. Starting at 16 Vac, the square pattern increased with voltage up to and including 40 Vac. During these experiments, it required about 50 Vac to induce the other pattern. Even at 50 Vac, the interferogram is not as crisp as normally obtained, a fact which hints at some mode instability during a portion of the 10-second exposure used to make the hologram.

The voltage needed to cause the second mode or pattern was not perfectly stable. Several times, the pattern switched at 40 Vac but, on occasion, it took higher voltages. When the excitation voltage was increased gradually, the second mode always occurred abruptly but upon lowering the voltage to about one-half, the square pattern reappeared. The occurrence of the high-voltage pattern was accompanied by a sudden small jump in voltage across the four elements connected in parallel. That is, the tuning dip was lost indicating that the electrical impedance looking into the transducer increased when it switched into the high-voltage mode.

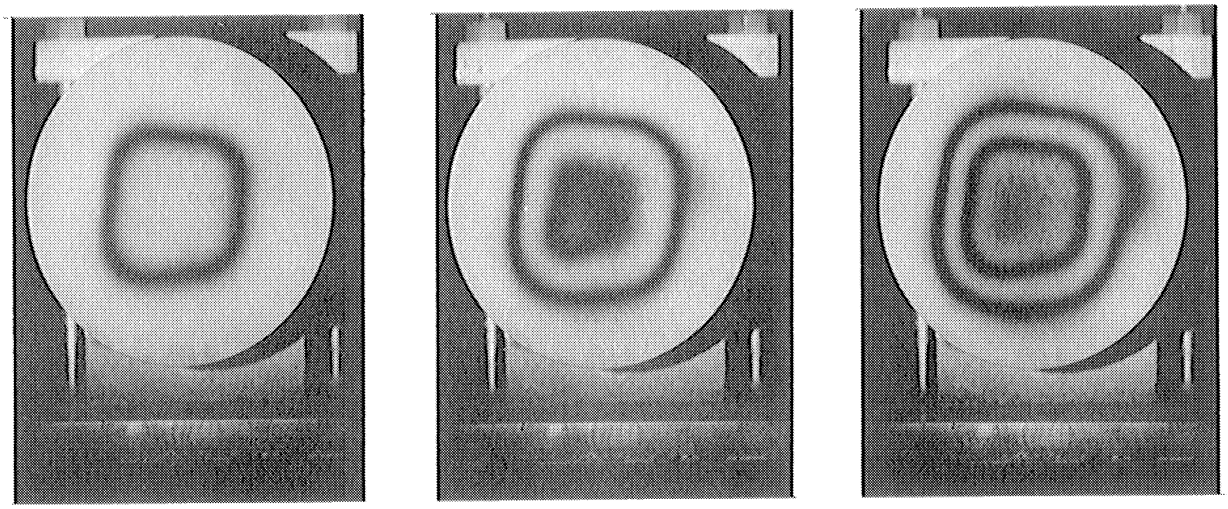

16.0 Vac 24.0 Vac 32.0 Vac

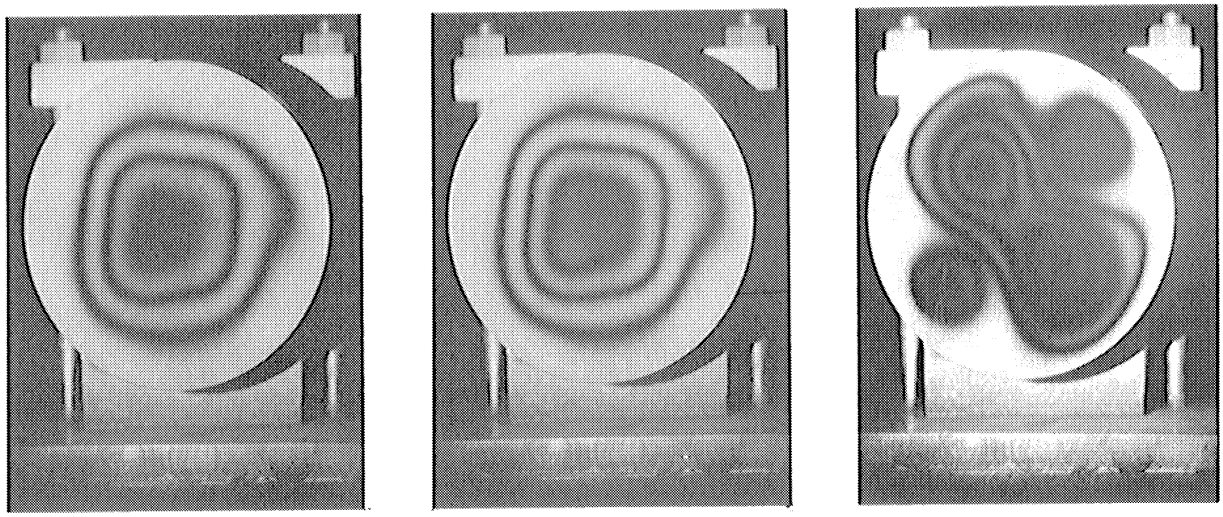

36.0 Vac 40.0 Vac 50.0 Vac

Fig. 24. Change in response with voltage; all four elements operated in phase in air at 34.600 kHz

A closer examination of the first five squarish patterns shown in Fig. 24 is in order. The first interferogram, made at 16.0 Vac, repeats an interferogram taken under similar conditions and shown previously in Fig. 23. Notice that the greater responsiveness of element B distorts the square into a more generalized quadrilateral form. The interior of the pattern approximates the value corresponding to the first bright fringe. Thus dark and bright fringes should alternate with successive (approximate) 8-volt increments if the electro-mechanical response is linear. The center of the pattern starts to darken again at 32.0 Vac which may indicate that the selected 8-volt increment was slightly too large. The interferograms for 36.0 and 40.0 Vac both show dark centers and some enlargement of the pattern area, but the expected additional dark fringe did not appear. This behavior suggests nonlinear response in the displacement at the free surface of the rubber as one plausible explanation.

The first five interferograms in Fig. 24 show another interesting feature, namely, a pronounced bulge in the outer dark fringe at about a 3 o'clock position. The effect is real but the exact cause unknown, perhaps a lack of bonding or an artifact of the internal construction.

The second-mode interferogram at 50 Vac has a peculiar fringe running from about 11 to 12 o'clock which cuts across the more prominent fringe pattern. Interpretation is ambiguous using just this one interferogram but it looks as if some instability, either in amplitude

or mode shape, occurred momentarily during the exposure time of about 10 seconds.

Attempts were made to obtain the two-mode behavior from each of the individual elements driven separately. At first, only element D could be made to switch modes, a feature inconsistent with the large response obtained in the figure-eight pattern at the location of element D. Mode switching of the individual elements was observed by watching for the little jump in voltage across the element as the resonant dip was lost. Near the transition voltage, one could make an incremental increase in the applied voltage. Next, the voltmeter would reach a stable indication for this new voltage at a reading consistent with the voltage increment. Then, after a few seconds, the meter would jump upscale by perhaps half a decibel. Subsequent exploration in frequency would show that the resonant dip had been lost. If the excitation voltage was then reduced to about 20 Vac, the resonant dip of about half a decibel would be found again.

As mentioned above, this behavior could be induced only in element D at first. After repeated trials, mode switching was observed for elements B, C and D, operated individually. It was never observed to occur for element A alone.

Figure 25 presents the motion observed in the rubber face of the transducer for element D in each mode of operation. In the low-voltage mode, the pattern has a slightly elliptical outline and exhibits an

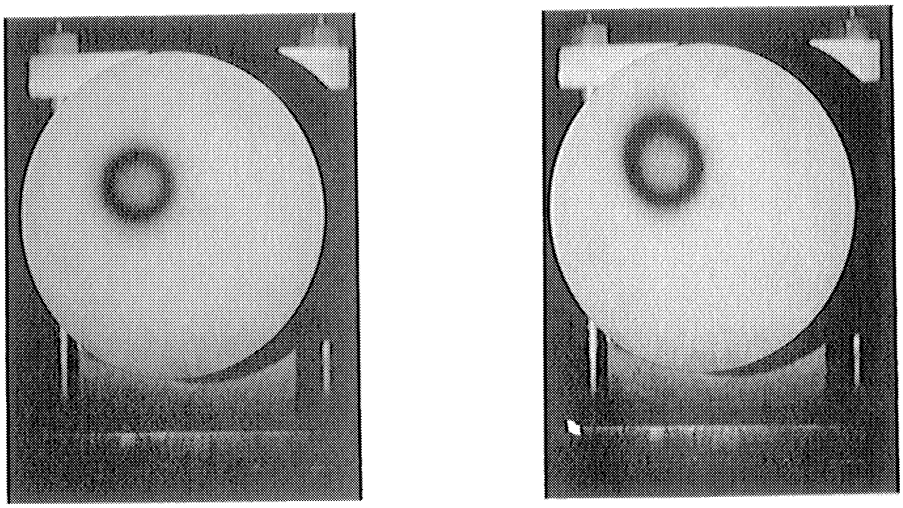

16.0 Vac 50.0 Vac

Fig. 25. Response of element D in low and high voltage states operating in air at 34.600 kHz

amplitude of about 1-1/2 dark fringes (roughly 8×10^{-6} inch single-peak excursion). In the second high-voltage mode, the interferogram shows a clearly circular pattern. If anything, the amplitude is slightly reduced and the region of maximum displacement amplitude lies closer to the center of the transducer face than for the low-voltage mode. Normally, in view of the ceramic piezoelectric elements, one would expect the response to be linear with applied voltage. Thus, in the second mode at 50.0 Vac, the displacement amplitude is roughly only one-third the expected amount.

The change in pattern shape argues for a change in the modal response of the head of the driver or for higher frequency action due to harmonic generation. In any event, the voltage jump observed at some voltage levels for individual transducer elements was accompanied by a corresponding change in the forced displacements seen on the free surface of the rubber.

4.1.5 Behavior Before and After Tests in Water. Figure 26 displays three time-average interferograms of the first transducer taken prior to experiments with it in water. The transducer had been positioned in the empty aquarium (Fig. 7). Thus the aquarium constituted a five-sided acoustically reflective enclosure located close to the transducer. (The other interferograms taken in air and discussed above, were taken with the transducer mounted in the open; the granite holography table was the closest extended acoustically reflective surface.) Because no

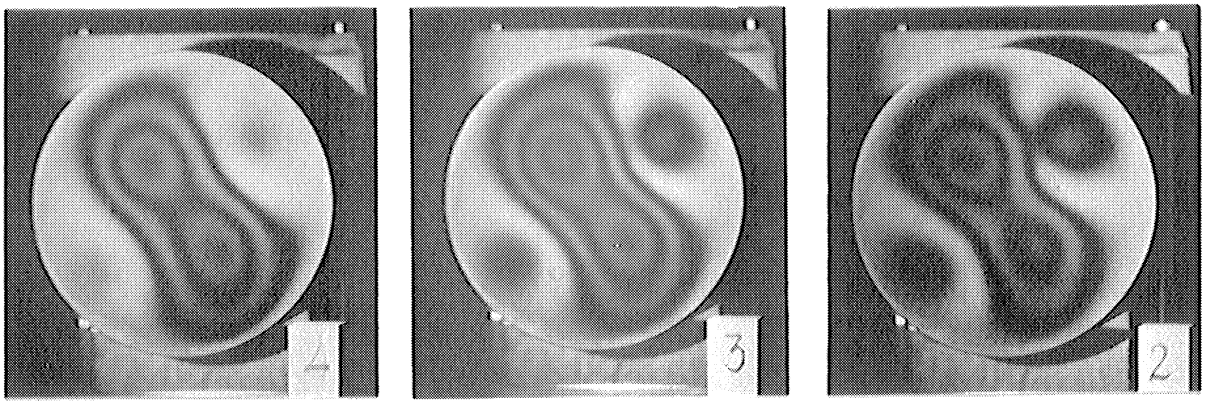

33.03 kHz 34.03 kHz 35.05 kHz

Initial trials before tests in water

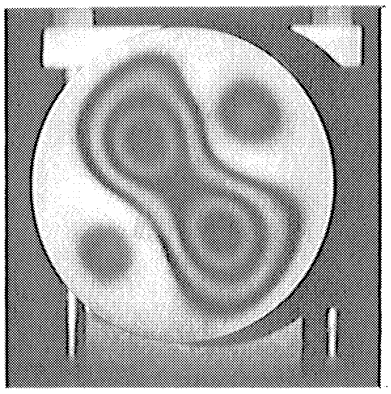

34.600 kHz

Subsequent to tests in water

Fig. 26. Comparison of initial and subsequent response; all four elements operating in phase in air at 40.0 Vac

specific frequency had been selected for in-air operation, these three interferograms were taken at one kilohertz increments and fortuitously, at a drive voltage which was discovered later to correspond to the high-voltage mode. These figure-eight patterns were thought peculiar at one time but, lacking specific knowledge about the array configuration or shading, we had proceeded with the experiments in water.

For comparison, an interferogram, taken in air at 34.6 kHz and 40 Vac after the water tests, is shown at the bottom of Fig. 26. Obviously, this first transducer displayed essentially the same behavior in air at 40 Vac before and after the tests in water. At this point, the first transducer became so erratic that further testing with it was cancelled.

4.1.6 Summary for the First Transducer. These studies of the first transducer in air have produced several significant results. At low driving voltages, the patterns generally have conformed to expectations for a 2 by 2 array interconnected in several ways. This result suggests that the rather unusual results obtained with it in water (Section 4.3.1) probably were more a consequence of the laboratory setup than untoward behavior of the transducer.

The location of the fringe patterns on the transducer's face, the contour shapes, and the areas enclosed by the contours all show features which probably result from the dynamic behavior of the viscoelastic layer of rubber covering the driving elements. Other features, such as the

large response at element B, relate to system performance and/or quality control. The mode switching in air at high driving voltages was not anticipated. It remains unexplained although its existence has been clearly documented.

The electromechanical response in air seems to have remained reproducible in spite of moisture entering the transducer during the studies in water. The final erratic behavior which ended these experiments is interpreted as an unfortunate and unrelated incident.

4.2 Second Transducer Operating in Air

The new transducer had a slightly larger face than the first. Also, it was a sealed, liquid-filled unit which operated at a significantly lower frequency, about 19 to 20 kHz, both in air and water. All four elements had to be operated simultaneously because their individual electrical leads were not accessible. Figure 27 shows front and rear views of this transducer as mounted for tests in both air and water. The position of the cable connection, rotated slightly counterclockwise from the vertical, provides evidence of the orientation of this transducer as it appears in the interferograms.

We elected to study the new unit in air before immersing it in water. It also had a flat-black rubber face and caused the same difficulties as the first transducer with respect to ease of reading the real-time fringes (Section 4.4.1). An initial survey indicated that the working

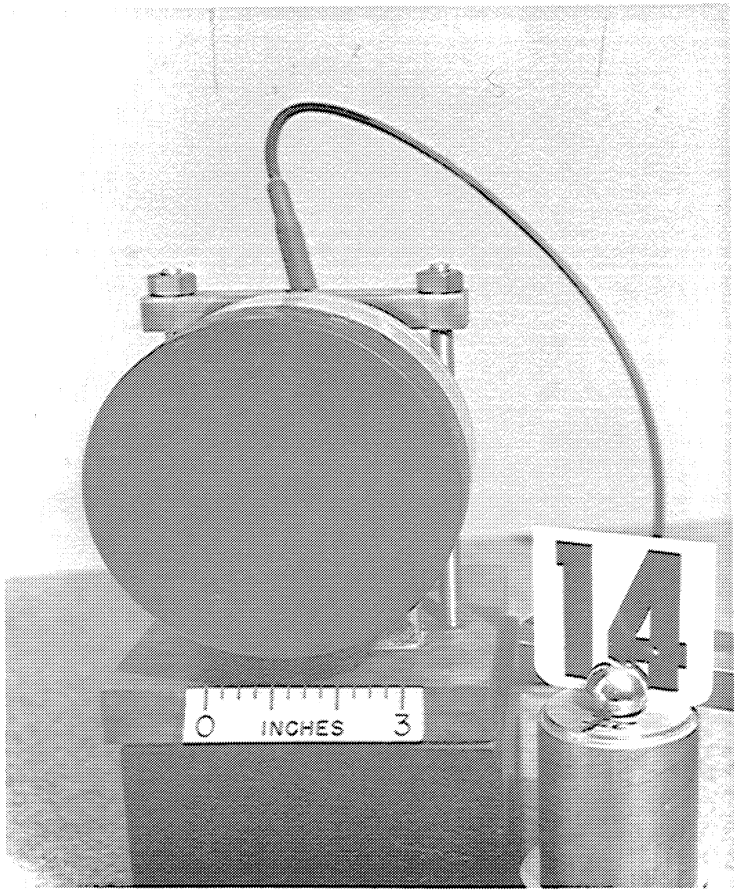

(a) Front View

(b) Rear View

Fig. 27. Second transducer mounted for air and water studies

mode occurred in air at about 19.950 kHz and was broadly tuned. Moreover, "nearest-neighbor" modes of completely different pattern occurred in air at about 14 and 22 kHz respectively.

The initial studies revealed an exercise phenomenon associated with the operating mode in which the shape and area of the pattern changed with operating time. Time-average interferograms were taken at 19.9 kHz and 12, 18 and 24 Vac with the results shown in Fig. 28. The 18 and 24 Vac interferograms show a brightening in the center of their patterns, verified by the displacement of the real-time fringes formed with the respective time-average holograms (Section 4.4.2). These patterns did not fully agree with the initial observations using real-time fringes, consequently, a thorough reexamination was undertaken.

A new real-time hologram was made after the transducer had remained unexcited for a day. Then, when first excited at 19.95 kHz and about 17 Vac, the surface displacement appeared to occur uniformly over most of the rubber face (stage one). Only a narrow annular region about a centimeter wide at the extreme outer edge did not move. This pattern appeared to be perfectly circular. Most of the central area of the rubber face exhibited reversed fringes indicating a single-peak amplitude of about 8×10^{-6} inch. As the observation was continued, the pattern appeared to shrink in from the outer edge slightly (stage two) and then to become race-track shaped (stage three) like the 24 Vac pattern of Fig. 28 and similarly tilted. Then the pattern became more irregular in outline

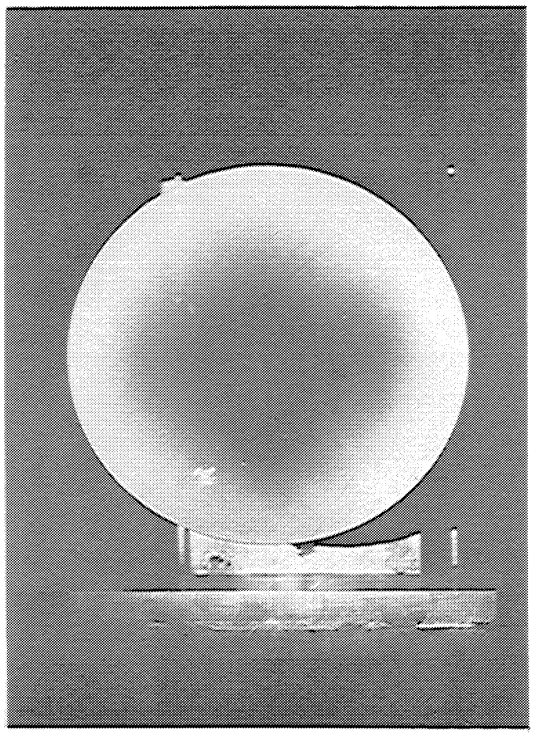

(a) 19.900 kHz, 12.0 Vac

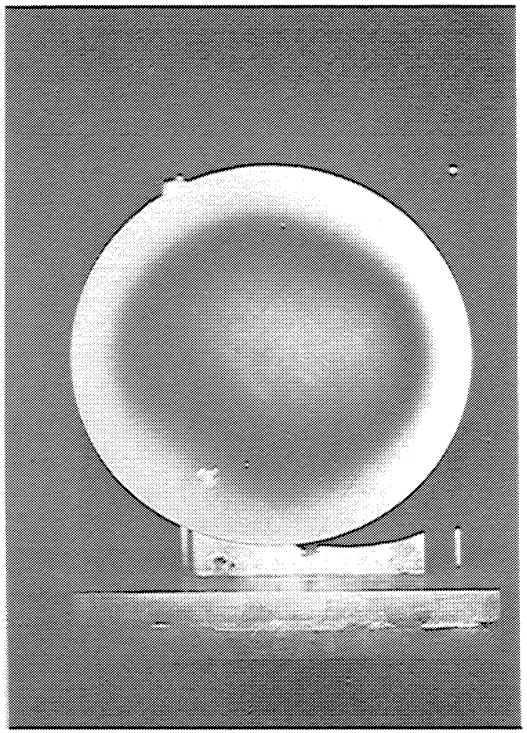

(b) 19.900 kHz, 18.0 Vac

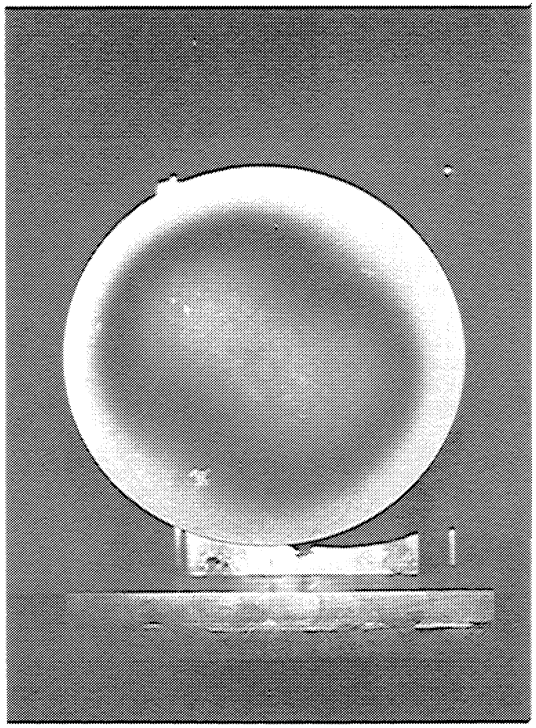

(c) 19.899 kHz, 24.0 Vac

Fig. 28. Second transducer operating in air

(stage four). Finally it shrank into an irregularly shaped patch at the lower right-hand portion of the face (stage five). There, only the first fade-out of the real-time fringes occurred indicating a reduced amplitude of about 5×10^{-6} inch single-peak motion. Thus, in a period of several minutes, the pattern shrank from a symmetrical concentric shape encompassing almost the entire rubber face to an unsymmetrical, off-center shape involving about one-quarter of the rubber area. Simultaneously, the maximum displacement amplitude decreased roughly by one-third. As the change of visual appearance took place, a change in the audible sound occurred also. When the excitation was first applied to the transducer, it was inaudible; 19.95 kHz lies above the audible range of this observer. Then as operation proceeded, a hissing sound occurred followed shortly by an irregularly timed chirping sound superimposed on the hissing sound.

Both the visual and audible sequences have been repeated many times with respect to their main features. The details and duration of events varied somewhat from test to test. If, after a sequence, the electrical driving signal was removed from the transducer for five to ten minutes, the general course of events could be repeated except that the sequence progressed more rapidly and some of the intermediate patterns were not as clearly delineated. If the transducer was rested longer between tests, a more complete duplication of the entire sequence of events was observed.

An effort was made to document some stages of this sequence by means of time-average interferograms. Figure 29a shows an interferogram taken at 17.25 Vac and 19.95 kHz. It indicates a motion encompassing most of the area of the transducer face and a single-peak amplitude of about 8×10^{-6} inch in the central portion of the pattern. However, the pattern has flattened sides instead of circular symmetry. From observations using real-time fringes as described above, the pattern in Fig. 29a looks like stage three in the progression of patterns.

The transducer was left undisturbed and unexcited over night and then the interferogram of Fig. 29b was obtained. The excitation was held constant at 19.95 kHz and 17.25 Vac. The result appears to be a very good repeat of Fig. 29a. The other intermediate stages in the exercise sequence were too furtive to record by time-average holography on our setup except for the final stage shown in Fig. 29c. It was obtained by exercising the transducer at 19.95 kHz and 25 Vac for several minutes before exposing the hologram with an excitation of 17.50 Vac. The voltage in this case was 0.25 V higher than before because of an accompanying change in the load impedance presented by the transducer. This time-average interferogram appears to correlate perfectly with stage five observed previously.

Figure 30 shows time-average interferograms at selected voltages of the nearest neighbor modes previously located by means of real-time fringes. These patterns are distinctly different both in appearance and

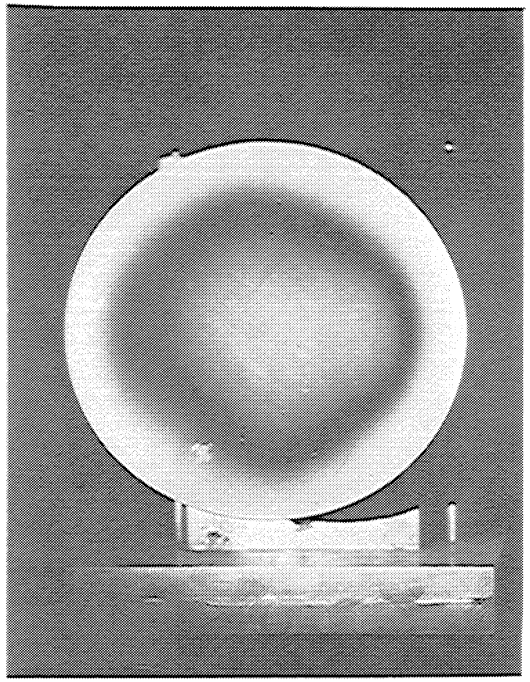

(a) 19.952 kHz, 17.25 Vac
Stage three

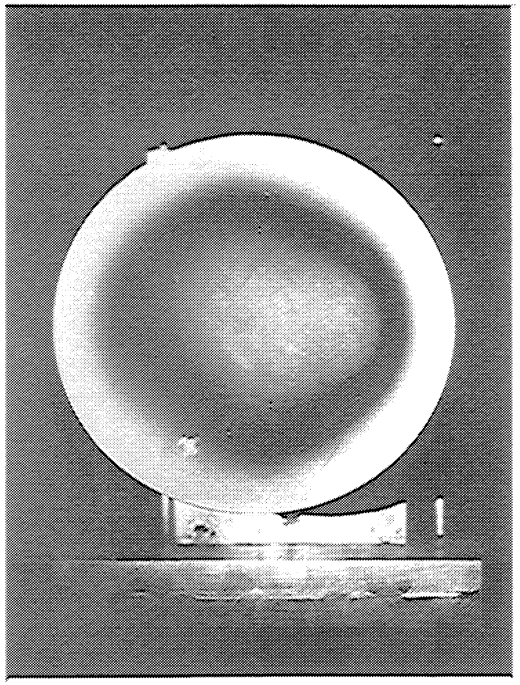

(b) 19.952 kHz, 17.25 Vac
Repeat of (a) one day later

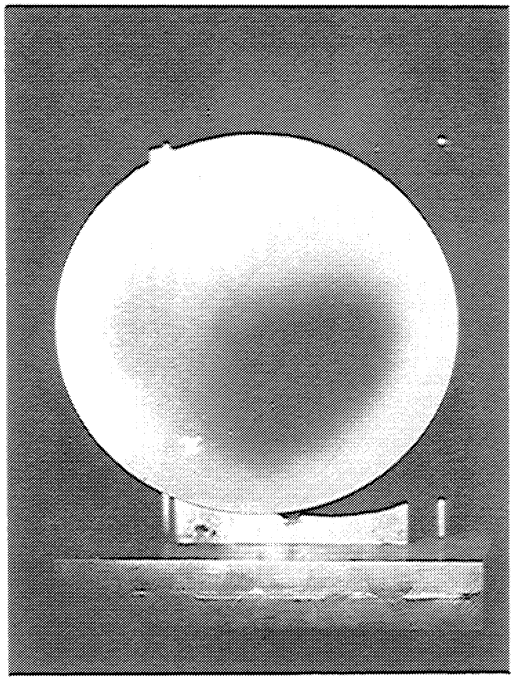

(c) 19.953 kHz, 17.50 Vac
After exercise at 25 Vac
Stage five

Fig. 29. Selected stages of exercise sequence

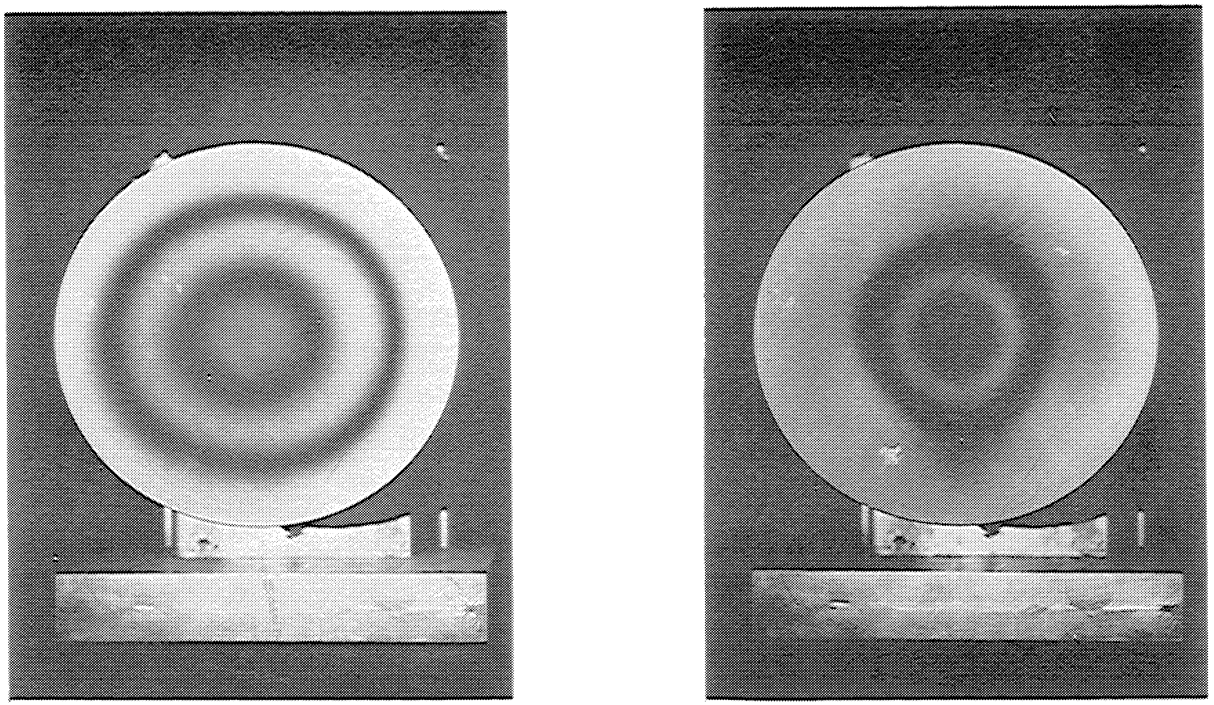

(a) 14.100 kHz, 10.0 Vac

(b) 21.950 kHz, 25.0 Vac

Fig. 30. Nearest neighbor modes

behavior from the patterns of the operating mode. They did not exhibit any temporal sequence of behavior resembling that found for the operating mode. To the limited extent that they have been studied, they appear stable and reproducible. These nearest neighbor modes were cleanly separated from the operating mode by frequency ranges where little or no motion of the rubber face was found for reasonable values of excitation voltage.

Supplementary experiments were performed on the exercise sequence characterizing the operating mode. The airborne sound close to the rubber face was examined using a 1/2-inch diameter condenser microphone (Bruel and Kjaer Type 4134). In contrast to the first transducer, the operating frequency of the second transducer fell within the useful range of this available microphone. The microphone diaphragm was positioned parallel to the rubber face at a distance of 1/2 inch and scanned over the transducer face. The strength of the direct sound field swamped residual standing-wave effects at this close spacing. Significant standing-wave effects were found when the microphone-to-transducer spacing was increased to 6 inches.

The airborne signal acting on the microphone was displayed on a cathode ray oscilloscope. Based on the nominal value of microphone sensitivity, the rms sound pressure one-half inch away from the face of the transducer was about 6.4 N/m^2 (or 110 dB re 2×10^{-5} N/m^2). This value of sound pressure corresponds to about 7×10^{-6} inch single-

peak displacement amplitude at 20 kHz. If we read the corresponding interferogram pattern to have a fully developed second bright fringe at the center, then by holographic reckoning, the single-peak displacement amplitude was about 8×10^{-6} inch, excellent agreement considering the rudimentary measurements associated with both procedures.

When the exercise experiment was repeated with the microphone as pickup, the oscilloscope displayed a corresponding sequence of patterns. When the 17.25 Vac excitation at 19.95 kHz was first applied, the scope showed a clean, constant amplitude sinusoidal waveform. After a brief period of exercise, the amplitude slowly diminished by about 10 percent and then remained clean and constant for a variable period of time up to several minutes. Eventually the next stage occurred in which the amplitude fluctuated between its recently acquired level and a new 10 percent smaller value. In this stage, the amplitude appeared to fluctuate continuously and randomly between those two bounding values and, at the same time, the audible hissing sound occurred. The transition to unsteady amplitude would occur immediately if the driving voltage was raised to 25 Vac, for example, for a few seconds.

As the exercise proceeded, a chirping sound soon accompanied the hissing sound. When this happened, the unsteady amplitude viewed on the scope exhibited recognizable, discrete transient envelope patterns of roughly one-tenth second duration which temporarily supplanted the more random fluctuations. Both fluctuations in amplitude seemed to be

bounded by the same limits. A scan with the microphone over the transducer's face confirmed the pattern shown in Fig. 29c.

If the transducer was allowed to rest for a few minutes and then excited again, it promptly returned to the unsteady amplitude state accompanied by the hissing sound. The transducer had to be rested at least 10 or 15 minutes to recover enough to exhibit the full sequence of states, even momentarily.

The behavior of the second transducer violated the condition for time-average interferometry of steady-state sinusoidal vibration. On the other hand, the amplitude was small enough (one dark fringe), and the amplitude variation was narrowly bounded, so that recognizable if not ideal interferograms were obtained as evidenced by Figs. 28 and 29 for example.

Incidentally, measurements with the microphone also indicated larger airborne sound signals for the nearest neighbor modes, especially at 14.1 kHz, than for the operating mode. This observation also agrees with the interferometric evidence. Likewise, observation by microphone confirmed the relatively unresponsive frequency regions either side of the operating mode.

4.3 Studies in Water

One of the first demonstrations by this laboratory was that successful holography could be accomplished on objects immersed in

water.[1] Since that time, we have conducted studies in water using both real-time and time-average interferometry of vibrating objects. Under appropriate conditions such holograms are fully as clear as those taken in air. Figure 31 is an example of such an underwater time-average interferogram. These interferograms, taken in January 1967, were mentioned in our progress reports[2] but reproductions of them have not been published previously. The vibrating object is an edge-clamped circular metal diaphragm of a modified waterproof marine horn. This diaphragm was driven at the center. The nearly invisible concentric marks at the center are a photographic rendering of a bolt and washer at this location, not interference fringes. The diaphragm was placed at the rear of the water-filled aquarium so that the total optical path in water amounts to about four feet in this instance. Since the frequency was about 183 Hz, the dimensions of the aquarium were small compared to the wavelength of sound in water.

A variety of experiments had been performed in water prior to undertaking the study of the two ORL transducers reported below. In summary, their results indicated that if mechanical stability of the water tank and the immersed object was achieved and if the water was allowed to reach thermal equilibrium (thermal expansion of the aquarium rather

---

[1] R. M. Grant, R. L. Lillie and N. E. Barnett, "Underwater Holography," J. Opt. Soc. Am., Vol. 56, 1966, p. 1142(L).

[2] January 1967 Progress Report, Subcontract No. R66-2476, dated February 13, 1967.

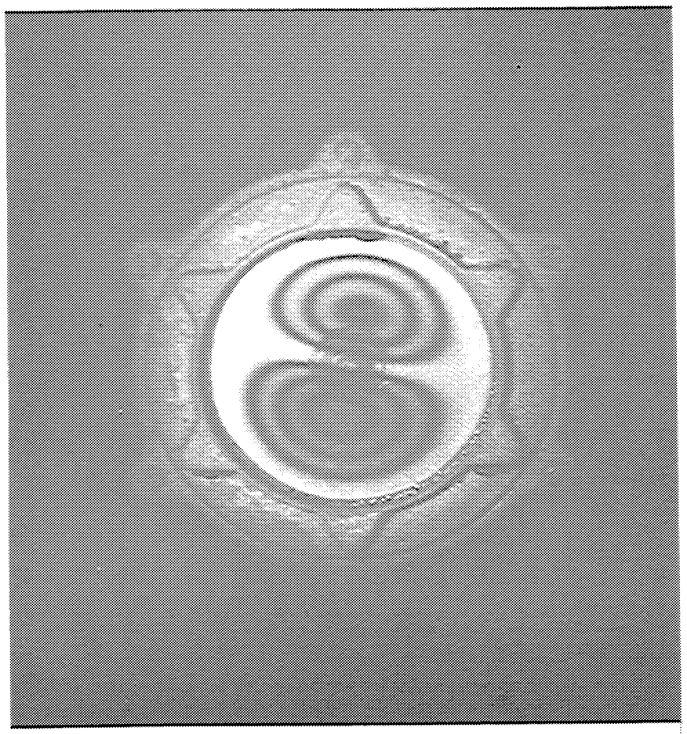

(a) 183 Hz, modified waterproof marine horn

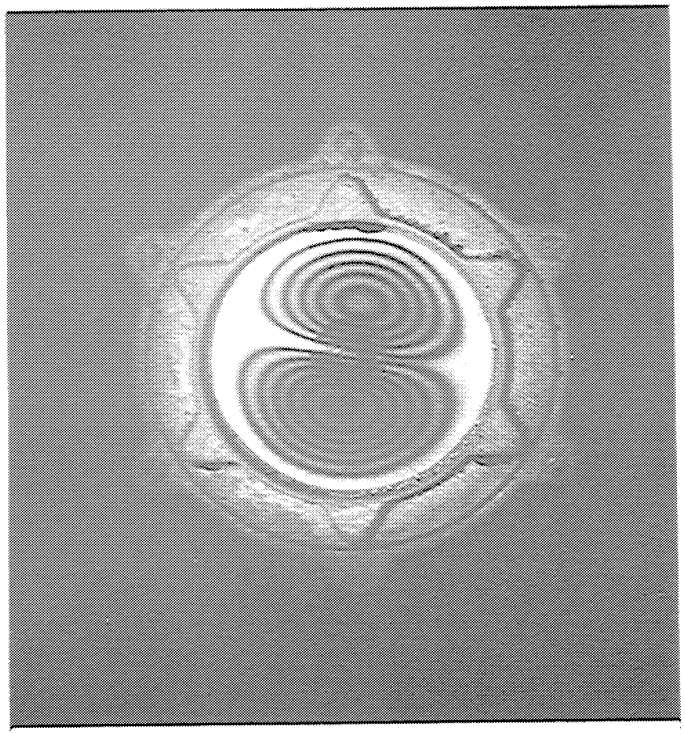

(b) 183 Hz, larger excitation

Fig. 31. Early example of time-average hologram interferometry of vibrating object submerged in water

than thermal variation of index of refraction of water), holograms of high quality could be obtained. Of course, when setting up the apparatus, due regard had to be paid to equilization of the optical path lengths (Section 2.5.1), to refraction of ray paths at the aquarium surfaces so that the sensitivity vector had the intended direction at the transducer face, and to the many optical reflections from the aquarium windows which tended to occur at visually disturbing positions.

The question of the acoustical characteristics of the sonic field surrounding vibrating objects is significant to the present studies. It was expected that a standing wave field in the aquarium might cause some difficulties. However, we had obtained apparently satisfactory results with vibrating structures which were loosely coupled to the water (Fig. 31, for example) and thus we were led to expect that useful observations might be made on sonar-type transducers also. In other words, we anticipated results that were not badly perturbed.

As it has turned out, standing wave effects, including pressure modulation of the index of refraction of water (Section 2.5.2) were so severe as to preclude a simple analysis of the interferograms. The acoustic interaction between a transducer and its surround is too strong. It now appears that anechoic facilities suitable for hologram interferometry are prerequisite to interpretable experiments with transducers. Even with an anechoic surround, the experiments necessarily would have to take the pressure modulation of the optical refractive index into consideration.

The following discussion presents the experiments performed with the two transducers in water. The cumulative results from these studies have led us to the conclusion that anechoic facilities are needed for the next stage of studies with transducers.

4.3.1 First Transducer Operating in Water. The apparatus was arranged as shown previously in Fig. 7. Figure 32 gives a more detailed plan of the aquarium and Fig. 33 is a photograph of the same setup. The near end of the aquarium was angled so that the subject beam, reflecting from the air-glass interface, would miss the hologram plate. The front face of the transducer was turned to align its normal with the sensitivity vector in water. The transducer was arbitrarily placed near the front of the aquarium but at an angle to the front window. Presumably this water wedge had some acoustical benefit by avoiding the extreme standing-wave field which would result from a parallel geometry.

The aquarium was filled with filtered tap water and allowed to outgas several days. When bubbles of dissolved air ceased to accumulate on submerged objects, a real-time hologram was made and the transducer inspected in the vicinity of its operating frequency. Some thirteen distinct patterns and many lesser ones were observed from 26.385 to 32.901 kHz with 15 to 20 Vac excitation. These patterns consisted of roundish spots, elongated ovals, L-shaped spots and horizontal striae. Indeed, one pattern of horizontal striae at 29.816 kHz was the most prominent "mode." We documented it the next day with five time-average

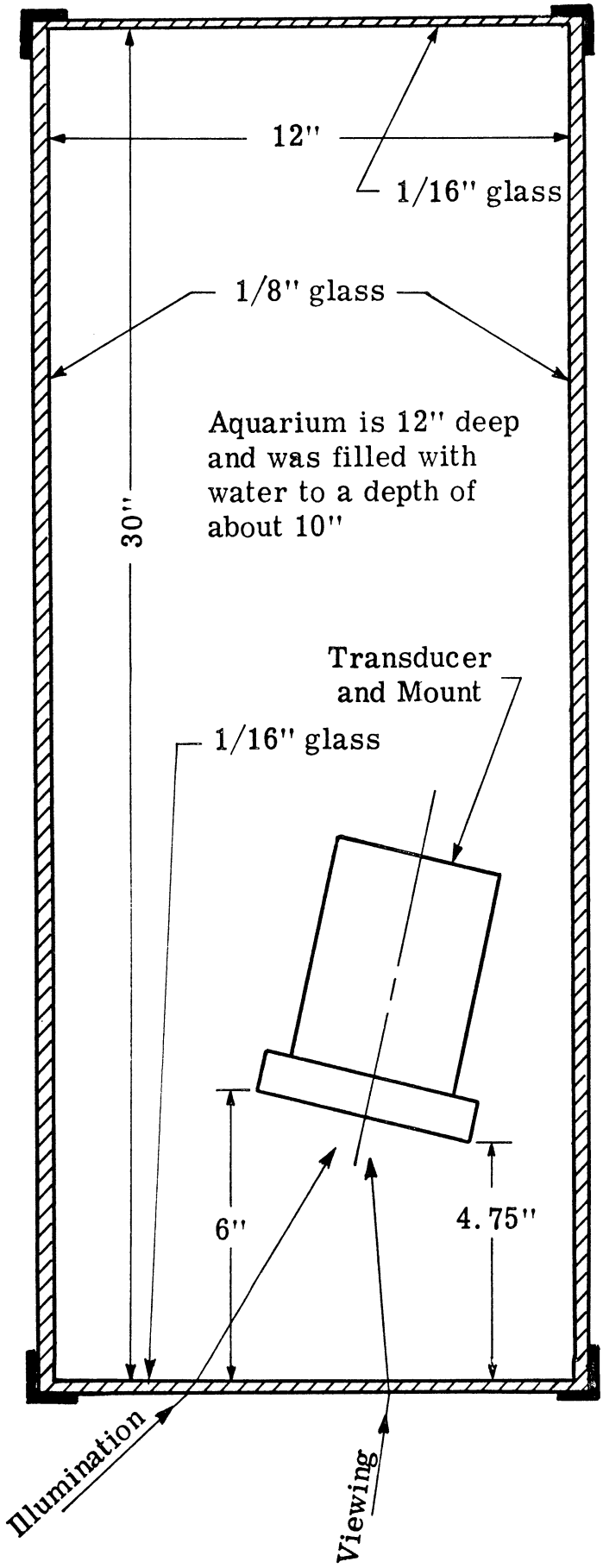

Fig. 32. Plan of transducer in aquarium

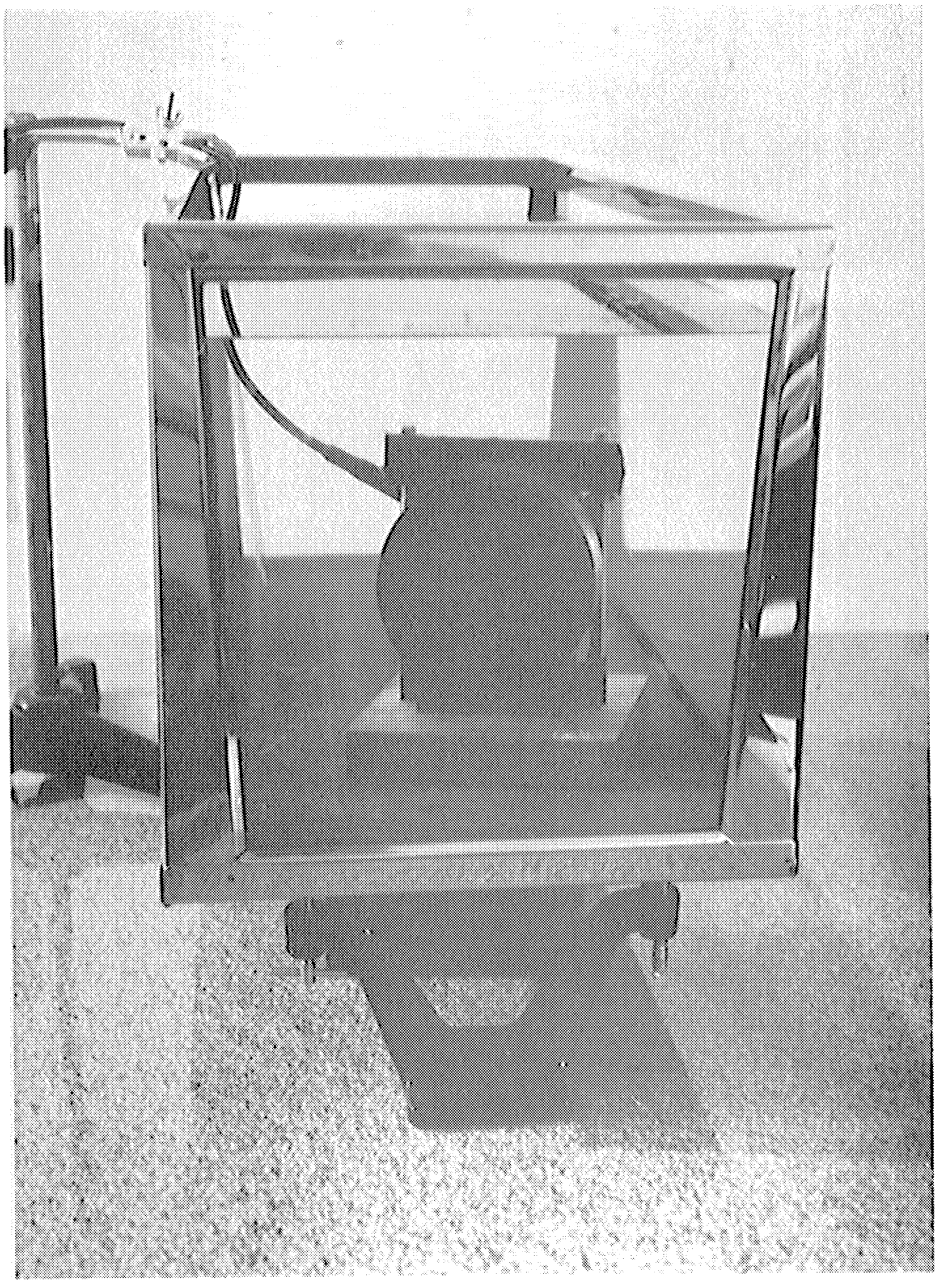

Fig. 33. Photograph of transducer in aquarium

interferograms taken at 15, 18, 21, 25 and 30 Vac. However, the frequency was found to have shifted upward to 29.955 kHz. This series of interferograms is reproduced in Fig. 34. Note the fringe pattern overlying the numbered metal blocks in the lower right-hand corner. Also notice that the striae on the transducer face bear scant relationship to the locations of the individual elements. (Refer to Fig. 20 which was taken in air.)

The next tests documented the frequency range from 29.0 to 30.6 kHz in 100 Hz increments at 25 Vac excitation. A diversity of splotchy patterns resulted but the pronounced striae patterns of Fig. 34 did not reappear at 29.9 or 30.0 kHz although a pattern, at least superficially similar, did occur at 30.1 kHz. Figure 35 shows six interferograms from this time-average series selected to indicate the diversity of patterns.

A specific study was conducted at 29.955 kHz to try to document what happened to the illusive striae pattern whose frequency appeared to shift upward with passing time. Interferogram Fig. 36a was the pattern first obtained at 29.955 kHz and 25 Vac excitation (shown previously in Fig. 34). Interferogram Fig. 36b was obtained after the frequency increment series when we specifically looked at 29.955 kHz again. The action bears no recognizable correlation with the previous pattern. To see if this last pattern was stable, the condition was repeated again at 29.955 kHz and 25 Vac, but the hologram consisted of a double exposure.

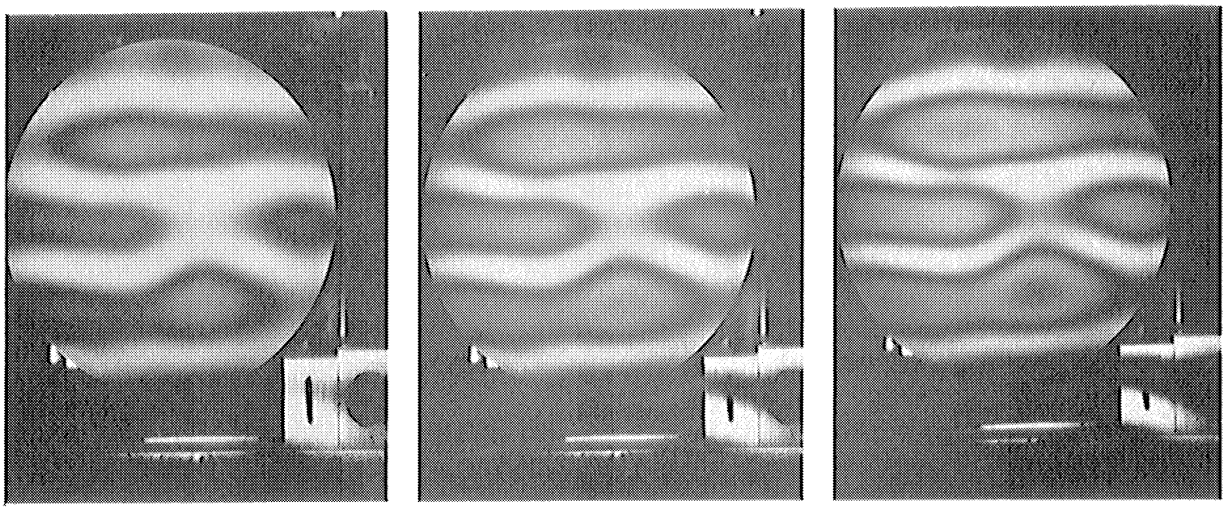

(a) 15 Vac (b) 18 Vac (c) 21 Vac

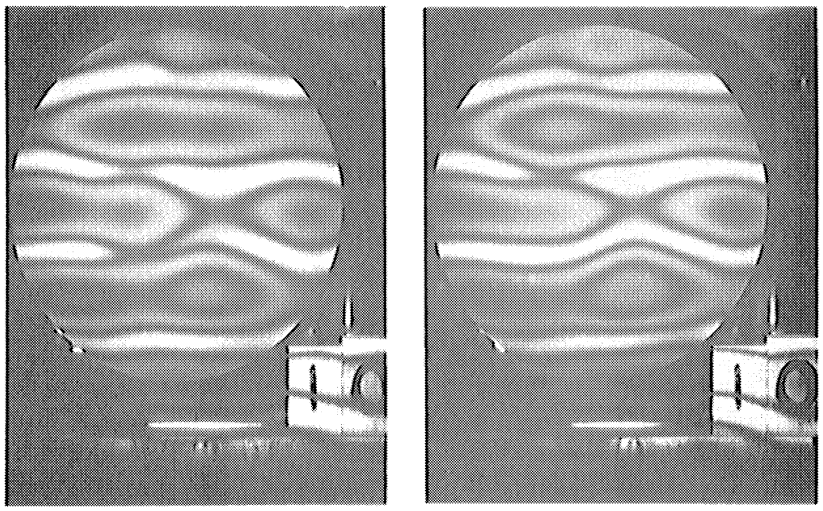

(d) 25 Vac (e) 30 Vac

Fig. 34. Striae patterns at 29.955 kHz in water

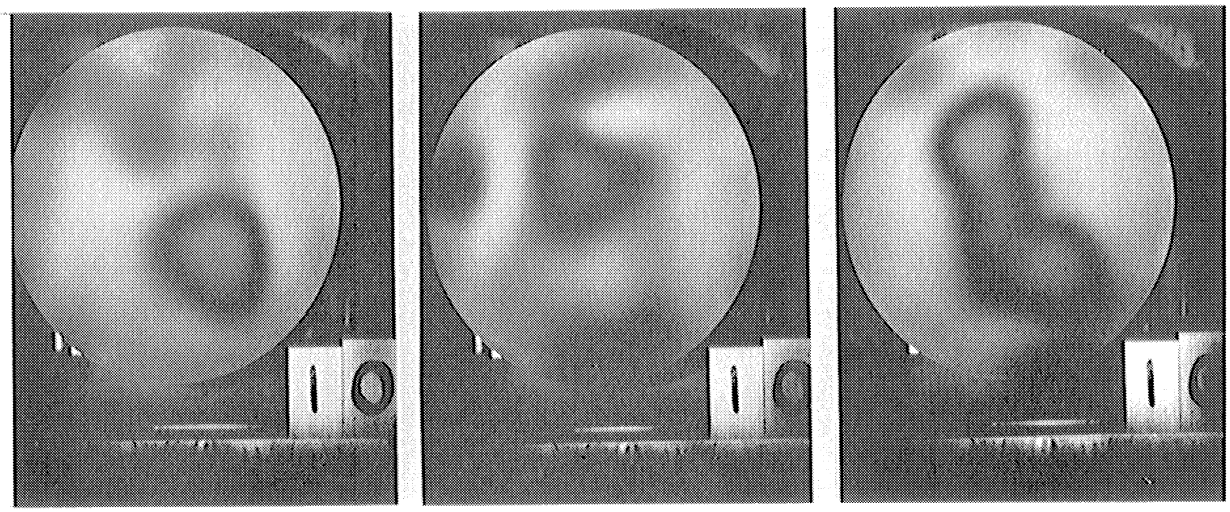

(a) 29.0 kHz, 25 Vac (b) 29.2 kHz, 25 Vac (c) 29.6 kHz, 25 Vac

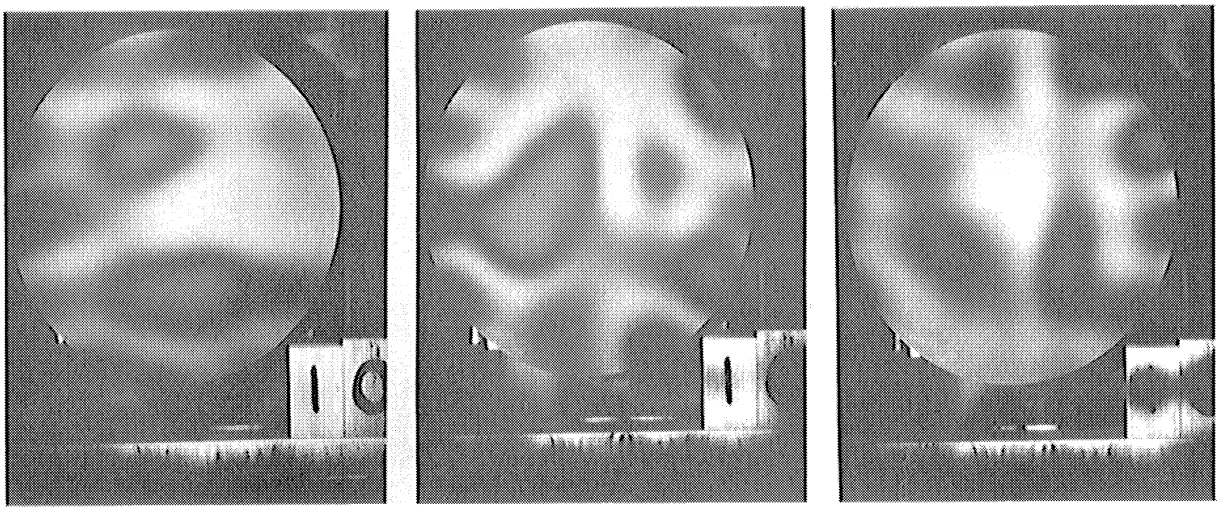

(d) 30.3 kHz, 25 Vac (e) 30.5 kHz, 25 Vac (f) 30.6 kHz, 25 Vac

Fig. 35. Diversity of patterns in 29.0 to 30.6 kHz region

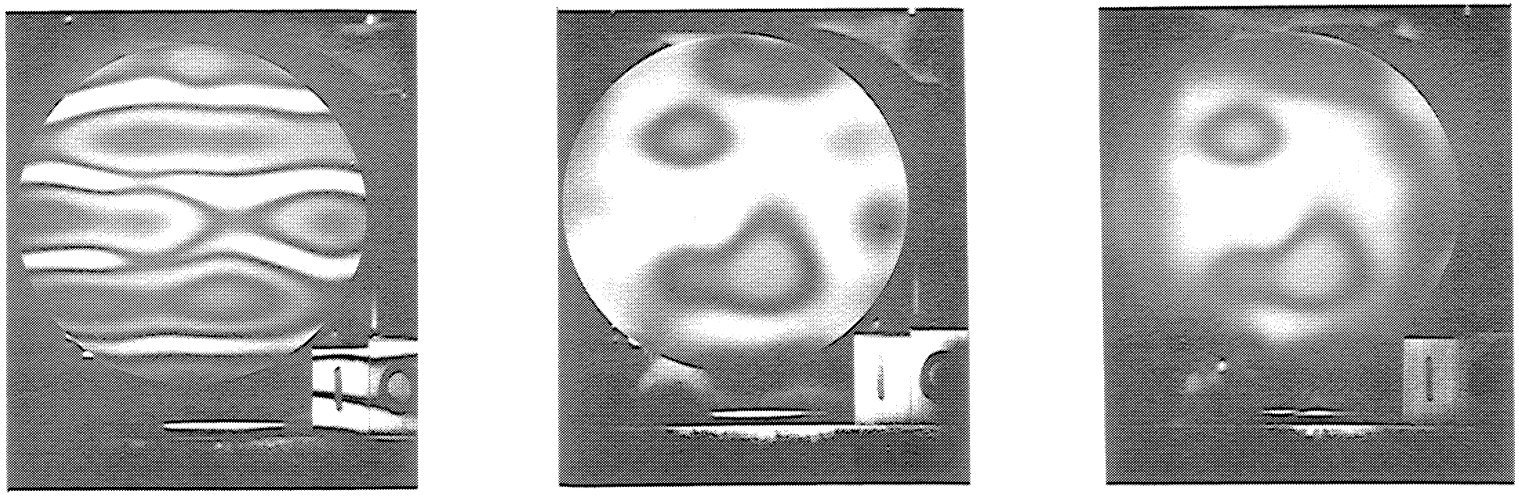

(a) Original striae pattern

(b) Attempt repeat after frequency series

(c) Double exposure showing change in one minute

Fig. 36. Study of behavior at 29.955 kHz and 25 Vac

Each half exposure was 2.5 seconds long taken one minute apart although the transducer was continuously excited. This double-exposure interferogram, Fig. 36c, has a strong resemblance to pattern (b) but, in addition, an irregular dark fringe now appears around the edge of the face. Obviously, something which was not revealed in a 5-second single exposure changed at a rate revealed by double exposures taken 60 seconds apart.

These time-average interferograms of a transducer in water furnished clear evidence as far as optical interferometry is concerned. Definite dark patches and various fringe contours indicated that specific amounts of optical phase modulation have occurred as a result of driving the transducer. The point, which was not clear, was what specific physical phenomena actually contributed the phase modulation recorded. The patterns were not recognizable in terms of the displacements expected from a 2 by 2 transducer array.

Section 2.5 has already suggested several mechanisms for optical phase modulation in the water-filled aquarium studies. Briefly, plausible mechanisms are:

1. Forced motion of the transducer face as expected from the driver configuration.
2. Motion of the aquarium windows under the action of the waterborne sound field.

3. Modulation of the optical index of refraction of the water by the acoustic pressure.

4. The acoustic standing wave field in the aquarium reacting on the rubber face of the transducer.

The problem was not how to obtain good interferograms under water but rather how to sort out, if possible, the causes of the optical phase modulation and how to render mechanisms 2, 3 and 4 insignificant, if possible, compared with 1.

Various experiments were performed to clarify the issue. One of these was a closer examination of the change in magnitude of the transducer's electrical impedance as a function of frequency. A 500-ohm resistor was inserted in series with the power amplifier to increase its source impedance. Figure 37 shows a typical result. Major fluctuations are spaced about every 50 to 60 Hz. Considering that the rectangular volume of water was roughly 0.76 by 0.30 by 0.25 meters, there should have been about 22 normal modes per 100 Hz bandwidth at 30 kHz center frequency.[1] The curve in Fig. 37 resembles frequency irregularities due to mode clustering more than individual mode effects. This curve undoubtedly indicates that a standing-wave phenomenon does exist in the aquarium strong enough to be observed in the reflected electrical characteristics of the transducer.

---

[1] Kinsler and Frey, Fundamentals of Acoustics, 2nd edition, John Wiley and Sons, New York, 1962; p. 446, eq. 14.48.

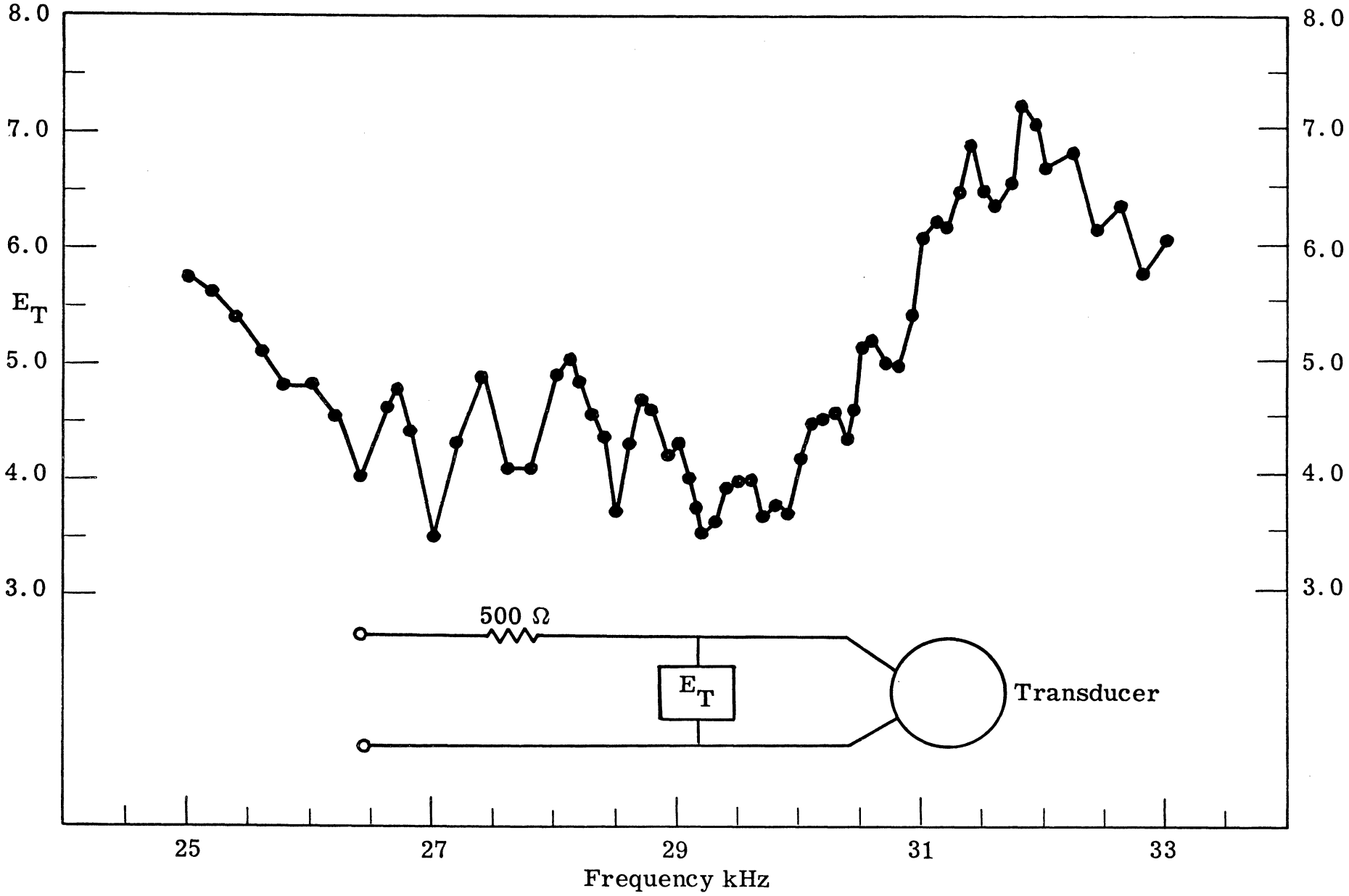

Fig. 37. First ORL transducer; fluctuation of impedance magnitude in aquarium

In another set of experiments, a plane, acoustically reflective boundary was introduced into the water at different locations and angular relationships. Two types of reflector were used. One was a rectangular piece of 1/4-inch plate glass about 4 by 5 inches across. The other was a glass-air-glass sandwich shown in Fig. 38. In some tests, these reflectors were located behind the transducer. In others, the transducer was viewed through them. Many curious interferograms were obtained. It seemed as if some effects, related to the standing-wave field, produced "ghost" fringe patterns and distorted the operating-mode pattern on the transducer's face.

A test was performed to see if the glass window in the end of the aquarium was vibrating appreciably. The window was sprayed with Krylon Dulling Spray No. 1310. It wipes off easily and does not significantly depolarize the reflected light. The reference beam path length was shortened to bring the end window within the coherence volume. Then both real-time and time-average holographic techniques were used to observe the window motion with the transducer excited as before. Figure 39 shows the time-average interferogram obtained of the front window. It shows a checkboard pattern with a single-peak amplitude approaching 5 by 10^{-6} inch although many of the active areas move appreciably less than this amount. The lateral spacing was about 1.9 cm; roughly 3/4 of $\lambda/2$ in water at 29.955 kHz. This wavelength discrepancy would appear to indicate that the motion of the glass was a high-order

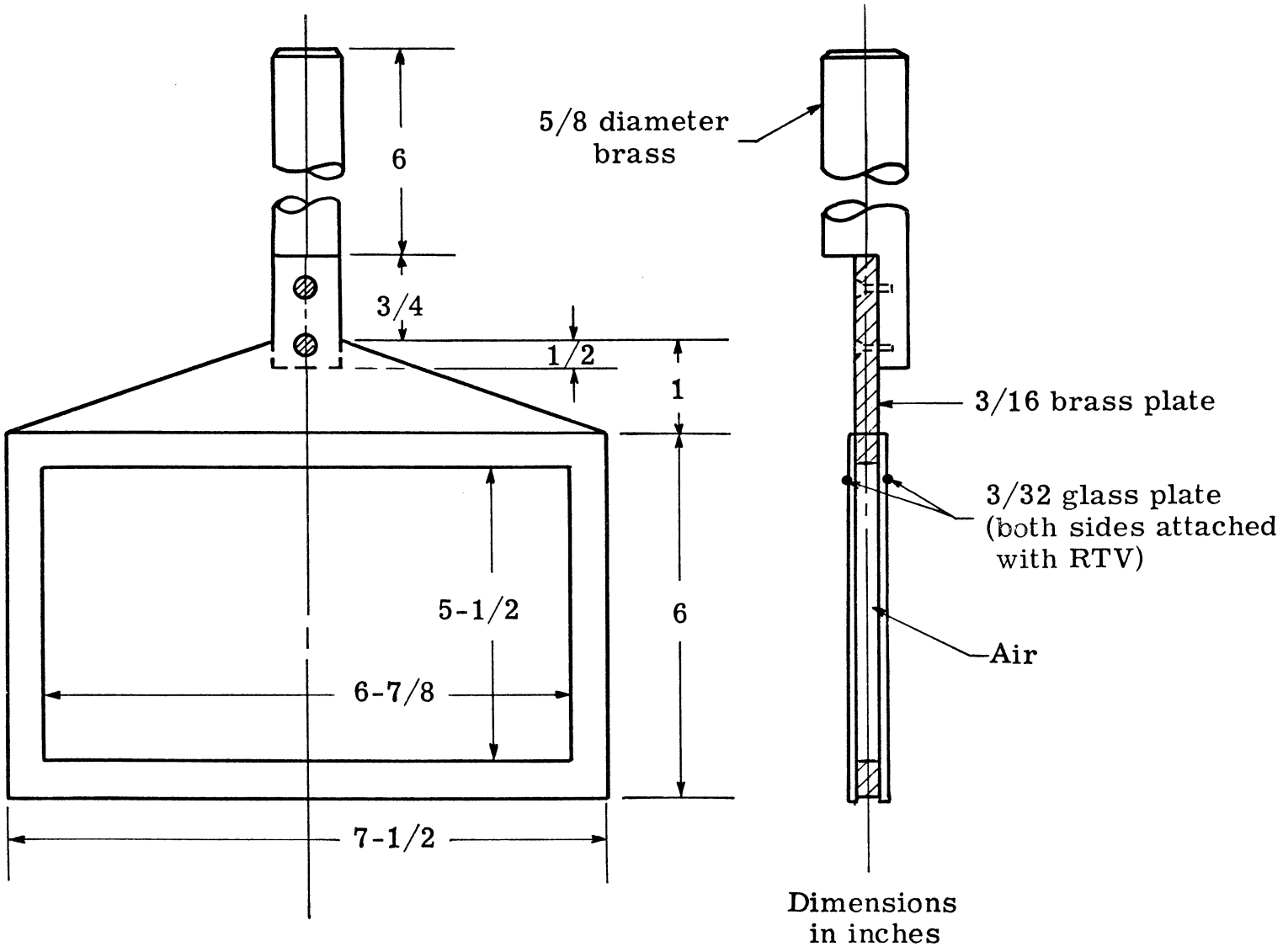

Fig. 38. Acoustically reflective vane used in water experiments

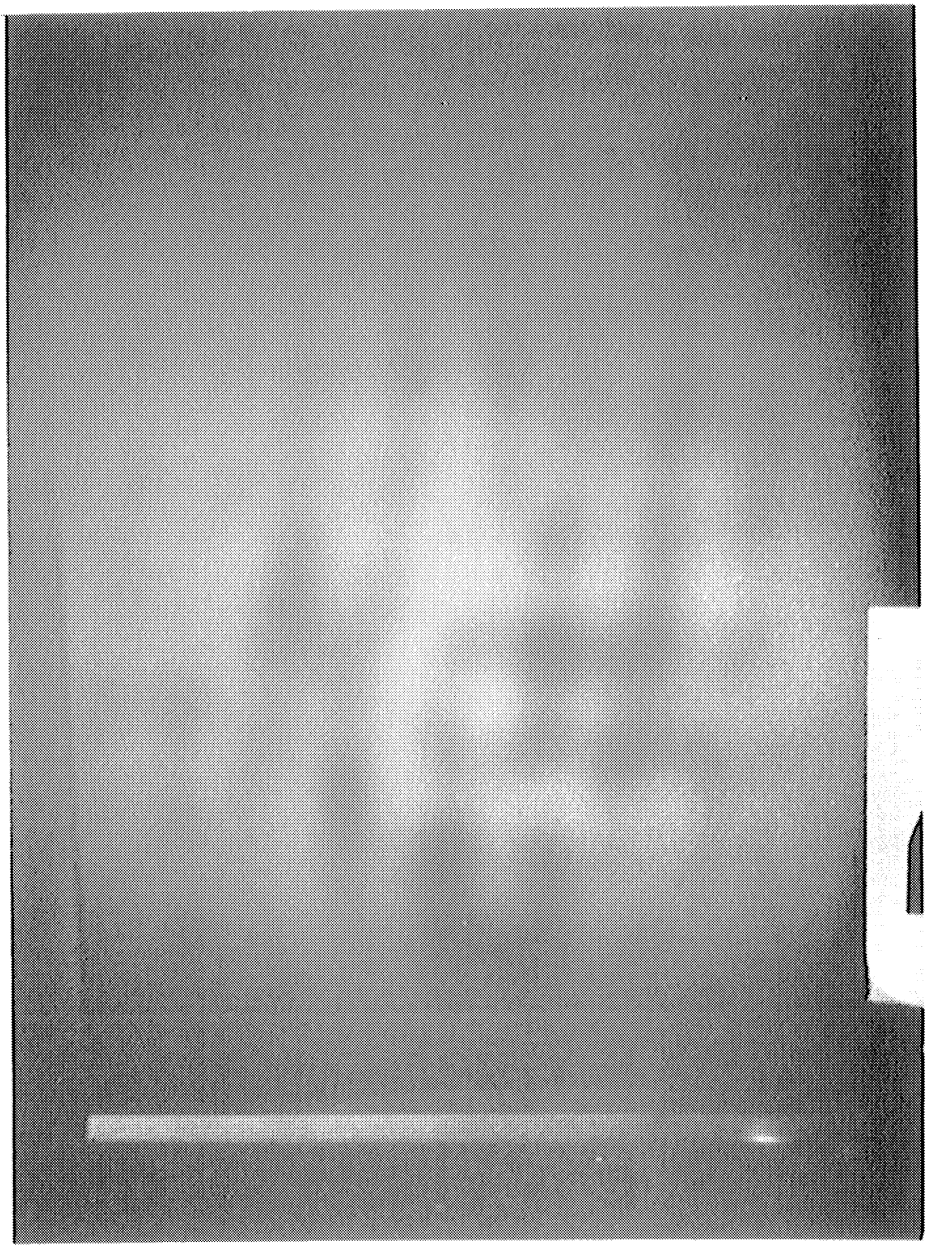

Transducer operating at 29.955 kHz, 25.0 Vac

Fig. 39. Vibration of aquarium window

flexural resonance rather than a forced motion representing the standing-wave field in the water. In any event, the displacement amplitude of the glass seemed too small to account completely for the ghost fringes. (See Section 2.5.2.)

The transducer was removed from the water and the tests in air were performed, as described in Section 4.1, to clarify the kind of displacement patterns to be expected of this 2 by 2 array. We had intended to continue the studies in water after the experiments in air. The erratic failure of the first transducer cancelled any further tests with it.

4.3.2 Second Transducer Operating in Water. Following the preliminary tests in air, as reported in Section 4.2, the second transducer was studied in water. The experimental apparatus and setup remained substantially the same as for the first transducer (Fig. 7). There was one important change; the front glass window of the aquarium was replaced by a panel of 1/2-inch thick plate glass.

At first, some difficulty was encountered with an accumulation of many small bubbles due to the large amount of dissolved air in the domestic water at this time of year (June, July). Observations concerning these bubbles are given later in Sections 4.4.4 and 4.4.5. When the bubbles had been eliminated, the operating mode of this second transducer was found at about 19.0 kHz with the aid of real-time fringes.

Figure 40 shows two successive locations, A and B, of the transducer in the forward part of the aquarium. Figure 41 shows the

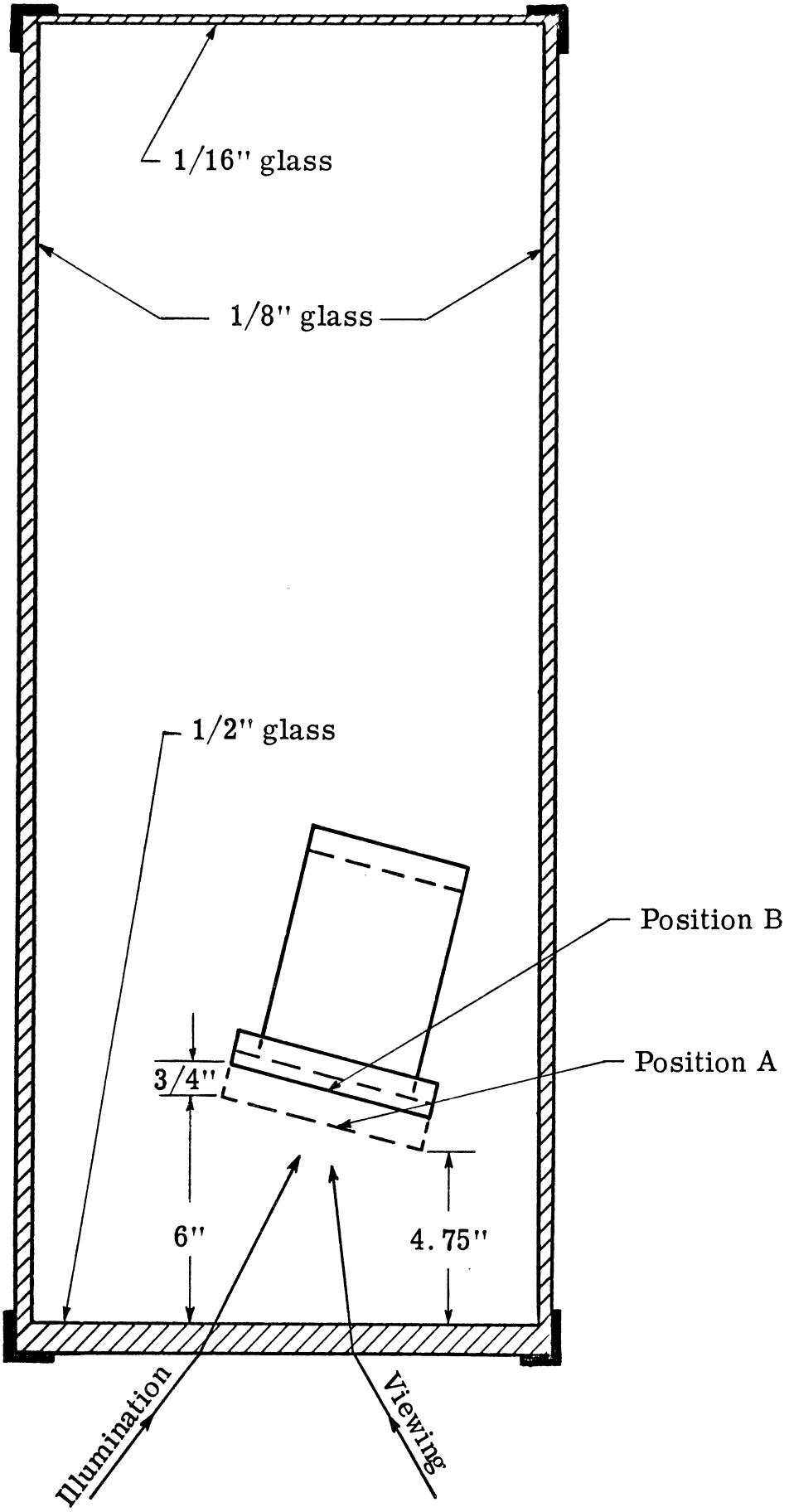

Fig. 40. Plan view of the second transducer in aquarium

Position A

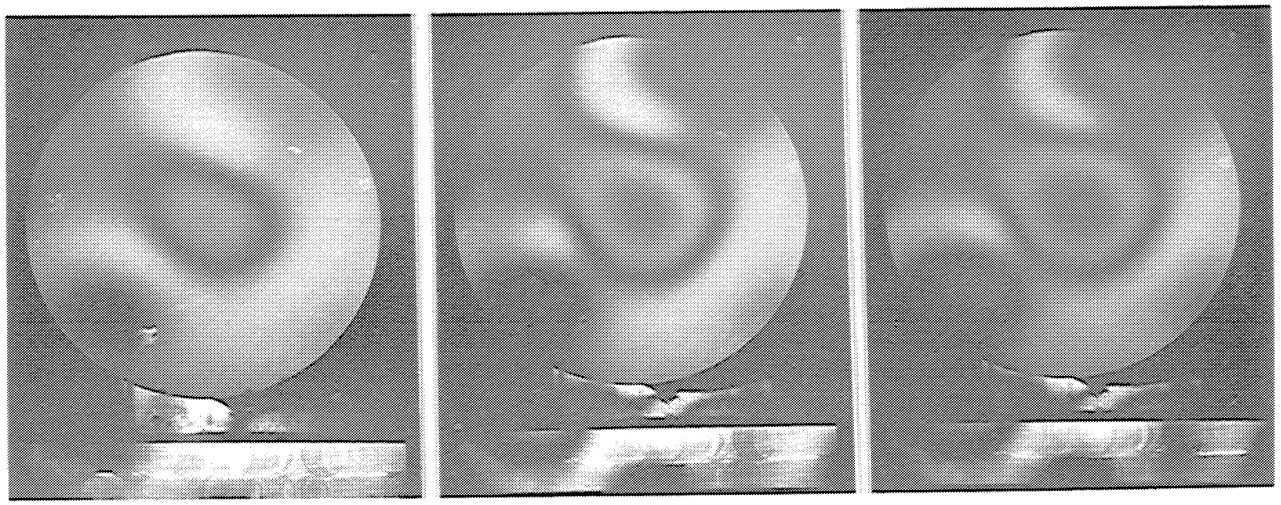

A1. 40.0 Vac A2. 80.0 Vac A3. 80.0 Vac

Position B

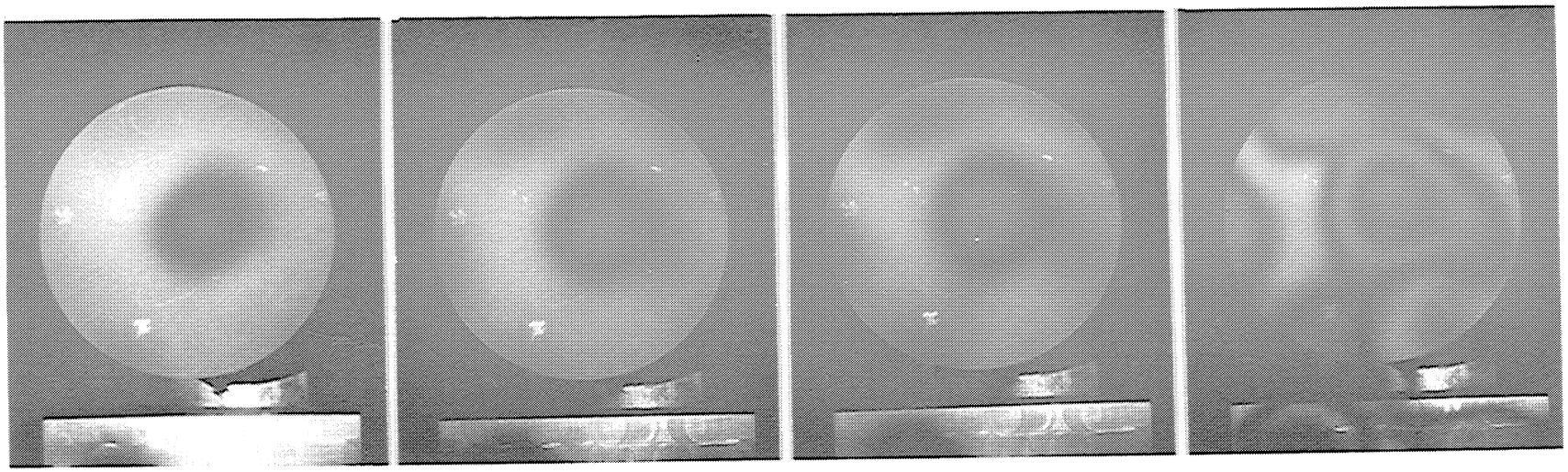

B1. 20.0 Vac B2. 32.0 Vac B3. 40.0 Vac B4. 80.0 Vac

Fig. 41. Second transducer in aquarium; 19.000 kHz

corresponding interferograms. Interferogram A3 was taken several hours after A1 and A2 as a check on reproducibility. Interferograms B1 through B4 were taken five days later after some intervening experiments. As can be seen, at low driving voltages, say 20 Vac, the ghost fringe patterns have almost vanished. On the other hand, at the higher levels and especially at 80 Vac, the ghosts are prominent. Position B of the transducer was 3/4 inch further back in the tank than position A. This distance corresponds approximately to a computed $\lambda/4$ in water at 19.0 kHz. The intent was to increase the acoustic path from the transducer's face to the glass and return by $\lambda/2$. Of course, the new location of the transducer altered the characteristic mode structure within the aquarium also.

In Fig. 41, both series A and B interferograms consistently displayed a region of activity near the center of the transducer's face. But the shapes of those patterns did not seem to correlate with any behavior expected for a 2 by 2 array. There were too many changes in pattern details from A to B, including changes associated with the ghost fringes, to make a complete interpretation. The patterns seemed reproducible and characteristic for the respective locations of the transducer. The optical phase modulation, which causes the fringes, appeared to increase proportionately with driving voltage in each series.

At the end of this research program, we have become convinced that Fig. 41 mainly shows the effect of acoustic pressure modulating the

index of refraction of the water. Simultaneously, there probably is some contribution to the recorded optical phase modulation by displacements of the rubber face and the aquarium window.

A parallel experiment to examine the motion of the 1/2-inch thick plate glass window was performed. As before, the glass was coated with Dulling Spray. The only change in the setup was to shorten the reference beam path to place the window within the coherence volume; all angles and other system parameters were held constant. Figure 42 shows the results at low and high driving voltages for transducer positions A and B (Fig. 40). At 20 Vac drive, motion of the window in the direct sonic beam of the transducer can just be detected by a slight darkening. At 80 Vac drive, the impingement of the direct beam is easily seen and amounts to roughly 8 by 10^{-6} inch single-peak displacement amplitude. Outside of the main pattern, several weaker displacement regions can be seen. Compared to the previous results with a thinner window (Fig. 39) the present situation has improved appreciably. Presumably both the thicker glass and the lower frequency were responsible but their respective roles have not been separated in these tests. The thicker glass was advantageous because it reduced fringe motion caused by residual sloshing of the water in the aquarium.

Other experiments were performed, some in which the transducer was moved to the rear of the aquarium as illustrated in Fig. 43. The transducer was aimed at the front corner of the aquarium. This object

Position A. 20.0 Vac

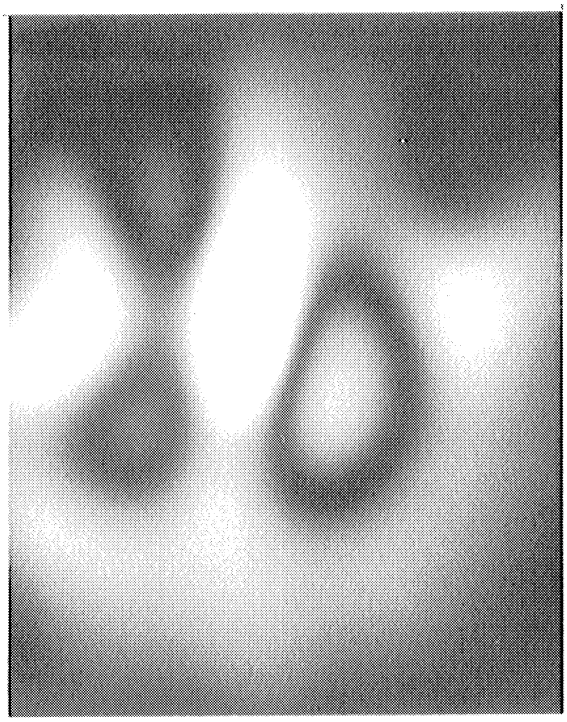

Position A. 80.0 Vac

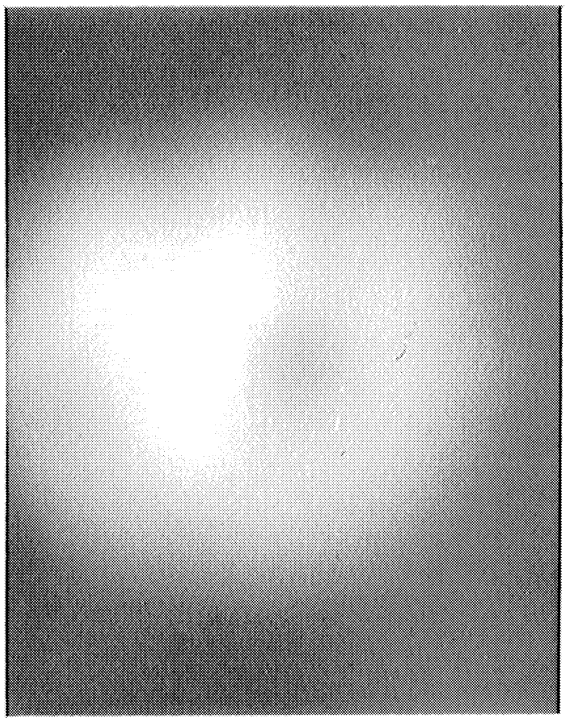

Position B. 20.0 Vac

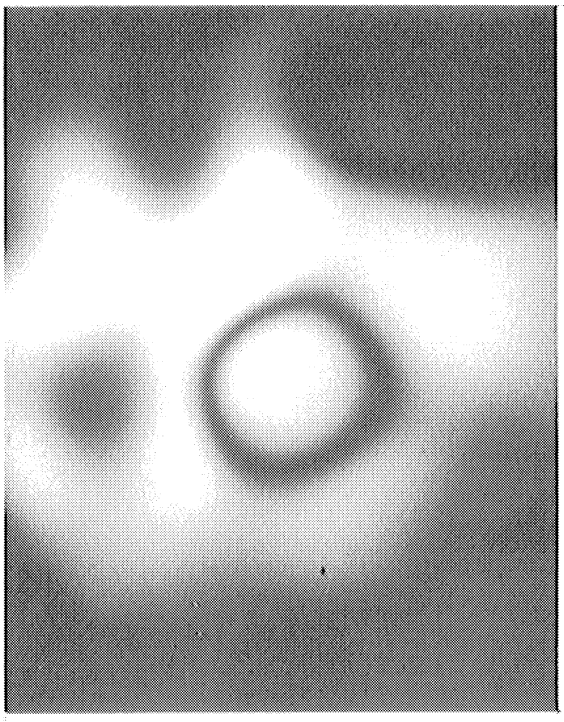

Position B. 80.0 Vac

Fig. 42. Interferograms of 1/2-inch glass window; 19.000 kHz

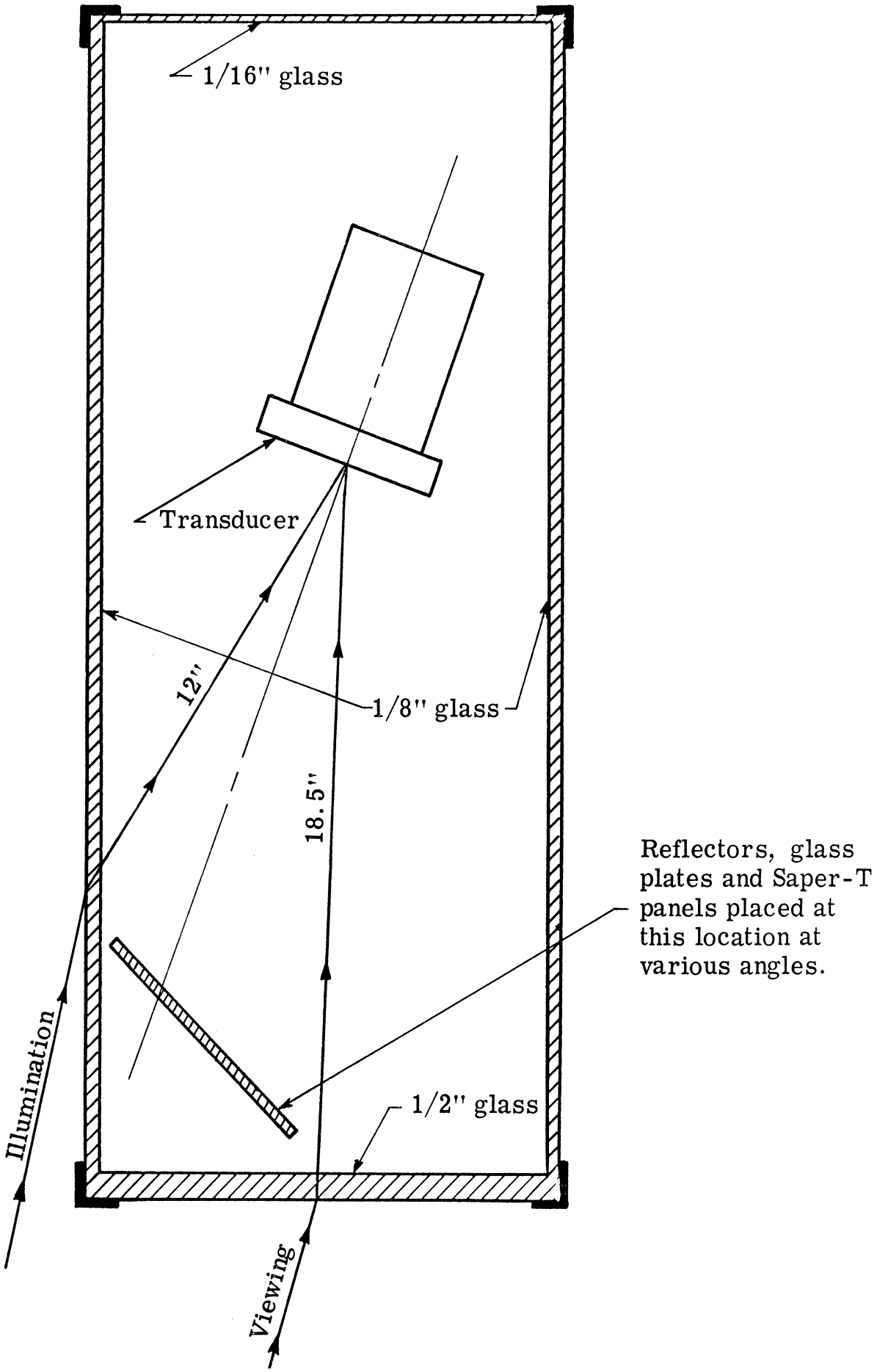

Fig. 43. Plan view of transducer placed at rear of aquarium

was illuminated through the thin side window and viewed through the thick front window. In several experiments, the direct acoustic radiation was reflected in different directions about the aquarium by placing either a piece of 1/4-inch plate glass or the glass-air-glass sandwich in the corner. Also a 1/2-inch thick brass plate, 6-1/2 by 10 inches and covered with SAPER-T (B. F. Goodrich Co.), was tried as a moderately lossy reflector at 19.0 kHz. Minor changes in the fringe patterns, especially the ghost patterns, resulted but none of these arrangements were effective enough to warrant adoption. It seemed, in fact, as if the relatively thin side window vibrated enough to mask any gains from the several experimental configurations.

One final experiment in water provided the most definitive and dramatic evidence relating to the standing-wave field. The transducer was placed near the front of the aquarium as shown in Fig. 44. An acoustically reflective vane, improvised from the glass-air-glass sandwich (Fig. 38), was placed near the rear of the aquarium. The vane rotated freely in a ball-bearing support bracket. A weight, attached to a cord which was wound around the shaft of the vane, provided several minutes of smooth, gentle rotation at rates up to about 12 rpm.

A real-time hologram was made of the transducer without excitation and with the vane stationary. Rotation of this vane did not degrade the real-time fringes on the unexcited transducer. Next, the real-time fringes were studied with the vane stationary and the transducer excited,

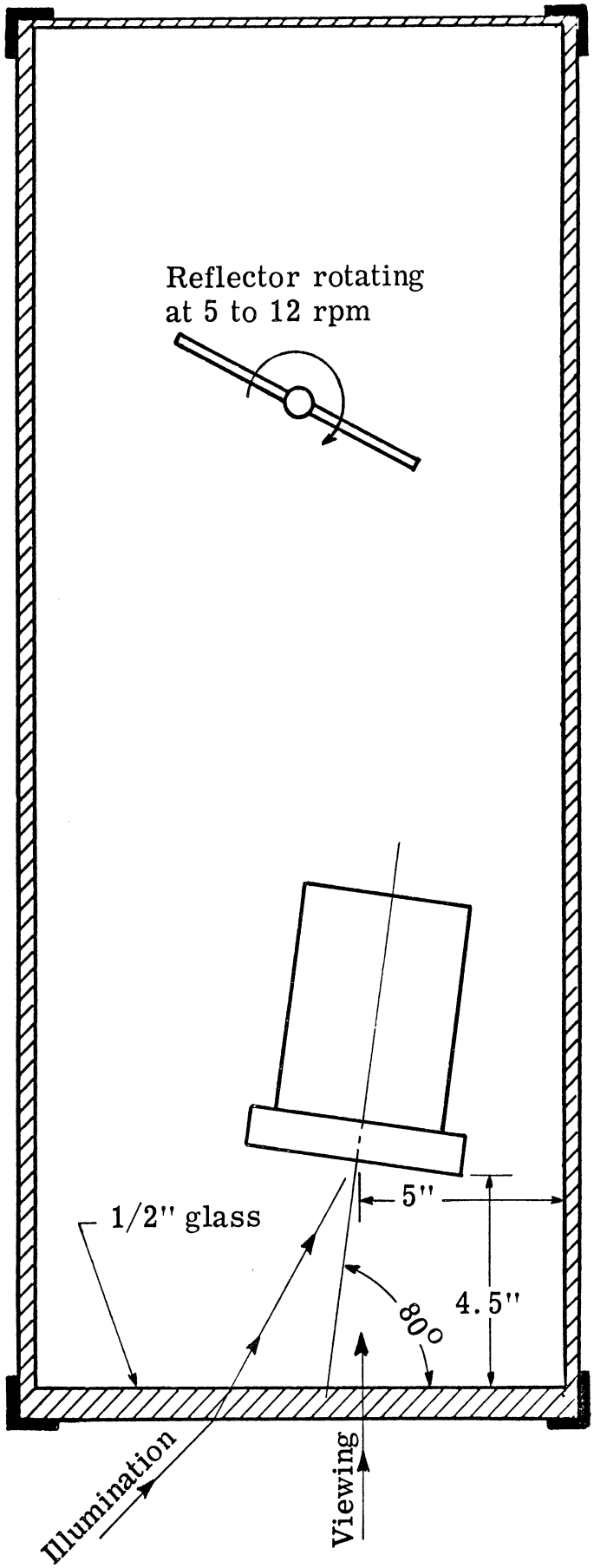

Fig. 44. Plan view of rotating vane arrangement

typically, at 19 kHz and 40 Vac. A particular pattern of fringe blurring resulted, both on the rubber face and elsewhere. Then the falling weight was allowed to rotate the reflector vane. The regions of blurred fringes jumped around, appeared and disappeared, in a most dramatic way. It was strikingly clear that the patterns observed by means of hologram interferometry were predominently influenced by the angular position of the vane. The particular patterns were controlled by the excited acoustic modal distributions in the aquarium. The rate of vane rotation was just right so that the eye observed the patterns flitting around, freezing momentarily in some configuration, then changing again. Even on the rubber face of the transducer, the variety of patterns suggested modal clumping of standing-wave phenomena rather than piston-like driving action expected for a 2 by 2 array.

Previously, we had taken series of time-average interferograms with this vane clamped at arbitrarily chosen angular orientations. These interferograms showed differences in pattern but left one puzzled about how detrimental the standing wave phenomena were. The moving vane experiment left no doubts. One cannot satisfactorily observe these transducers in water in the acoustically reflective confines of an aquarium. The optical interferometry functions adequately, but the acoustical situation is hopelessly confused. An anechoic tank accommodating hologram interferometry (Section 4.4.3) would constitute a large step in the direction of obtaining useful underwater observations on transducers. Optical

phase modulation caused by acoustic waves in water (Section 2.5.2) would occur even with an anechoic surround but the problem of definitive interpretation ought to be reduced to a more manageable level.

The only adequate ways to communicate the observations from the rotating vane experiment would be to view the live experiment or to see a movie of it. Neither was possible in this report; however, time-average interferograms can provide partial documentation. Those in Fig. 45 were made with assistance from the rotating vane experiment. Interferograms (a) and (b) were taken of two selected patterns which illustrate one of the more extreme differences. The only change was the angular position of the stationary vane behind the transducer. Interferogram (c) was taken with the vane rotating at roughly 12 rpm. Some of the ghost fringes appearing in (a) and (b) have been considerably suppressed in (c). However, interferogram (c) cannot be interpreted easily because it has resulted from the time average of two simultaneous optical phase modulations. The first modulation was the sinusoidal excitation of the transducer which, taken alone, would involve the usual zero-order Bessel function. The other modulation was caused by the effect of the rotating vane on the standing wave pattern. The details of this latter modulation are not known completely enough to attempt analysis. (Note also the evidence of a tiny air bubble at the 8 o'clock position on the edge of the rubber face which escaped detection at the time of exposing the holograms. See Section 4.4.5.)

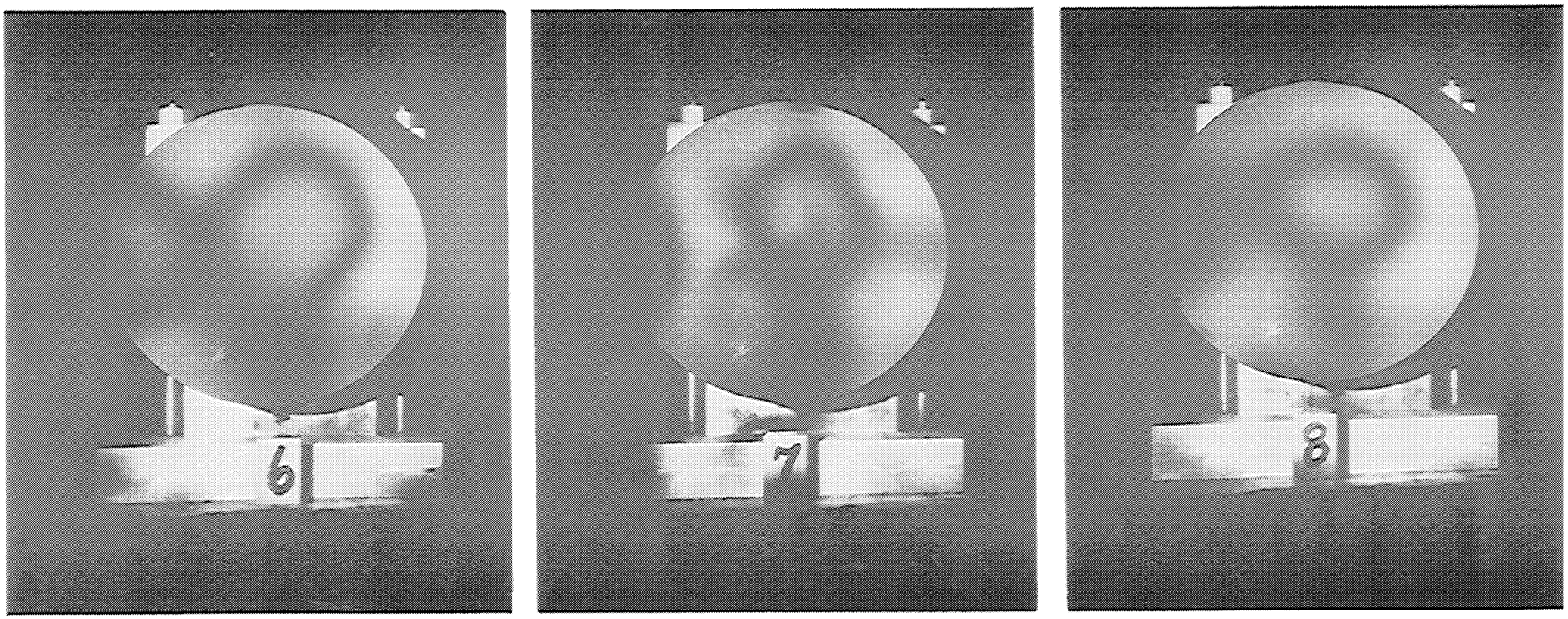

(a) Vane stationary

(b) Vane stationary but rotated from (a)

(c) Vane rotating

Fig. 45. Effects of reflector vane orientation; transducer excited at 19.003 kHz and 60.0 Vac

We do not propose the rotating vane as a means for obtaining interpretable results on transducers. The rotating vane was used successfully here only to demonstrate the serious magnitude of interference caused by the standing-wave field in the water.

4.4 Peripheral Observations

In the course of the transducer studies, observations occurred which did not fit conveniently into the main organization of that research. Such observations are collected in this section.

4.4.1 Degraded Real-Time Fringes. The remarks about tuning for maximum response in Section 4.1.1 implied a degree of uncertainty about the observations and consequently an explanation is in order. Our usual procedure is to apply the method of real-time fringes for initial exploration of an object's behavior. Then, based on those observations, we select appropriate test conditions for time-average interferometry. Photographic reconstructions from the time-average interferograms constitute most of the final documentation presented in our technical reports.

Many of the vibrating devices which we have studied have been interferometrically stable and reproducible, or could be arranged to so behave. Then the procedure outlined above leads to clear observations which can be reported precisely. The transducers were not so ideally behaved. Thus, a degree of equivocation enters the reported observations. Three factors seemed to contribute to the difficulty.

1. The first factor is the distinct impression that the real-time fringes were more difficult to observe visually on these two transducers than we have learned to expect from other objects under similar conditions. This impression occurred immediately, before the transducers were operated. We do not attribute the degradation to the flat, black optical property or to any depolarization at the rubber face. The precise cause of the impression remains unknown.

2. The rubber face was sensitive to thermal gradients produced both by internal heating when driven, and by slow changes in the ambient temperature. The real-time fringes soon departed from straight lines; they curled up, became closely spaced on some areas and widely spaced on others. This variable spacing and orientation of the fringes appreciably complicated visual observation of vibrational effects. It was possible to maintain real-time fringes with a given hologram for a period of several days. Nevertheless, within a few minutes, the fringes often became sufficiently distorted to make the usual dynamic observations difficult.

3. Exercising the rubber even briefly by driving the transducer noticeably degraded the fringes. Just as for the thermal effects, observable fringes could be maintained for several days with a given hologram. However, any exercise of the rubber introduced some non-recoverable degradation. Probably this behavior should be expected of a viscoelastic material. Perhaps, with exercise, each microscopic surface area,

which, for a diffuse surface, must return within the resolution limit in order to produce optical interference, does so incompletely. Thereby the degree of correlation between the two interfering wavefronts is reduced and fringe contrast is degraded. On the other hand, such a loss of correlation was not extensive enough in the present study to degrade the fringes completely. (Perhaps this phenomenon of contrast degradation with exercise might be usefully applied to study the microscopic surface-stability characteristics of viscoelastic materials.)

In total, there seemed to be at least three distinguishable phenomena which worked against precise interferometry of the rubber face both in air and water. The degrading effects were not severe enough, either collectively or individually in these studies, to spoil the real-time fringes completely. However, the effects were large enough to make interferometric observations less precise than customary. As a consequence, one feels less certain that the explorations based on real-time fringes have detected all significant vibrational phenomena. Lastly, the same degradations will affect time-average interferograms also but may not be as noticeable.

4.4.2 Real-Time Fringes with Time-Average Holograms. A time-average hologram, exposed under conditions of steady-state sinusoidal vibration, may be replaced in the plate holder as for real-time interferometry. Except for the regions of black time-average fringes where there is no reconstructed image, real-time fringes will cover the object.

That is, the time-average plate is manipulated to give straight, parallel fringes at a convenient spacing in exactly the same way as with the ordinary real-time hologram.

Of course, the image reconstructed from the time-average hologram has characteristics described by the zero-order Bessel function (Fig. 46). Ordinarily we view or photograph the reconstruction from a time-average hologram alone and then the square of the function plotted in Fig. 46 correctly describes the intensity distribution in the image. However, the wavefront information stored in the time-average hologram actually corresponds to the amplitude and phase of the electric field vector as plotted in Fig. 46. In the regions where the Bessel function is negative, the stored wavefront is reversed in phase compared to the positive regions. Therefore, when a time-average hologram is used for real-time interferometry, the real-time fringes will be reversed in the corresponding negative regions, i.e., a dark fringe occurs where a bright fringe would otherwise be expected.

This reversal of real-time fringes upon crossing a time-average black fringe was observed several years ago and considered to be a minor point of academic interest. However, during the transducer studies, we have encountered at least two situations of practical application for it:

Case A. Many of the time-average holograms taken of the transducers both in air and water evidenced rather small amplitudes of vibration, often only one dark fringe. Recall that the ordinary real-time

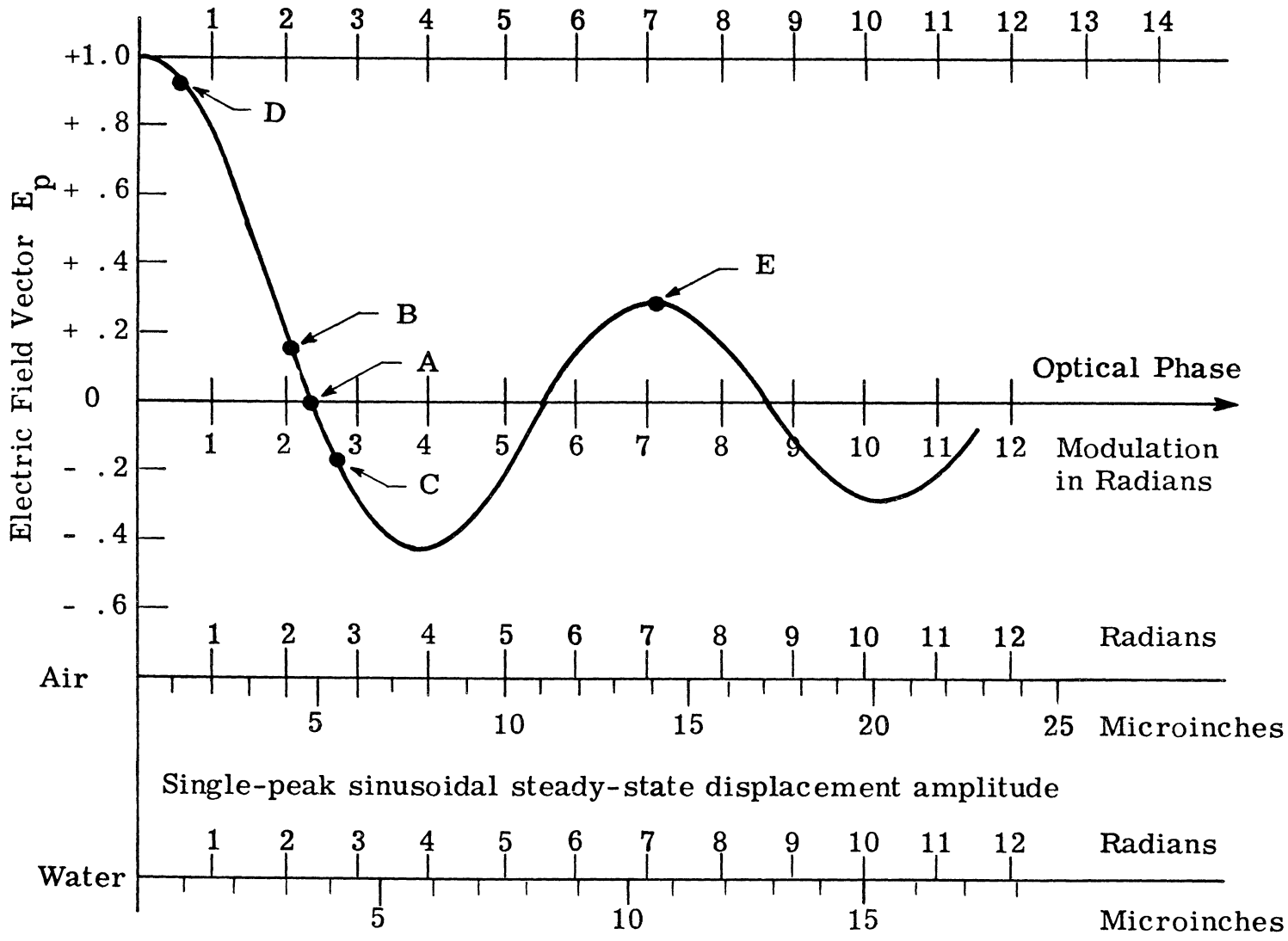

parallel to maximum sensitivity vector for 632.8 nm HeNe laser light

Fig. 46. Zero-order Bessel function applying to time-average interferometry (see Fig. 3)

fringes often were not easy to read. Furthermore, the second transducer was not particularly stable so that the precise amplitude of vibration acting during a subsequent time-average exposure was somewhat in doubt. In Fig. 28b, for example, what amplitude occurred at the center of the face? Did the vibration amplitude decrease slightly as from point A to point B in Fig. 46 or did it increase to point C?

When the time-average hologram was replaced to yield real-time fringes, the ambiguity was immediately resolved. The real-time fringes reversed phase indicating a slight increase in amplitude beyond the first dark fringe into the first negative loop region of Fig. 46.

This type of observation was applied almost routinely throughout the transducer studies. It might seem as if the darkish areas would reconstruct too weakly to see the real-time fringes. To the contrary, it was found that one could detect the real-time fringes in areas that appeared almost totally black in normal time-average reconstruction. Furthermore, the observation of reversed or not reversed fringes could be made with real-time fringes whose contrast and brightness were much too low for any other observational prupose. The method, of course, only works when one knows from external evidence which two adjacent positive and negative loops of the Bessel function (Fig. 46) apply.

Case B. This case, like case A, seemed most valuable when the ordinary real-time fringes were not easily read. The transducer studies in water were plagued with "ghost" patterns. These occurred in random

locations and shapes, e.g., Fig. 35. Although the ordinary real-time fringes were studied, it was easy to forget precisely what amplitude had been observed in some of the many splotches. Had the real-time fringes not quite blurred out, blurred out completely, or had the weaker reversed fringes reappeared? In this case also, real-time interferometry with the time-average interferogram supplied the forgotten answer.

4.4.3 Aquarium as an Acoustic Chamber. The glass-walled aquarium used in the transducer studies was a convenient laboratory apparatus with which to start underwater studies. Its size and weight could be accommodated on our holographic table. The positional stability needed for optical interferometry was achieved without extreme difficulty and many excellent interferograms have been obtained using it. On the negative side was the fact that it constituted an acoustic reverberation chamber of small dimensions. Since to date interferometric studies usually are conducted in the sinusoidal steady-state, the reverberant acoustic surround constituted a questionable choice. The techniques commonly applied in air, such as using signals comprised of band of noise, multitones, or warble tones are not acceptable, and the use of a time-varying boundary condition is questionable also. The aquarium was too small for pulse techniques in view of exposure times of the order of ten seconds.

In reality, it had been obvious from the beginning that sooner or later one should use anechoic surround conditions for interferometry of

acoustic transducers both in air and water. However, initial studies had demonstrated that useful hologram interferometry could be performed in an ordinary laboratory environment having nondescript acoustic boundary conditions. Furthermore, appreciable engineering knowledge already existed to guide the design of anechoic acoustic surrounds for both air and water. Design knowledge about facilities for hologram interferometry was not as complete. Thus, it was more appropriate to explore the demands of holography and to postpone the design of integrated holographic and acoustic facilities. Up to this point, that approach has been justified. Many successful and interpretable interferograms have been made, especially in air but also in water. The vibrating objects tended to be mechanical structures rather than acoustical transducers. Perhaps fortuitously, most such structures couple only loosely to the surrounding fluid medium and therefore display behavior largely independent of the acoustical surround.

Acoustic transducers generally couple tightly to the surrounding fluid medium. The studies conducted in water, described in Section 4.3, have now reached the point where the acoustical field in the surrounding medium must be appropriately selected for the experiment at hand. It is not a question of accomplishing successful hologram interferometry but rather interferometry which can be interpreted uniquely in terms of acoustical cause and effect. A similar point was reached in air while

studying microphones under a different project. In that case also, the residual interference caused by standing waves needed to be eliminated.

It is still difficult to recognize quantitatively the level of coupling between the vibrating object and the medium at which an anechoic surround becomes essential. At least, this statement seems true in terms of current experimental laboratory technique.

How then should an anechoic water tank be constructed for holographic interferometry studies? We have not considered this question thoroughly but preliminary thoughts may be of some value.

Any or all parts of the optical interferometer may be placed in the water if need be. The hologram plate itself may be placed directly in water. The most critical requirement in that case is to allow the emulsion time to swell, perhaps a minute or so, and to attain positional equilibrium before exposure. The swelled emulsion is delicate, the plate may exhibit a different photographic speed when wet, and photographic development occurs at a different rate for a preswelled emulsion, but these factors are mere details.

A slow circulation of the water due to small temperature or pressure gradients is not serious because the corresponding changes in optical index of refraction are insignificantly small. The problem of interferometric stability of objects in water is somewhat more severe if the water is moving. The large energy of moving water, the density of which is about one thousand times that of air, tends to move submerged

objects along with it. We have already mentioned that a long-period sloshing of water in the aquarium produced difficulty by slightly fluctuating the hydrostatic pressure operating on the glass walls and bending them. Higher frequency wave action or stirring had little optical effect. It seems best to avoid the sloshing as much as possible and to use thick, massive windows if they are part of the internal path of the interferometer. Some automatic compensation for bending of the windows could be accomplished by sending both interferometer beams through the same part of a moving window but such an arrangement usually is inconvenient for other reasons.

The acoustic particle velocity in water is comparatively small but the acoustic impedance of a glass plate or plastic film base does not differ widely from water. An immersed hologram plate will tend to move with the local particle velocity. Therefore assuming negligible gross motion of the water, direct immersion of a photographic plate looks acceptable until the peak-to-peak amplitude of particle displacement approaches roughly 1/10 wavelength of light in water ($\approx 0.5 \times 10^{-7}$ m for HeNe laser light). At 20 kHz in water, such a particle displacement would occur at roughly 105 dB re 10^{-12} W/m^2. Pressure modulation of the index of refraction of water appears more troublesome. (See Section 2.5.2.)

The metal and glass parts comprising immersed elements of the interferometer would be subject to similar forces except that many of

them can be made physically small whereas the hologram plate inherently has appreciable area. Incidentally, a small hydrophone could be used to investigate the acoustic field even in the field of view of the hologram; the obscuration would be small. In air, the difference of acoustic impedance between the apparatus and the medium is so large that acoustic excitation of the optical apparatus need not be particularly troublesome.

Both in air and water, the hologram plate is the one part of the interferometer which can hardly be considered acoustically nonreflecting, at least at high frequencies where the plate dimensions are several acoustic wavelengths. However, in an otherwise anechoic field, the hologram plate is seldom placed normal to the direction of viewing and it could be angled to reflect acoustic energy away from the direction of the transducer. A smaller than conventional (hologram) plate could be used; indeed, it could be just the size of the entrance pupil of the final viewing system without loss of resolution. Alternatively, a small field lens might replace the aquarium window if the loss of light could be tolerated.

The sketch shown in Fig. 47 represents a first-thought design of an anechoic tank for moderately high-frequency research. The transducer is beamed at an acoustically absorbing area between the illuminating and viewing ports. This area could be simply absorbing, but it could also be convex for dispersion for residual reflections or it could be a hollow absorbing wedge. If the transducer is beamed at this spot

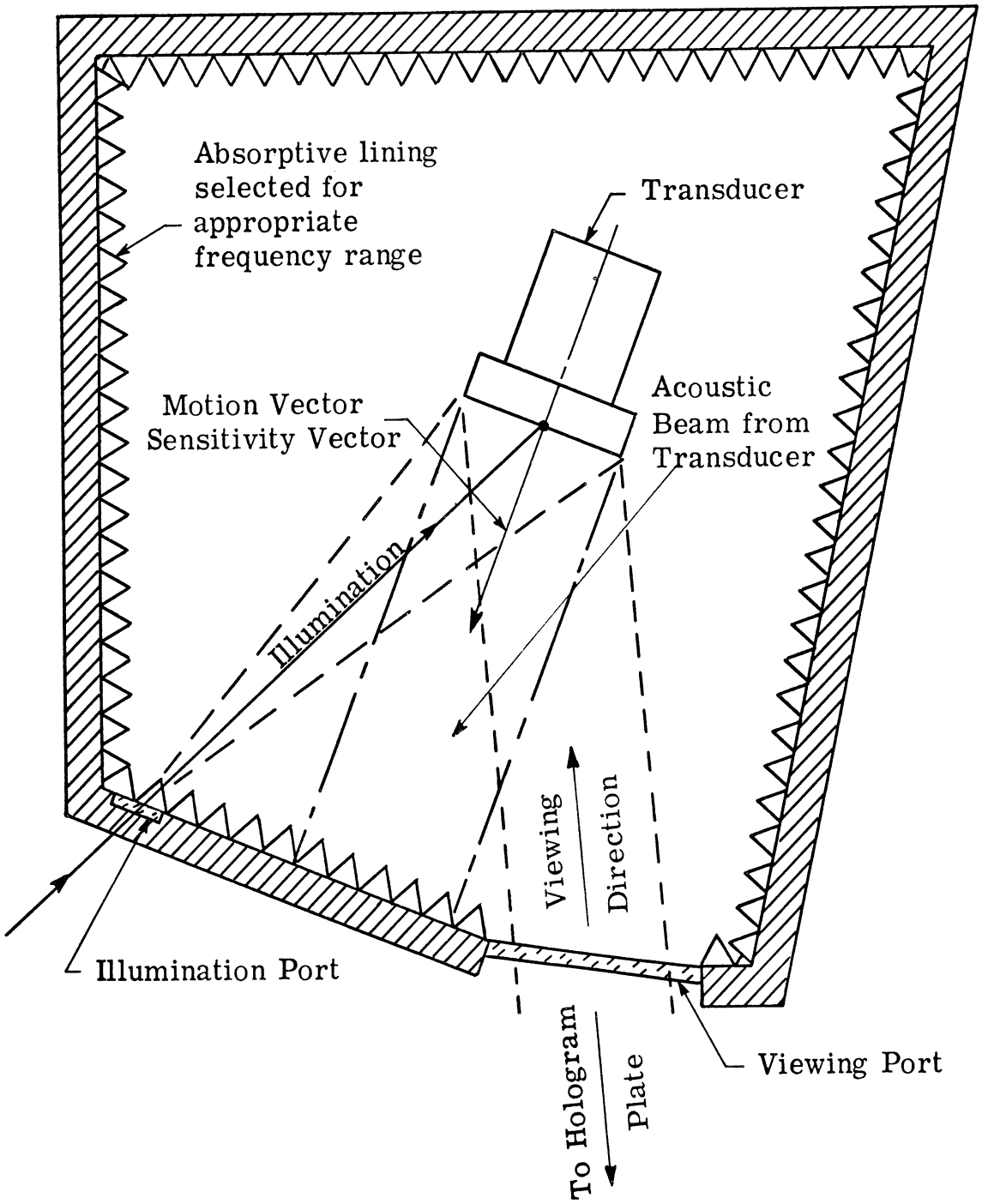

Fig. 47. Sketch of possible anechoic tank for hologram interferometry

midway between the illuminating and viewing ports, its motion vector and the optical sensitivity vector would be aligned for maximum sensitivity. Transducers with other directional patterns will suggest different arrangements.

A geometrical arrangement similar to that in Fig. 46 was applied successfully in air for studying microphones. A sound projector was placed between the illuminating beam and the hologram to produce a normally-incident plane-wave field at the microphone. Then the microphone's motion vector and the sensitivity vector were aligned for maximum sensitivity.

4.4.4 Underwater Techniques. The aquarium was filled with filtered tap water. This water was drawn through a line filter intended for photographic applications (CUNO Aqua Pure Water Filter Model P-10). It removed the larger particulate matter and optical scatter was noticeably reduced. For extensive research in water, it might be worthwhile to invest in a finer filter, one capable of removing submicron-sized particles.

Deaeration of the water is a notorious problem in underwater acoustic measurements in the laboratory. We had no special cure for it other than to allow the filled aquarium to stand for a day or two. The accumulation of bubbles was dislodged every few hours until they ceased to collect. Impatience with this deaeration process led to the observations on bubbles presented in Sections 4.4.5 and 4.4.6.

Some difficulty was encountered with chemical reaction between the water and objects placed in the water. These reactions were troublesome because they produced debris which clouded the water. More attention to selecting compatible materials and protective finishes would help considerably to keep the water clear. In the case of steel parts, rusting was inhibited by adding sodium nitrite to the water. This chemical did not seem to cause any interference with successful holography. Automotive (radiator) rust inhibitor was found to be too strongly colored and it produced an opalescence which was unacceptable. When both brass and steel were immersed together, the addition of sodium nitrite inhibited rusting but slowly discolored the brass. However, for a period of a week or two at a time, the effects on the brass were of much less consequence than rust from uninhibited steel. Galvanize on steel rapidly scaled off in the presence of sodium nitrite and formed little piles of debris on the bottom of the aquarium.

We have made some use of the ordinary aquarium air pump and filter system to circulate the water in order to filter cloudiness from the water. This pump system circulated the water effectively and could be allowed to operate even while exposing holograms as long as the pump did not mechanically contact the granite slab or aquarium structure. The circulation of the water and the air bubbling through the pump tube did not cause detectible holographic troubles. The effectiveness of the filtering operation in clearing the water was poor. Either a better filter

medium needs to be found or more emphasis should be placed on avoiding water-beclouding reactions.

Holographic studies of microphones had revealed a problem of thermal distortion of the object by heating produced by the subject illumination. Because the transducer faces were black and had to be intensely illuminated, we checked for the existence of similar thermal difficulties. There seemed to be no evidence of heating due to laser illumination although we could produce detectible fringe distortions on the rubber faces in air with the light of a small flashlight.

The real-time fringes on the transducers showed increased curvature with operation time. This effect probably was caused by internal heating and expansion of either the driving units or the rubber face. Thus, for the two transducers studied, thermal effects were sometimes a nuisance but were not too severe.

We have examined another type of high-frequency transducer in water which exhibited a thermal convection problem. It was a ceramic bimorph element in direct contact with the water on one side. At some levels of excitation, thermal convection blurred the real-time fringes on the active face after only a few seconds of operation. The fringes would recover after a few seconds if the excitation was removed but interferometric observations had to be made very quickly in several widely spaced bursts of operation.

4.4.5 Bubble Sheath. An observation of the acoustic consequences of a bubble sheath occurred during studies on the second ORL transducer. The acoustic isolation provided by a bubble sheath is, of course, a well-known phenomenon of underwater acoustics. The observation of it by means of hologram interferometry is unique enough to justify reporting it.

The transducer was placed in an aquarium and the aquarium was filled with filtered tap water. A real-time hologram was made within about three hours of filling the aquarium, and the transducer, especially its rubber face, was covered almost completely with a sheath of fine bubbles which had formed as the dissolved air separated out of the water

The fringes must have been formed principally by light which reflected from the rubber face of the transducer between the bubbles. The bubble sheath appeared so dense and complete that it was hard to imagine there being enough exposed area between the bubbles to produce a wavefront suitable for interferometry. Nevertheless, it did occur and the observer was not conscious of any discontinuity in the fringes where they were superimposed on the bubbles or of any significant degradation of contrast due to the bubbles. That the interfering wavefronts actually represented the rubber surface and not light passing through the bubbles was proven subsequently by gently sweeping the bubbles away; the fringes remained.

With the real-time fringes and the bubble sheath present, the transducer was excited. The same pattern of interferometric observations occurred as found previously in air for this transducer. (See Section 4.2.) The patterns occurred at the same frequencies and drive voltages as in air. This behavior was observed at 19.950 kHz as well as at 21.950 and 14.100 kHz. Thus, on the basis of hologram interferometry, the vibrational phenomena were identical in air and in water when covered with a bubble sheath. When the bubble sheath was removed, the vibrational characteristics of the transducer changed.

These observations, made by means of hologram interferometry, are consistent with the known acoustical effects of bubble sheaths. It would have been surprising and disturbing if it were not so. Nevertheless, we found the actual occurrence of this observation most interesting and gratifying.

4.4.6 Isolated Bubbles. A related observation occurred after the water had become somewhat deaerated. We were making time-average interferograms of the transducer in water under selected conditions of steady-state excitation. Small dark circular spots appeared in the reconstruction on portions of the rubber face (Fig. 48) which were not moving appreciably; at least they were not partaking of the main displacement activity. A careful inspection showed that there was a tiny bubble attached to the rubber face at the center of each such spot. Where a larger, more irregularly shaped spot appeared, several small bubbles

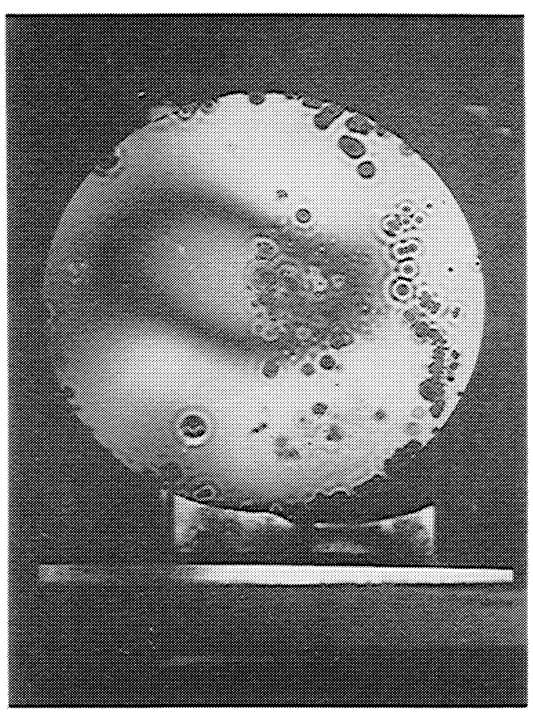

(a) Many bubbles

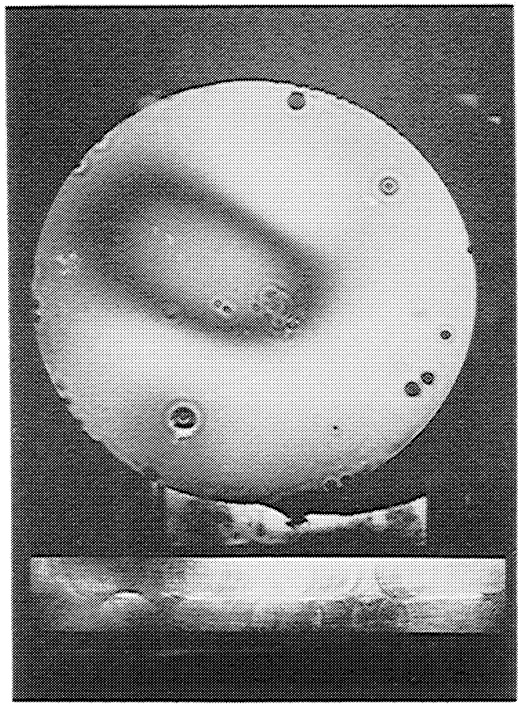

(b) Few bubbles

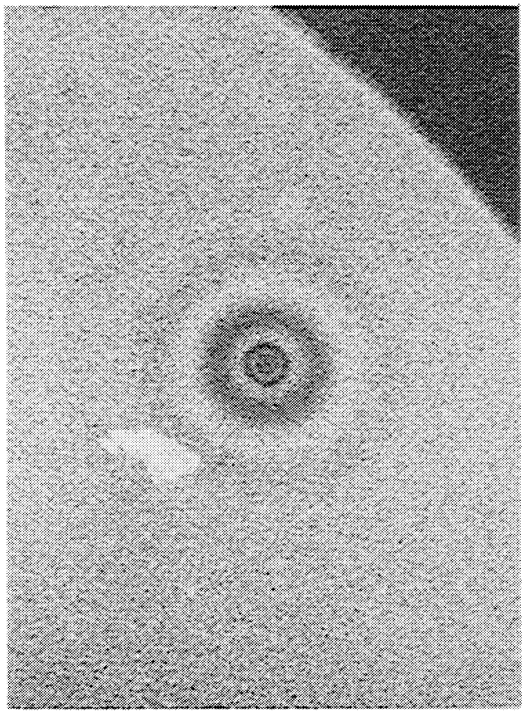

(c) Enlargement of bubble pattern

Fig. 48. Time-average interferograms showing effects of isolated, small bubbles

occurred fairly close together. These bubbles were quite persistent in that they remained in place for an hour or more. Perhaps they grew in size between the time when the time-average hologram was exposed and when they were observed directly in juxtaposition of reconstructed spot and visible bubble. But they were not dislodged even by excitation of the transducer.

The local effect of such bubbles had not been noticed previously when observing real-time fringes. Thus a new real-time plate was exposed when a few persistent small bubbles were on the transducer face. Upon observing the real-time fringes and shifting one's viewing point to cause a dark real-time fringe to superimpose over a bubble, then, excitation of the transducer caused the fringe to blur in the immediate vicinity of the bubble but not in the general neighborhood of the bubble.

The explanation, referred to the time-average situation, is as follows. When the transducer was excited, a portion of the rubber face moved with forced motion and gave rise to the predominant contour fringe patterns. Away from this major pattern, the rubber had vibrational energy in it but the surface motion was too small to cause even the first dark fringe. Generally, the rubber in such areas was only slightly less bright than when not excited. In terms of Fig. 46, we might observe a region of the rubber where the motion would correspond to point D, for example. If, then, a small bubble occurred on the surface of the rubber in such an area, it introduced a tiny local region more

compressible than the water. As a consequence, the rubber surface in the neighborhood of the bubble moved with increased amplitude. A small circular pattern of one or more dark fringes occurred, corresponding for instance to point E in Fig. 46 representing roughly 2-1/2 fringes amplitude. The lateral spread of this enhanced displacement is perhaps 10 or more bubble diameters wide. The actual diameters of the bubbles were not measured but can be estimated at about 0.5 millimeter. Fig. 48c shows an enlargement of the reconstruction of one of the spots.

These small, high amplitude regions surrounding a few isolated bubbles probably have little direct significance with respect to transducer power or beam shape. The indirect deductions are more profound. That is, the whole rubber face is insonified with energy and behaves like a fluid in some respects. If a bubble can cause the effects described above, then conversely, the principal motionat the rubber surface must be a dynamic resultant of the whole force field. It may not faithfully transfer the beam characteristics of the underlying driving elements.

4.4.7 Rubber Creep. We observed a slow creep phenomenon in the rubber face of the second ORL transducer for a period of several weeks after it was received. During this time period, we were studying the transducer in air. A hologram for real-time fringes would be exposed for 5 to 10 seconds, processed, and replaced in the plate holder. Initial adjustments produced the conventional pattern of straight or nearly straight real-time fringes over the transducer's face. After an

elapsed time of an hour or two, the fringes over a small region in the center of the face showed a pronounced kink. In the normal course of experiments, we had exercised the transducer so that the original straight fringes had become curved due to thermal expansion among other things. Even in the presence of such curled fringes, a localized effect near the center of the face was easily distinguished and it became more pronounced as time proceeded. This local effect was a slow outward creep in a small, clearly defined region of the rubber.

Figure 49 shows two reconstructions of real-time fringes taken roughly 24 hours after the reference hologram was exposed and four days after we had received the transducer from ORL. Also shown in Fig. 49 is a sketch indicating a small triangular marking which could just be made out on the rubber face under grazing illumination.

The origin of this creep pattern is unknown to us. The pattern was similar to those which can be obtained by pressing some hard object briefly into the rubber. Squeezing the rubber with one's fingers produces both local thermal and pressure distortion that will persist for perhaps ten minutes. However, the creep pattern found on the transducer lasted much longer and appeared more sharply defined at its edges than any pressure mark which we made deliberately. The packing over the transducer's face when received from ORL would scarcely have allowed the marking to have occurred in shipping and we cannot account for it by any occurrence in our laboratory. We think, therefore, that it originated

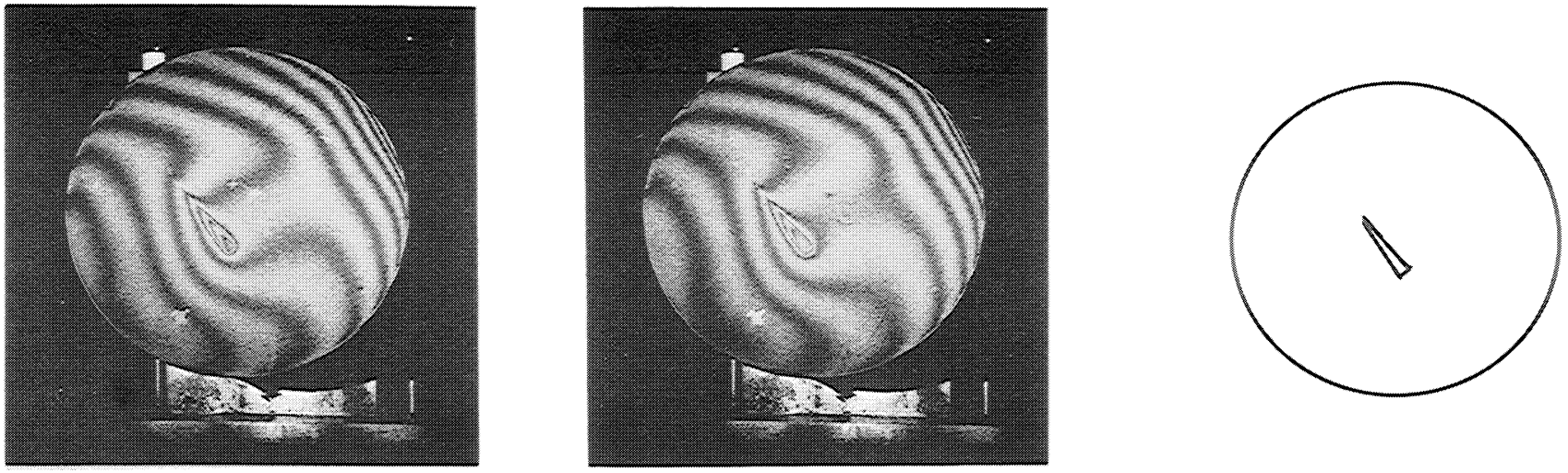

(a) (b) (c)

Fig. 49. Real-time fringes showing creep phenomenon in rubber

at ORL. Whether it is a trivial result of the transducer resting face down on a triangular sliver of tape or metal for several days, for instance, or the result of something in the vulcanizing process, we do not know. If it were caused by the latter, then the creep pattern might be a clue of some importance.

Figure 49b also shows a slight dumbbell shape above and to the right of the main creep pattern. This also appears to be a weak, creep pattern. There is a white X-shaped spot at about the 7 o'clock position. This appears to be a bit of foreign white material firmly stuck to the black rubber. Whatever it is, it is not interferometrically stable; real-time fringes will not occur on it. After several weeks, the creep phenomenon discussed above subsided to the point where it was no longer obvious and eventually it disappeared completely.

5. CONCLUSIONS

The field of vibration analysis by hologram interferometry is maturing rapidly. A more complete understanding of the underlying science is developing and simultaneously the range of useful laboratory procedures is expanding. The following conclusions may be drawn from the studies reported here:

1. The contrast of real-time fringes has been completely analyzed in terms of two limiting cases.

2. The practical manipulation of this fringe contrast has been demonstrated and several practical laboratory techniques for doing so are described.

3. More sophisticated techniques of hologram interferometry have been considered and several of them promise significant practical value. They should be thoroughly explored in the laboratory. Thses techniques, in concert, promise:

   (a) Analysis of periodic vibrations of any complexity in contrast to the present single-component, sinusoidal, steady-state vibration.

   (b) The possibility of detecting and mapping smaller vibrational amplitudes.

   (c) Direct sensing of vibrational phase.

4. A large object can be usefully examined by hologram interferometry even when the axial coherence length of the laser

source is smaller than the object's dimensions.

5. Hologram interferometry may be directly extended to objects immersed in water. Displacement sensitivity is then increased by the index of refraction of water.

6. Acoustic pressure modulation of the index of refraction of water introduces a fundamental complexity into the vibrational analysis of sonar transducers.

7. The effective study of acoustic transducers by hologram interferometry requires anechoic surround conditions in both air and water. The study of vibrating mechanical structures, less tightly coupled to the fluid medium, can be successful in a non-descript acoustical surrounding.

8. Hologram interferometry may be used to detect and map the distribution of nonlinear effects, unstable operation, and time-dependent operation such as occurred during the transducer experiments.

APPENDIX

Note: The table of contents of Technical Report No. 1 (December 1968) is repeated here for reference only. It does not apply to the present report.

Technical Report No. 1 (08160-1-T)

TABLE OF CONTENTS

APPENDIX (Cont.)